CONTROLLED SWITCHING APPLICATON FOR TRANSMISSION LINES AND POWER APPARATUS

Ph.D. THESIS

by

BHATT KUNAL ASHVINKUMAR

DEPARTMENT OF ELECTRICAL ENGINEERING
INDIAN INSTITUTE OF TECHNOLOGY ROORKEE
ROORKEE – 247 667 (INDIA)
MAY, 2019

CONTROLLED SWITCHING APPLICATION FOR TRANSMISSION LINES AND POWER APPARATUS

A THESIS

Submitted in partial fulfilment of the requirements for the award of the degree

of

DOCTOR OF PHILOSOPHY

in

ELECTRICAL ENGINEERING

by

BHATT KUNAL ASHVINKUMAR

DEPARTMENT OF ELECTRICAL ENGINEERING
INDIAN INSTITUTE OF TECHNOLOGY ROORKEE
ROORKEE – 247 667 (INDIA)
MAY, 2019

INDIAN INSTITUTE OF TECHNOLOGY ROORKEE, ROORKEE

CANDIDATE'S DECLARATION

I hereby certify that the work, which is being presented in the thesis entitled "**CONTROLLED SWITCHING APPLICATION FOR TANSMISSION LINES AND POWER APPARATUS**" in partial fulfilment of the requirements for the award of the Degree of Doctor of Philosophy and submitted in the Department of Electrical Engineering of the Indian Institute of Technology Roorkee, Roorkee is an authentic record of my own work carried out during a period from July, 2015 to May, 2019 under the supervision of Dr. Bhavesh R. Bhalja, Associate Professor, Department of Electrical Engineering, Indian Institute of Technology Roorkee, Roorkee – 247667, Uttarakhand, India.

The matter presented in this thesis has not been submitted by me for the award of any other degree of this or any other Institution.

(BHATT KUNAL ASHVINKUMAR)

This is to certify that the above statement made by the candidate is correct to the best of my knowledge.

(Bhavesh R. Bhalja)
Supervisor

Date:

Acknowledgement

I would like to thank and express my sincere gratitude and deep regards to my supervisor Dr. Bhavesh R. Bhalja, Associate Professor, Department of Electrical Engineering, Indian Institute of Technology Roorkee for his constant encouragement, inspiring guidance, moral support, and keen interest in minute details of the work.

I express my sincere thanks to the SRC committee members: Prof. N.P. Pathy, Dr. Vinay Pant, and Dr. Sanjay Upadhyay for sparing their valuable time in reviewing and critically examining the work.

My heartfelt gratitude and indebtedness go to all the faculty members of the Department of Electrical Engineering for their caring words, encouragement and providing support with necessary facilities to carry out this research work. I would also like to extend my special thanks to Prof. N. P. Padhy, Dr. G.B. Kumbhar, Dr. Vinay Pant, Dr. C.P. Gupta and Dr. P. Sumathi for his moral support & facilities provided in the PSS laboratory and making my stay pleasant during this period.

I extend my special thanks to Prof. R. P. Maheshwari, Retired Professor, Department of Electrical Engineering, Indian Institute of Technology Roorkee for his kind support, encouragement, and necessary help provided during this work.

I would also like to extend my gratitude to Dr. Urmil B. Parikh, Global principle engineer, ABB India Pvt. Ltd., Vadodara, Gujarat for providing valuable suggestions & comments and sparing his valuable time throughout my research work.

I would like to acknowledge the support and help provided by Shri. Ravindraji, Shri. Amir Ahmadji, Mr. Manoj and Mr. Vinit, and Mr. Sanjay for his kind support and facilities provided in PSS laboratory. Further, I would also like to acknowledge the support provided by Mr. Mohan Singh, Mr. Rishabh and Mr. Bhopal Singh in all departmental administrative work.

I express my thank to my co-researchers Mr. Soumitri Jena, Mr. Vishal Gaur, Mr. Ashish Doorwar, Mr. Tejeswara Rao, Miss Rinalini, and Mr. Abhishek for sincere support and respect. In addition, a special recognition must be given to Mr. Haresh Shabhadia, Dr. Nawab Alam, Dr. Akhilesh Mathur, Dr. Afroz Alam and Mr. Sukhlal Sisodiya, Mr. Saran Satsangi, Mr. Kanhaiya kumar and Dr. Shriniwas for their valuable suggestions and comments on my progressive work time to time. Further, it would be unfair if I forgot my co-researchers Dr. Hari Krishna, Mr. Sanjeev Panala, Mr. Chaithanya, Mr. Gururaj, Mr. Phanindra, Mr. Naveen, Mr. Abhishek, Miss

Rashmi, Miss Satabdi, Miss Sandhya, and Mr. Arpit. They help me directly or indirectly for my research work.

I would express my sincere regard to Dr. B. K. Gandhi, QIP Coordinator, QIP Centre, Indian Institute of Technology Roorkee and all the administrative staff member of the QIP Centre for providing their valuable support during my stay at Roorkee.

My heartfelt gratitude and indebtedness to go Mr. A. M. Patel & his family, Mr. Dixit Pathak & his family, Mr. H.D. Patel & his family, Mr. Jatinbhai Patel Mr. S. B. Prajapati & his family, Dr. Sricharan & Bharti, and Mr. Z. R. Chhaya, Mr. Sachin Patel, and Mr. Vanzara for providing their support and homely environment during my stay at Roorkee.

I am grateful to Dr. P. K. Brahmbhatt and Dr. U. K. Khare, In-charge Principal, Government Engineering College, Dahod for his continuous support. At the same time, I am very much thankful to my departmental colleague Prof. J. I. Patel, Prof. A. D. Joshi, Mrs. Minaxi Patel, Mr. Ashesh Shah, Mrs. Megha Mahida, Mrs. Prafulla Bamaniya, Mrs. Mumtaz Makrani, Mr. Pratik, Mr. Hardik Patel and Mr. Rakshit Patel for their kind support provided during the process of obtaining deputation for higher study.

During my journey of doctoral degree, Dr. Yogesh kumar Makwana and Mr. M. A. Maniar has been continuous motivational force for me to pursue my work. Dr. Makwana has been with me right from the very first day to the last day of stay at Roorkee. He helped me a lot in my academic work and domestic need. I am really very much thankful to him for his help.

I extend my heartfelt gratitude to my parents with their blessing only I am able to complete my work. I would also like to express my deep regards and gratitude to my both the elder sisters & her family and friends for their consistent support and patience.

Word can hardly explain the co-operation and patience of my daughter *Ananya*. I have no words to express the support of my wife *Murli* provided me to fulfill my endeavor of doctoral work. She stood by me at every moment and kept me free from almost all the responsibilities of domestic issues during my work.

At last but not least, I very much thankful to my God for giving me an opportunity to live few years of my life at the bank of holly river *Ganga*

(**Kunal Ashvinkumar Bhatt**)

Abstract

Since the inception of power system network, utility uses transmission lines along with different power apparatus to transfer bulk amount of power from source to load end. Sometimes, it is essential to perform switching operations of transmission lines and power apparatus during normal/abnormal conditions. However, the switching operations may cause switching transients. At Extra High Voltage (EHV) and Ultra High Voltage (UHV) levels, switching transients gain more importance than lightening surge. At the same time, frequency of switching of transmission lines and power apparatus are increasing day by day due to increase in penetration of renewable energy resources in the grid, which in turn generates switching transients. The switching transients develop thermal and dielectric stresses in the power system network. They may cause problems such as degradation of quality of power supply, loss of life of power apparatus, lower efficiency, and poor reliability of the system. Two types of switching practices namely, uncontrolled switching and controlled switching are normally used by the utilities.

In past, uncontrolled switching of transmission lines and power apparatus has been performed using Circuit Breakers having Pre-Insertion Resistor (PIR-CB). Though PIR-CBs offer better performance in terms of minimization of the level of switching transients compared to simple Circuit Breaker (CB) (i.e. which does not have pre-insertion resistor) they are not able to eliminate switching transients completely.

In order to minimize the level of switching transients, point on wave switching technique (also known as controlled switching technique) has been reported in the literature. In this case, the level of switching transients has been limited by controlling the opening/closing instant (point on wave) of the CB. The opening/closing instants of CB are known as controlled switching targets and the device attached with the CB is known as Controlled Switching Device (CSD). Depending on the power system equipment to be switched ON/OFF, opening/closing instant of the CB is controlled by CSD. For successful implementation of the controlled switching, the targets must be repetitive in nature. This type of nature helps in predicting occurrence of point on wave target. Accordingly, the controlled switching command can be raised and mechanism of the CB can be activated. However, CB is a mechanical device with different mechanical and electrical closing instants. The electrical opening/closing target of the CB has been achieved using mechanical opening/closing target. Due to effect of Mechanical Operating Time (MOT) scatter, it is difficult to attain precise electrical opening/closing target using mechanical opening/closing target of the CB. This is one of the setback faced by the controlled switching technique during its implementation in real field. The main objective of

this thesis is to reduce the level of switching surge during energization/re-energization of different types of transmission lines and power apparatus along with the consideration of the effect of MOT scatter of the CB.

In case of uncompensated and shunt reactor compensated transmission line, energization/re-energization has been performed at zero crossing instant of gap voltage across the contacts of CB (V_{GAP}), which is the difference between line side and source side voltages. Energization of fully discharged Un-Compensated Transmission Line (UCTL) has been carried out at zero crossing instant of supply side voltage. Due to absence of trapped charges, zero crossing instances of supply side voltage and V_{GAP} occur at the same time. On contrary, it is required to study polarities and variations in the magnitude of the trapped charges during energization of a partially discharged transmission line (i.e. re-energization). It has been reported in the literature that the trapped charges attain unidirectional polarity during dead time of the CB in case of UCTL. Conversely, in case of Shunt Compensated Transmission Line (SCTL), the nature of trapped charges is oscillatory and achieve bidirectional polarity. Therefore, it is difficult to identify the controlled switching targets during energization of a partially discharged SCTL due to non-repetitive waveform of V_{GAP}.

In order to determine optimal controlled switching target during energization of a partially discharged SCTL, different controlled switching targets have been identified. In the presented work, supply side voltage has been considered as the reference. Seven points on wave targets from one complete cycle of supply side voltage ($0 - 360^0$) have been tested (each at 45^0). Out of all seven targets, zero crossing instant of the supply voltage is considered as an optimal controlled switching target for fully and partially discharged SCTL. Whereas, half of the peak value of the supply side voltage (having same polarity of the trapped charge) is considered as an optimal controlled switching targets for a partially discharged UCTL. As the above mentioned targets are repetitive in nature, they can be easily implemented in real field. Here, the transmission line has been modeled by the frequency dependent phase model, available in Power System Computer Aided Design (PSCAD)/Electro Magnetic Transients including DC (EMTDC) software package, as it is commonly used for transient overvoltage study. In order to evaluate performance of the proposed controlled switching target, a simulation study has been carried out. At this point, different power system parameters such as fault type, fault inception angel, fault distance, compensation level, load angel, and fault duration are varied to generate large numbers of cases. Further, the proposed technique has been tested considering effect of MOT scatter of the CB and Short Circuit Current Level (SCCL) of the source. Considering all above cases, the suggested technique is able to limit the level of switching surge up to 1.9 p.u.

and hence, can be easily adopted by utilities. At last, comparative evaluation of the proposed scheme with the existing scheme clearly indicates its superiority in terms of reduction in the level of the switching surge for fully and partially discharged SCTL.

Similarly, controlled switching targets for energization of fully and partly discharged SCTL have been obtained using analysis of line side voltages. In order to determine optimal controlled switching target, Discrete Fourier Transform (DFT) of the line side voltages has been performed. It has been observed that the derived optimal controlled switching target is repetitive in nature. The simulation model has been developed in PSCAD/EMTDC software package environment considering an existing 400 kV Indian power transmission network. In order to test wide range applicability of the proposed technique, a simulation study of energization of a partially discharged SCTL has been performed. Variation in fault type, load angel, fault duration, compensation level, and distance of fault have generated large numbers of simulation cases. The proposed technique has also been evaluated considering impact of Switching Arrestor (SA), effect of MOT scatter of the CB, and different SCCL of the sources. It has been observed that the proposed technique is capable to maintain the level of switching surge below 1.5 p.u. At the end, comparison of the proposed scheme with the existing scheme proves the supremacy of the proposed scheme.

The presented work has been further extended to identify controlled switching target for Single Phase Auto Reclosing (SPAR) for SCTL, which has been determined using line side voltages. In order to assess the performance of the proposed technique, a simulation study has been carried out. Large numbers of simulation cases have been generated by varying power system parameters such as fault duration, load angel, instant of fault inception, fault distance, and compensation level. The modeling of an existing 400 kV power transmission network has been carried out in PSCAD/EMTDC software package. Further, the performance of the proposed technique has been verified considering effect of MOT scatter of the CB and different SCCL of the grid sources. Unlike the existing technique, the proposed technique is able to restrict the level of switching surge up to 1.5 p.u.

Shunt reactors are widely used in power system network at 400 kV and above level. They are switched ON and OFF multiple times in a day for reactive power management. Uncontrolled energization of the shunt reactor draws high charging current from the supply, which creates high thermal stress in the winding of the shunt reactor. As this charging current contains asymmetric dc component it takes a very long time to decay. At the same time, presence of asymmetric dc component in the charging current may saturate the instrument transformers due to which the protective device may maloperate. Based on analytical analysis, optimal controlled

switching targets have been determined during energization of the shunt reactor. The simulation model has been developed in PSCAD/EMTDC software package. The proposed technique has been tested considering different connection configurations of the shunt reactor. Moreover, the effect of MOT scatter of the CB is also analyzed. The proposed technique has also been implemented in real field and the results are discussed thoroughly. It has been observed that the proposed technique is able to limit the level of charging current up to 1.1 p.u., which authenticates its wide range of applicability.

Occasional switching of power transformers is converted in to frequent switching due to penetration of more and more renewable energy sources because of deregulation of power system network. Uncontrolled energization of power transformer draws very high level of inrush current from the source. This inrush current contains asymmetric dc component and different harmonics component, which degrades power quality and may develop severe thermal stresses in the winding of the transformer. At the same time, it also creates Transient Voltage Dip (TVD) for the equipment connected with the same line. The level of inrush current depends on winding resistance, residual magnetic field, and instant of switching. In order to limit the level of inrush current during controlled energization of a power transformer, it is essential to minimize the effect of MOT scatter of the CB. In the presented work, a detailed study of the parameters, which are responsible for the MOT scatter of the CB, has been carried out. Further, the behaviour of the dynamic fluxes is also investigated, as it is entirely different for electrically and magnetically coupled power transformers. The performance of the proposed technique has been evaluated by modeling two different types of power transformers (electrically and magnetically coupled) in PSCAD/EMTDC environment. In order to validate the simulation model, field testing for implementation of the proposed technique for electrically (1500 MVA, 765 kV) and magnetically (500 MVA, 400 kV) coupled power transformers have been performed. It has been observed that the proposed technique effectively limits the level of inrush within 1.0 p.u. At the end, comparison of the proposed scheme with the existing scheme proves the supremacy of the proposed technique in terms of reduction of the level of inrush current.

The presented work is likely to contribute significantly to the area of controlled switching applications for transmission lines and different power apparatus. The different techniques developed will be particularly useful for shunt compensated transmission line, shunt reactor, and power transformer. Some suggestions, based on observations and simulations in this area, are proposed at the end of the thesis for the benefit of potential researchers.

Contents

List of Abbreviations

Acronym	Full name
ADC	: Analog to Digital Converter
CB	: Circuit Breaker
CS	: Controlled Switching
CSD	: Controlled Switching Device
CT	: Current Transformer
DERs	: Distributed Energy Resources
DFT	: Discrete Fourier Transform
DL Fault	: Line-to-Line Fault
DLG Fault	: Double-line-to-Ground Fault
DR	: Disturbance Recorder
EHV	: Extra High Voltage
EIT	: Electrical Insertion Time
EMTDC	: Electro Magnetic Transients including DC
FACTS	: Flexible Alternating Current Transmission Systems
GOOSE	: Generic Object Oriented Substation Events
HTTP	: Hyper Text Transfer Protocol
HV	: High Voltage
IED	: Intelligent Electronic Device
KVL	: Kirchhoff's Voltage Law
LHMI	: Local Human Machine Interference
MIT	: Mechanical Insertion Time
MOT	: Mechanical Operating Time
N_{cycles}	: Numbers of half cycles
OHB	: One-and-Half-Breaker scheme
PCT	: Primary Current Transient
PIR	: Pre-Insertion Resistor
PIR-CB	: Circuit Breaker Having Pre-Insertion Resistor
POW	: Point On Wave
PSCAD	: Power System Computer Aided Design
PT	: Potential Transformer
R	: Value of Pre-Insertion Resistor
R_C	: Core loss component of winding
RDDS	: Rate of Decay of Dielectric Strength
RRDS	: Rate of Rise of Dielectric Strength
SA	: Switching Arrester
SCADA	: Supervisory Control And Data Acquisition
SCCL	: Short Circuit Current Level
SCT	: Secondary Current Transient
SCTL	: Shunt Compensated Transmission Line
SF6	: Sulphur Hexafluoride
SIR	: Source to line Impedance Ratio
SLG Fault	: Single-line-to-Ground Fault
SPAR	: Single Phase Auto Recloser
T_{AR}	: Arcing time period of circuit breaker
T_{close}	: Mechanical closing time of the circuit breaker
T_D	: Total time delay introduced for controlled switching operation
T_{elect}	: Electrical closing time of the circuit breaker

Tin	: Insertion instant of PIR
T_L	: Lingering time delay introduced by controller
TL Fault	: Triple-Line-to-Line Fault
TLG Fault	: Triple-Line-to-Ground Fault
t_m	: Mechanical closing instant of the circuit breaker
TOV	: Transient Over Voltage
T_{pre}	: Time duration for pre-strike
t_r	: Instant of random switching command of the circuit breaker
Tr	: Removal instant of PIR
t_{sep}	: Instant of contact separation of circuit breaker
TVD	: Transient Voltage Dip
T_{wt}	: Waiting time interval
UCTL	: Un-Compensated Transmission Line
UHV	: Ultra High Voltage
V_{GAP}	: Gap voltage across circuit breaker contacts
V_L	: Line side voltage
V_{L2H}	: Second harmonic component of line side voltage
Y	: Ungrounded star configuration
Yg	: Grounded star configuration
Δ	: Delta Configuration
Z_C	: Characteristics impedance of transmission line

List of Tables

List of Figures

Chapter 1
Introduction

1.1 General Background

Utilities across the globe are trying to find the most economical way to transfer the electrical power to the users. Right from the inception of the interconnected power system, overhead transmission lines are used to transmit the bulk amount of power over a long distance. This is achieved by transmitting the power at High Voltage (HV), Extra High Voltage (EHV) and Ultra High Voltage (UHV) levels through a transmission line from the source end to user end. In order to improve efficiency and performance of power transfer, various power apparatus such as power transformers, reactors, and capacitors are used. Moreover, situations in power network such as load shedding or fault conditions cause repetitive switching of power apparatus. At EHV and UHV levels, random switching of transmission lines and power apparatus creates severe switching transients, which leads to reduction in performance, efficiency, reliability, and stability of the power system network [1], [2]. In the worst case, it may result in insulation breakdown. In order to maintain the reliability and economic power transfer from one end to another end, it is required to energize/re-energize the transmission line and power apparatus. Similarly, in case of abnormal/emergency conditions, de-energization of transmission line and power apparatus is also indispensable.

1.1.1 Energization/re-energization of power apparatus

The process of connecting electrical power apparatus with the source is called as energization/re-energization of the power apparatus. It has been observed that during energization of the power apparatus installed at EHV and UHV levels, it is required to handle a large amount of electrical energy. Therefore, in order to energize/re-energize the power apparatus, a special switching device is required, which can handle such a large amount of electrical energy in a controllable manner. Since the inception of power transmission, Circuit Breakers (CBs) have been used for such applications at HV/EHV/UHV levels. However, CB is a mechanical device in which electrical closing occurs prior to mechanical closing in the form of electric arc during energization of a power apparatus. The closing of the CB occurs on a random basis, which creates severe switching transients [3], [4]. These high switching transients may affect efficiency and reliability of the power system. This kind of switching is known as uncontrolled switching. Therefore, a specific technique/device is required to mitigate switching transient during energization/re-energization by controlling closing point on wave of a power

apparatus, which is known as Controlled Switching (CS).

1.1.2 De-energization of power apparatus

The process of disconnecting the power apparatus from the supply source is known as de-energization. During de-energization, it is critical to handle the large amount of energy released due to the separation of contacts of the CB. In case of faulted condition, scheduled opening, and emergency conditions, it is required to de-energize a power system network either fully or partly. However, improper de-energization of power apparatus may create severe switching transients. These switching transients further leads to restriking in the CB. In worst case, repetitive restrike events lead to failure of the CB [5].

1.1.3 Overview of past/existing techniques

In the past, simple CBs have been used for energization, re-energization, and de-energization of the transmission lines and power apparatus. Thereafter, switching of transmission line is carried out by Pre-Insertion Resistor (PIR) along with Switching Arrestor (SA) to minimize the level of switching overvoltages [6]–[14]. Though, PIR reduces the level of switching transients up to certain limit, space requirement and mechanical linkages of PIR with CB are the issues, which restrict its usage. Afterwards, a state of the art technology (known as CS) has been developed, which ensures cost-effectiveness and safety and also improves the reliability of a system. It is termed as predefined switching strategies for closing and/or opening of each independent circuit breaker pole (staggered pole) in an effective way to minimize the switching overvoltages, equipment failures, and enhance power quality [3], [4], [15]–[17]. In addition, the dielectric and thermal performance of power system components are also improved [15], [16], [18], [19]. In controlled switching, the electrical closing/opening instants of the CB are defined as closing/opening targets. Basically, energization of power apparatus is carried out in two ways, namely, (i) uncontrolled (random) switching and (ii) controlled switching.

1.2 Uncontrolled switching

Switching of power apparatus at any random instant is known as uncontrolled switching. Uncontrolled switching causes a steep change in voltage and current of the network [20]. Uncontrolled switching of the transmission lines and other power apparatus causes severe switching transients in the power system network. The effects of uncontrolled switching of transmission line and different power system apparatus are elaborated in the following subsections.

1.2.1 Uncontrolled switching of the transmission lines

Energization and re-energization (i.e. closing and reclosing) of the transmission line during terminal fault and out of phase conditions, may develop severe switching transients. It also reduces the life of power components and SAs [7]. In case of transmission lines, following situations are responsible for development of switching transients in the power network [21].

(i) Energization of fully discharged transmission lines.

(ii) Energization of partially discharged transmission lines (Auto reclosing operation).

(iii) Energization of transmission lines during out of phase conditions.

(iv) Energization/re-energization of transmission lines on the terminal fault condition.

Energization of fully discharged transmission line is as good as energization of newly installed transmission line. In this case, there is no trapped charge on the transmission line. Therefore, the value of line voltage (V_L) is zero. Based on published literature, it has been reported that the level of the switching surge developed, during switching of the transmission line, is proportional to the level of voltage across the contacts of CB (V_{GAP}) at the closing instant [22], [23]. The V_{GAP} is the difference between the source side and line side voltages. Here, due to the absence of V_L, the magnitude of V_{GAP} is proportional to local end supply side voltages (V_S). The V_{GAP} will attain a maximum value, if the closing of the CB will be performed at the peak of the supply voltage. This will cause severe switching surge at the remote end of the line.

In the second case, energization of a partially discharged line is similar to reclosing of the transmission line. In this case, the trapped charges remain present on the line and V_L attains non-zero value along with polarity. Therefore, it is required to monitor the value and polarity of the V_L continuously. In out of phase condition, the polarity of supply side and line side voltages are opposite to each other at the time of energization (case-3). Hence, the V_{GAP} attains very high value. Subsequently, it creates severe switching surge and multiple strikes (overvoltages) on the terminals of SA [8]. In worst cases, these multiple strikes may damage the SA [9], [24]. Similarly, in case of energization/re-energization of the transmission line at terminal fault, a large amount of current is drawn from the supply, which develops high thermal stresses on the contacts of the CB as well as on other power components connected with the same line.

In order to identify the severe effect of uncontrolled switching of transmission line, a simulation study has been carried out. In this study, energization of partially discharged 200-km long Un-Compensated Transmission Line (UCTL) has been carried out considering the out of

phase condition and Fig. 1.1 shows the simulation results. It has been observed from Fig. 1.1 that the maximum level of switching surge generated at the remote end (load end) of the line is of the order of 2.59 p.u. This high level of switching surge may damage the power system equipment connected to the same line [25].

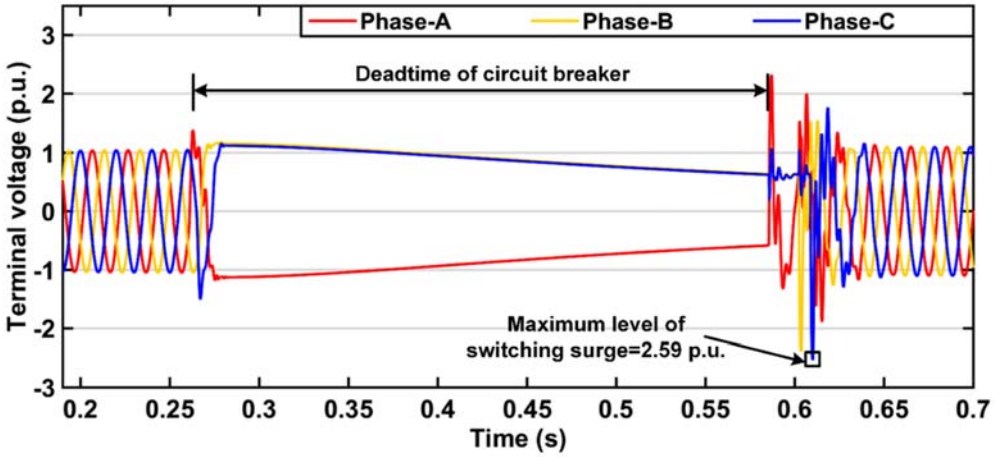

Fig. 1.1 Level of switching surge during uncontrolled reclosing of the UCTL.

Recently, in order to improve the performance and efficiency of the power system, different types of configurations of transmission lines such as shunt reactor compensated, series capacitor compensated, and shunt & series compensated are used. Sometimes, these configurations may contain Flexible Alternating Current Transmission Systems (FACTS) devices [26]–[30]. Incorporation of different private power producers increases the complexity of the power system [31]. Due to this, the possibility of variation in the voltage and frequency of the supply increases [32]–[34]. This motivates researchers to identify new techniques to minimize the level of the switching transients during controlled energization, re-energization, and de-energization targets for above-mentioned configurations of the line. Moreover, in order to identify optimal controlled switching targets for the aforementioned configurations, it is important to conduct an in-depth study of V_{GAP} and V_L.

1.2.2 Uncontrolled switching of a shunt reactor

Shunt reactors are widely used at EHV and UHV levels for reactive power management and maintaining a flat voltage profile [35], [36]. The shunt reactor is a gapped core type power apparatus [5]. The variation in core length controls the amount of reactance offered by the reactor. However, the main application of shunt reactor is to maintain a flat voltage profile by controlling the flow of reactive power. This is achieved by switching ON the reactor during light load conditions and switching OFF in case of peak load conditions [36]. In addition, it also limits

the level of switching overvoltage for the long transmission lines [37]. However, uncontrolled energization of a shunt reactor at 765 kV and 400 kV draws high charging current from the source [38], which contains decaying asymmetric dc component. The asymmetric dc component not only takes a long time to decay but also saturates the magnetic cores of the Current Transformer (CT) and Potential Transformer (PT) [39], [40]. Due to this, the measurement error has been introduced in the instrument transformers, which in turn causes malopeartion of differential/earth fault relay [37], [41]. Inadvertent tripping of the relay enhences the chances of restriking of an arc due lower magnitude of current flowing through the CB compared to higher magnitude of fault current. In worst case, it may cause severe thermal and dielectric stresses on inter-winding insulation of the shunt reactor [5], [36], [42]. In order to observe the effect of uncontrolled energization of a shunt reactor, the simulation study has been carried out. In this study, energization of a shunt reactor has been performed at supply voltage zero. Fig. 1.2 shows the simulation results in terms of level of asymmetrical charging current flowing through the shunt reactor.

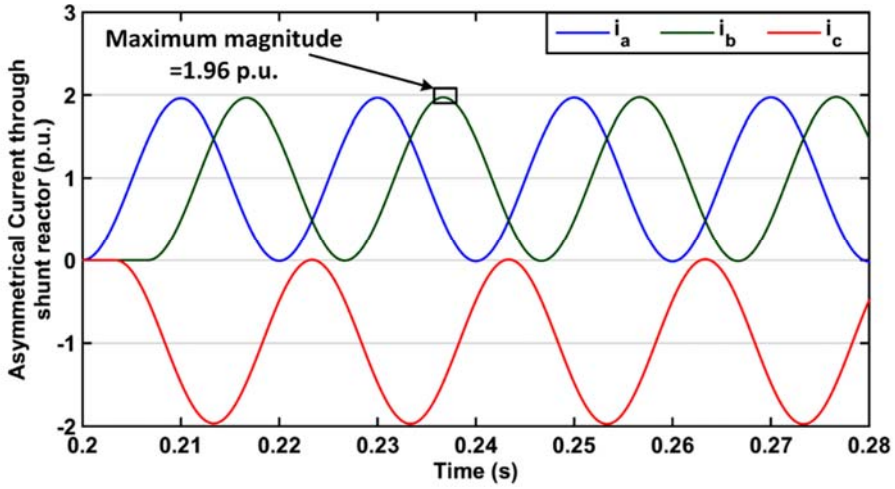

Fig. 1.2 Level of asymmetric charging currents during uncontrolled energization of shunt reactor.

It has been observed from Fig. 1.2 that the maximum level of asymmetric charging current is of the order of 1.96 p.u. To limit the level of asymmetric charging current, PIR-CB was used during energization of a shunt reactor. However, energy dissipation in PIR due to repetitive energization is the prime limitation of its usage [5], [43], [44].

1.2.3 Uncontrolled switching of a power transformer

Conventionally, the switching of power transformer has been performed infrequently.

However, restructuring of power system leads to incorporation of Distributed Energy Resources (DERs), which are usually renewable in nature. Due to intermittency of renewable energy sources (solar and wind), switching of power transformer is carried out on a frequent basis [45]–[48]. Malopeartion of cyber sensors also enhances the frequency of switching of power transformer [49]. Uncontrolled energization of power transformer draws large amount of inrush current from the supply, which causes loss of life of transformer and malopeartion of differential relay [48], [49], [50]–[57]. In order to notice the effect of uncontrolled energization of an unloaded power transformer, a simulation study has been carried out. Fig. 1.3 shows the simulation results in terms of inrush current during uncontrolled energization of a power transformer. It has been observed from Fig. 1.3 that the maximum level of inrush current is of the order of 7.22 p.u.

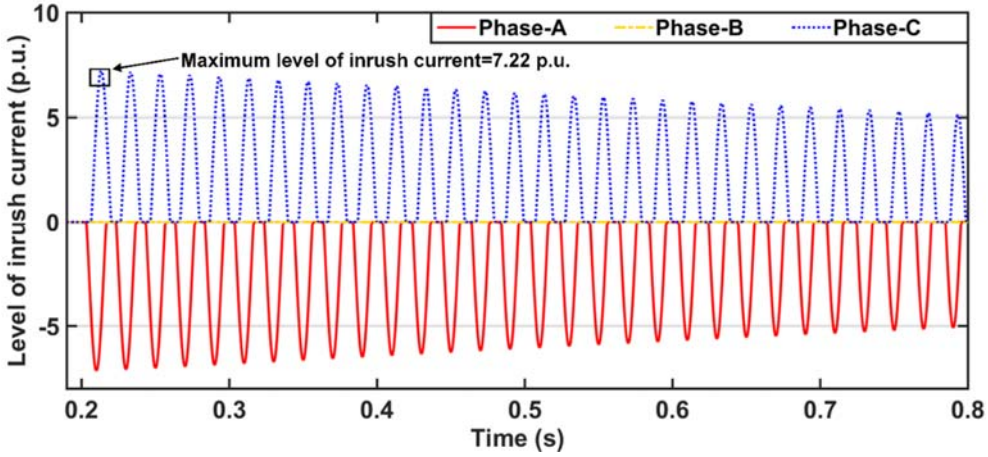

Fig. 1.3 Level of inrush currents during uncontrolled energization of a power transformer.

The level of inrush current during uncontrolled energization depends on parameters such as level of residual flux in the core, winding resistance, magnetizing characteristic of the core, and phase angle of the supply voltage at the closing instant [61]. It has been mentioned in past published literature that high level of inrush current causes Transient Voltage Dip (TVD) in the network [47]. The magnitude of this TVD depends on Short Circuit Current Level (SCCL) of the source [47]. Utilization of philosophy of CS for power transformer helps in minimizing the level of inrush current during energization of a transformer. However, it is difficult to attain an optimal controlled energization target due to the effect of MOT scatter of the CB [58], [62].

1.2.4 Uncontrolled switching of a shunt capacitor

Shunt capacitors are used to counterbalance the effect of lagging reactive power of the power system network. However, they draw high charging current during uncontrolled

energization. In order to identify uncontrolled energization of a shut capacitor, a simulation study has been carried out. In this study, shunt capacitor has been energized on random basis. Fig. 1.4 shows the simulation results in terms of level of charging current during uncontrolled energization of a shunt capacitor.

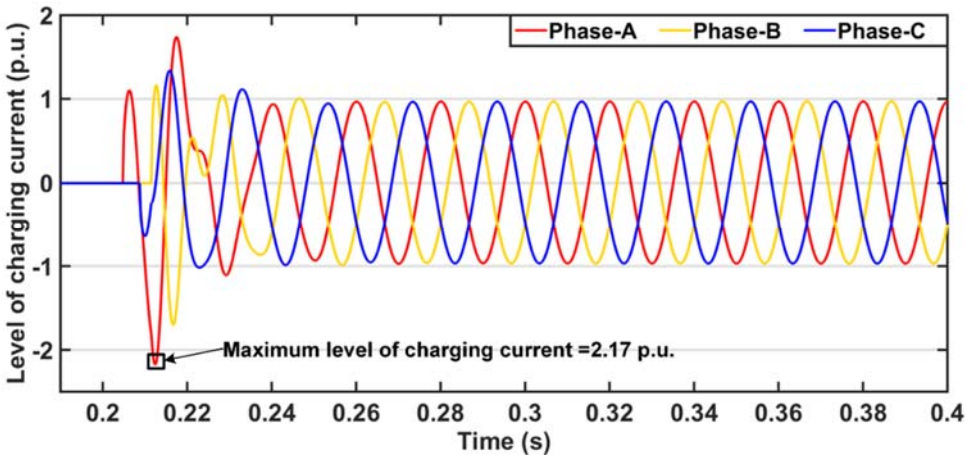

Fig. 1.4 Level of charging currents during uncontrolled energization of a shunt capacitor.

It has been observed from Fig. 1.4 that the maximum level of charging current is of the order of 2.17 p.u. Occasionally, this uncontrolled energization also generates overvoltage at the load terminals [4], [63]. These switching transients degrade the power quality of the supply and loss of life of power apparatus connected to the same line [64].

1.2.5 Disadvantages of an uncontrolled switching

The major disadvantages of an uncontrolled switching of the transmission lines and different power system apparatus are as follows.

1.2.5.1 Malopeartion of the protective device

The uncontrolled switching of transmission lines and power apparatus cause switching transients [1]. These switching transients attain high level of voltage/current compared to its rated value, which in turn may cause malopeartion of the protection relay [65]–[68]. In case of uncontrolled energization of a shunt reactor, capacitor bank, and power transformer, very high level of inrush current is drawn from the supply. This inrush current is asymmetric in nature due to which there is a possibility of malopearation of the protective device [37]. Due to such mal-opearation, the reliability and stability of the system may decrease [69]. Moreover, inclusion of FACTS devices also creates chaos in the dynamic stability of the power system network [70], [71].

1.2.5.2 Power quality issue

Nowadays, it is required to supply electrical power to the user without violating the pre-specified limits of power quality. In case of violation in the pre-specified limit of power quality, the penalty will be imposed on the utility by power system authority [47], [57]. In this context, the uncontrolled switching of power apparatus generates severe switching transients. Due to the asymmetric nature of switching transients, power quality issues such as TVD, harmonics, dc offset, and power frequency variations are developed [54]. These can degrade the power quality of the supply.

1.2.5.3 Loss of life of power apparatus

The switching transients during uncontrolled energization of the transmission line and power apparatus cause severe thermal and dielectric stresses, which in turn creates an adverse effect on the windings and the life expectancy of the power apparatus [65]. In the worst case, it may cause an inter-turn fault or external flashover. Further, switching transients such as high inrush current and voltage surge increase contact pitting of the CB, which reduces the life of CB [69]. The growth and complexity of the power system network enhance due to involvement of renewable energy sources. This further increases the frequency of switching of power apparatus such as CB and power transformer [52], [72]. In this case, uncontrolled switching will further reduce the life of the power apparatus.

1.2.5.4 Economy and safety issues

As mentioned earlier, due to switching transients, the life of the power system apparatus reduces. On contrary, the other solution is upgradation of the level of insulation of the power apparatus, which is extravagant. The possibilities of occurrence of an accident will also increase due to the loss of life of power apparatus. Hence, both economy and safety are compromised. In addition, these switching transients may cause disturbance in telecommunication and control systems.

1.3 Controlled switching

It has been observed that during uncontrolled operation of the CB, high level of switching transients such as high magnetic inrush or severe switching voltage surge creates problem to all power system apparatus. They produce a variety of dielectric and thermal stresses on power system auxiliaries, which in turn damages the power system equipment immediately or gradually [16], [17], [23]. As mentioned earlier, conventional CBs use either PIR or damping reactors along with SA to limit the switching transients [6], [8]. On the other hand, upgradation of

insulation class of equipment is another option to withstand the switching transients. But it is costly and unreliable as the magnitude of transients depends on Point On Wave (POW) switching [4]. In the last decade, a POW switching concept has been introduced for the reduction of the level of the switching transients. This is commonly known as Controlled Switching (CS) or synchronous switching. The controlled switching is a strategy that controls the POW switching to minimize the level of the switching transient. The CS technology uses micro-controller to control the opening and closing instant of the independent pole of the CB with respect to the phase angle of either current or voltage signal [65]. In other words, it is a strategy, which optimizes the opening/closing instant of CB to minimize the switching transients and failures of power apparatus [4], [73]. However, the required accuracy and precision to attain the target of specific POW switching are within the range of ± 1 ms or even less [4], [62]. In order to perform successful application of controlled switching in real field, it is required to achieve the CS targets for closing or opening of CB accurately. Hence, the following conditions must be satisfied.

(i) The controlled closing/opening targets must be determined prior to actual operation.

(ii) The controlled switching targets must be repetitive in nature.

(iii) Variation in the operating time of the CB due to the statistical and systematic variation of the CB must be counterbalanced [74], [75].

The phenomena of controlled closing and opening are explained below.

1.3.1 Controlled closing of CB

Controlled closing is the strategy for controlling the closing instant of each pole of the CB with respect to the phase angle of the voltage. In such case, the controller has to monitor the voltage across the contacts of CB and compare it with the reference voltage signal. Fig. 1.5 shows the waveform of V_{GAP} during operation of CB. As shown in Fig. 1.5, t_r is the instant of random CB closing command, T_D is the total time delay, T_L is the deliberate lingering time delay introduced by the controller, T_{wt} is the waiting-time interval, T_{pre} is the time duration for pre-striking, T_{close} is the mechanical closing time duration of CB, T_{elect} is the electrical operating time of CB, t_e is the electrical closing instant of CB, and t_m is the instant of mechanical closing of CB. Here, the closing operation has been controlled by the controller in such a way that electrical closing of the CB occurs at zero crossing instant of the V_{GAP}. Therefore, T_{pre} should be minimum. At the same time, it is further noticed from Fig. 1.5 that at an instant of t_r, the random closing command of CB is issued either by Supervisory Control and Data Acquisition (SCADA) or manual mode.

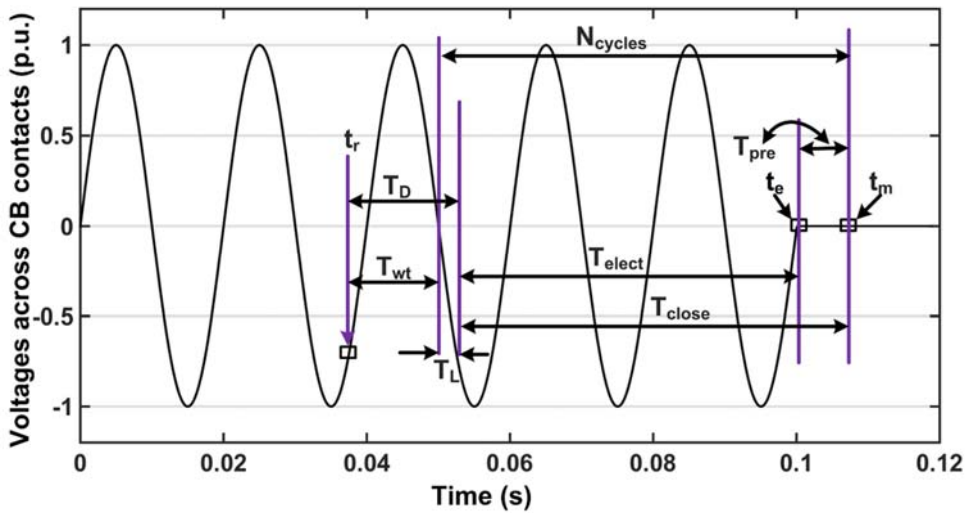

Fig. 1.5 Sequence of controlled closing.

This randomly generated command has been converted to controlled closing command with the help of controller. As soon as the random closing command has been raised, the controller tries to identify the zero crossing instant of V_{GAP} by collecting data from actual field. T_{wt} is the time taken by the controller to collect data from the field. Afterwards, based on this data, T_L has been calculated. In order to convert this randomly raised closing command to controlled closing command, the controller introduces time delay (T_D), which is an addition of T_{wt} and T_L. Subsequently, the electrical closing of the CB occurs precisely at t_e instant, which is an optimal controlled closing instant of CB. It is to be noted that for successful implementation of controlled closing operation, T_{close} must be known in advance. It is the time from the activation of the closing coil to the instant at which the contacts of CB physically touch. Similarly, the time from closing coil activation to the prestrike instant is known as electrical operating time (T_{elect}) [4]. It is also controlled by controller to obtain minimum prestriking time. Furthermore, N_{cycles} indicates the numbers of half cycles required to attain the controlled closing target.

1.3.2 Controlled opening of CB

The controlled opening is defined as controlling the instant of contact separation of each pole of CB with respect to the phase angle of reference signal. This ensures the least possible arcing time for the contacts of CB. In addition, it leads to prevention of failure of CB. The optimal opening is performed when the current flowing through the breaker becomes zero. Moreover, the same task can be performed by using a bus voltage as a reference signal. In such cases, the phase displacement between voltage and current must be known priory. As the contacts separate out, it will lead to the formation of an arc. This arc must be extinguished within a half-cycle time. In case of CB, the rate of rise of dielectric strength plays vital role for arc

extinguishing. The level of dielectric strength of CB ensures the capability of CB to withstand the recovery voltage at a particular instant. Hence, whenever the level of dielectric strength is higher than recovery voltage, CB does not encounter a reignition or restrike. Though, reignition and restrike seem to be the same kind of event, the difference between them is as follows [4], [23].

- Reignition means a dielectric breakdown that restores current within ¼th of the cycle time.
- Restrike is defined as dielectric breakdown beyond ¼th of the cycle.

Fig. 1.6 shows waveform of current during controlled opening of the CB. It has been observed from Fig. 1.6 that T_{AR} is an arcing time duration and t_{sep} is an instant of contact separation of the CB. Here, the opening operation has been controlled in such a way that contact separation occurs precisely at zero crossing of the current through the CB. Therefore, the arcing time can be minimized.

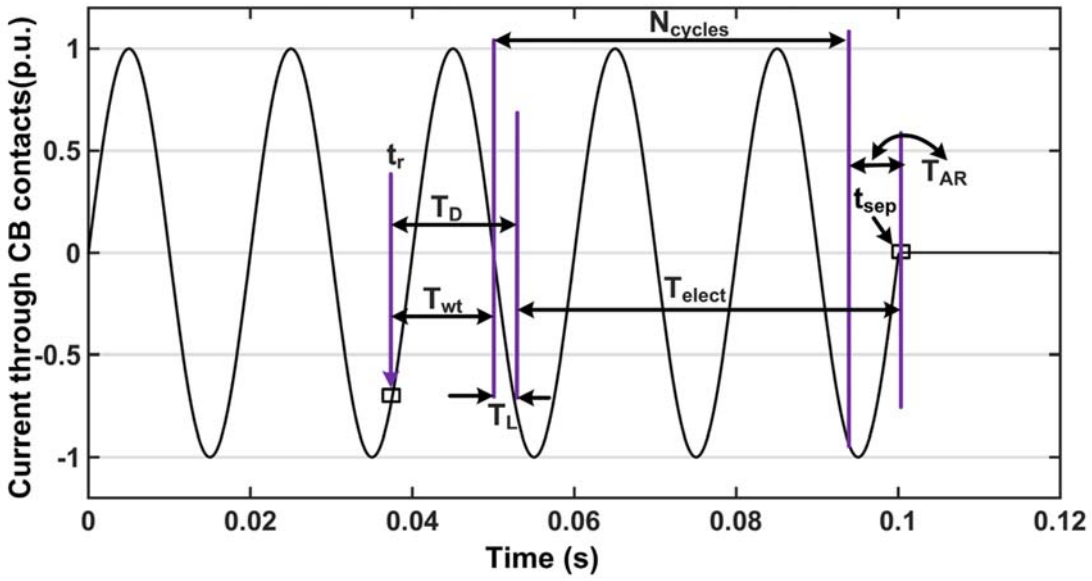

Fig. 1.6 Sequence of controlled opening.

At the same time, it has been further observed from Fig. 1.6 that the opening command initiated haphazardly with respect to the reference signal at t_r instant. The controller postpones the opening command by 'T_D' seconds, which is the addition of T_L and T_{wt}. The controller utilizes the waiting time (T_{wt}) to judge the next current zero instant from the real field. T_L is a function of the opening time and it determines the appropriate time of zero crossing instant of the current through the CB, which is an optimal controlled opening target. T_{elect} is the time defined by the electrical opening time duration from activation of the trip coil to the starting

instant of contact separation of the CB. However, T_{AR} is defined as the arcing time of contact separation till current interruption occurs at natural current zero[4], [74], [75].Here, the number of half cycles used to attain the optimal target is indicated by N_{cycles}.

1.3.3 Controlled switching device

In order to convert the random opening/closing command of the CB to controlled opening/closing command, it is essential to attach an additional device, which works along with CB. This device is known as Controlled Switching Device (CSD). It contains controller, which is the heart of the CSD. It has been observed from Fig. 1.5 and Fig. 1.6 that for successful implementation of a controlled switching strategy, acquisition of the signals from the power system network is required. Subsequently, these signals are further utilized by CSD for controlled switching targets. Fig. 1.7 shows the block diagram of CSD.

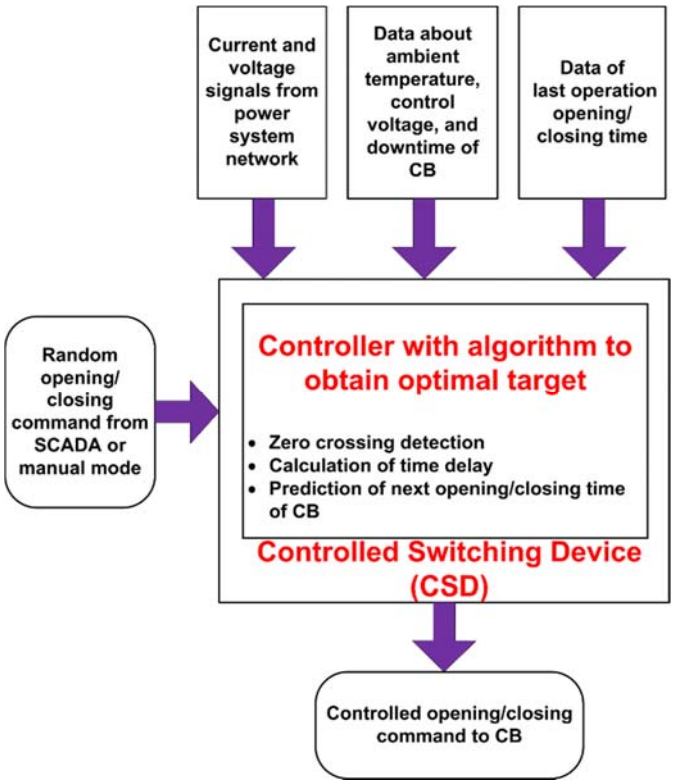

Fig. 1.7 Block diagram of controlled switching device.

As shown in Fig. 1.7, the controller collects current and voltage signals from the power system network, ambient temperature, control voltage, down time, and last operating time of the CB. The main task of CSD is to calculate the required time delay that depends on different parameters such as ambient temperature, control voltage, and downtime of the CB. Further, in order to predict the next opening/closing instant (target), it is required to consider the last operation (opening or closing) time of the CB. Therefore, based on the analysis of the aforementioned

data, the controller has to perform following tasks.

- Detection of zero crossing of voltage and current signals.
- Calculation of time delay.
- Prediction of the next opening/closing time of the CB.

Thereafter, the controller issues controlled opening/closing command to the CB [74]. It is to be noted that the controlled switching targets must be predicted/determined prior to actual operation. In addition, it is preferred that the controlled switching targets must have a repetitive pattern.

1.3.4 Advantages of controlled switching

The benefits of controlled switching are as follows.

- It reduces the switching transients of the power system during normal and faulted conditions.
- It improves the power quality of the electrical supply system.
- It reduces pitting of CB contacts, improves performance of CB, and enhances the lifespan of CB.
- It boosts the lifespan of power system components by reducing the risk of failure due to transients.
- The controlled switching relay offers retrofit feature. Hence, it can be easily accommodated in the existing CBs [3], [74].

1.4 Historical development of controlled switching techniques

The historical development of controlled switching techniques for transmission lines and other power apparatus is explained below.

1.4.1 Transmission lines

In case the transmission lines having Source to line Impedance Ratio (SIR) less than 0.5 at EHV and UHV level, the switching surge has gained more importance than lightening surge [35]. Uncontrolled energization of transmission line without SA may develop switching surge up to 3 p.u. [6], [22]. This may lead to a reduction in the lifespan of the equipment connected with the same line. In the worst case, it may result in flashover of line or insulation failure of the equipment. In order to mitigate the switching overvoltages, the conventional CBs are provided

with PIR. In this case, the switching surge is minimized by inserting PIR in the circuit for few milliseconds at the time of energization of the line. However, the sudden insertion and removal of PIR causes two types of surges, known as

(i) Primary surge: It is defined as the level of switching surge generated due to insertion of PIR in the circuit.

(ii) Secondary surge: It is defined as the level of switching surge generated due to the removal of PIR from the circuit.

Generally, both of these surges are known as switching surges [1]. The magnitude of switching surge depends on insertion instant, Mechanical Insertion Instant (MIT), Electrical Insertion Instant (EIT), the value of PIR, and surge impedance of the line (Z_C) [8], [11], [12], [76], [77]. In the last decade, controlled switching becomes more popular compared to PIR for minimization of switching transients. This is achieved by precisely controlling the switching instant with reference to the V_{GAP} across the individual pole of the CB [8], [15]. In case of transmission line, zero crossing instant of V_{GAP} is considered as an optimal closing/reclosing target.

The main four conditions, which are responsible for the development of high level of switching surge have been explained in section 1.2.1. In this regard, energization of fully discharged line is as good as energization of line with zero trapped charges on it. Therefore, zero crossing instant of V_{GAP} occurs at zero crossing instant of supplyside voltage, which is the controlled closing target for the CB. In this case, the energization phase sequence is A-C-B. Considering phase-A as the reference, the controlled energization targets for phase A, C, and B is 0, $\pi/3$, and $2\pi/3$ radians, respectively. Similarly, the de-energization targets for phase A, C, and B is $\pi/2$, $5\pi/6$, and $7\pi/6$ radians, respectively [74]. Particularly, the application of controlled switching is difficult in case of energization of a partially discharged (i.e. auto reclosing) UCTL and Shunt Compensated Transmission Line (SCTL) compare to energization of fully discharged line. In this case, the line carries trapped charges. These trapped charges develop a voltage on the conductor of the line, which is equivalent to V_L. The V_L attains polarity and magnitude both during the dead time of CB. Whereas, in case of UCTL, the trapped charges attain unidirectional polarity and gradually reduce during the dead time of CB. Therefore, it is essential to analyze the polarity and nature of the trapped charges to obtain controlled reclosing targets [24], [69]. Heresh *et. al* [24] suggested a reclosing technique for UCTL considering controlled reclosing targets based on local end supply side voltages. However, the effect of operating time scatter of the CB has not been considered.

Nowadays, in order to counterbalance the effect of capacitive reactance of the long transmission lines, shunt reactors are located at both ends of the line. Such type of configuration of the line is known as shunt compensated transmission line. As reported in [69], [78], the nature of line voltage is oscillatory (bidirectional) during the dead time of CB. The single-line-diagram of SCTL and the line/source side voltages are shown in Fig. 1.8 (a) and (b), respectively, during the dead time of CB for SCTL. It has been observed from Fig. 1.8 (b) that the line side voltage is bidirectional and oscillating in nature whereas the supply side voltage remains pure sinusoidal in nature. Hence, it is difficult to predict the optimal reclosing target for SCTL. Furthermore, Fig. 1.8 (c) shows the variation in V_{GAP} during the dead time of the CB obtained from the abovementioned simulation study. It has been observed from Fig. 1.8 (c) that the position of the optimal controlled reclosing target (minima beat) occurs after random time intervals, which is non-repetitive in nature. However, based on the available literature, the controlled switching targets should be repetitive in nature. Therefore, it is necessary to identify reclosing targets other than V_{GAP}. Froehlich *et. al* [69], [78] proposed a controlled switching technique based on local end supply side voltages for closing/reclosing of SCTL. However, the aforementioned controlled strategy may generate a high level of switching surges during reclosing of SCTL particularly, when the effect of MOT scatter (± 1 ms) of the CB has been considered. Afterwards, Dantas *et. al* [79] suggested controlled reclosing scheme based on prediction of a zero crossing instant of V_{GAP} for SCTL. In this technique, the variation in operating conditions due to aging of CB contacts and ambient temperature are compensated using adaptive control method. Nevertheless, the accuracy of this technique depends on the correct identification of the type of fault. In case of inaccurate identification of fault type, this technique may develop high level of switching surge. Thereafter, Mestas *et. al* [80] proposed a controlled reclosing technique for SCTL based on envelop pattern of V_{GAP}. However, this technique is useful only in non-faulted situations. At the same time, it would not provide satisfactory results during low level of compensation. Recently, Luo *et. al* [81] and Dias *et. al* [82] presented different algorithms based on odd/even harmonic factor and line voltage harmonic content measurement of faulted phase, respectively. Though the above techniques are able to differentiate between temporary and permanent faults, delay of 20 ms is one of the drawbacks of the abovementioned schemes.

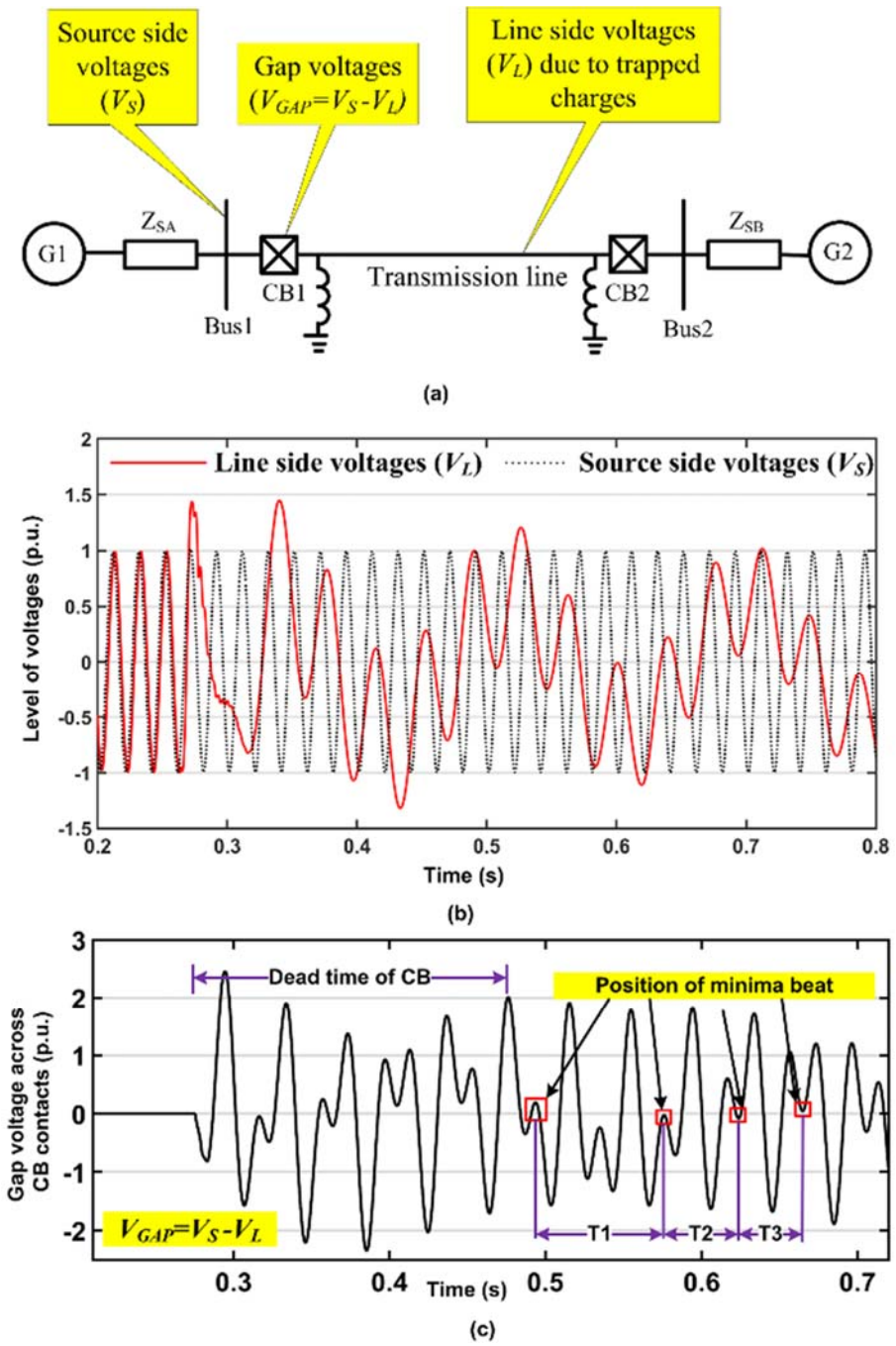

Fig. 1.8 (a) Single-line-diagram of SCTL, (b) line & source side voltages, and (c) V_{GAP} during dead time of the CB.

The above mentioned literature has focused only on three-phase controlled reclosing of SCTL. The literature based on application of controlled switching for Single Phase Auto Reclosing (SPAR) of SCTL is missing due to oscillatory nature of line side voltages during the dead time of CB.

1.4.2 Shunt reactors

In case of energization and de-energization of a shunt reactor, the main motive is to minimize the level of the asymmetric dc component of the charging current. In case of de-energization, controlled switching helps to provide restrike free operation of the CB. In this regard, various algorithms have been reported in the literature to mitigate the level of switching surge during energization/de-energization of the shunt reactor [4], [15], [65]. Table 1.1 shows the summary of controlled energization and de-energization targets for different configurations of the shunt reactor [4], [15], [65]. As depicted in Table 1.1, different configurations of shunt reactor such as Grounded Star (Yg), Non-grounded Star (Y), and Delta (Δ) have been considered for controlled energization and de-energization. Here, the sequence of controlled closing is determined considering anticlockwise phase sequence and gap voltage of phase-A as a reference phase. It has been reported in various literature that energization/de-energization of the shunt reactor is carried out at the peak of V_{GAP} [23], [38], [75]. In [38], controlled energization technique for variable shunt reactor has been proposed. In this methodology, detailed modelling of variable shunt reactor and CB (with two switching chambers) have been carried out considering different capacitor and variable reactor using PSCAD/EMTDC software package [83].

Table 1.1 Summary of controlled energization and de-energization targets for shunt reactor.

Sr. No	Power apparatus	Connection configuration	Phase-A	Phase-B	Phase-C
Controlled energization targets (radian)					
1	Shunt reactor	Yg	π/2	7× π/6	5× π/6
		Δ	π/3	π/3	5×π/6
		Y	π/3	π/3	5×π/6
Controlled de-energization targets (radian)					
2	Shunt reactor	Yg	π/2	7× π/6	5× π/6
		Δ	π/2	π	π
		Y	π/2	π	π

Here, the application of controlled switching during energization and de-energization of the shunt reactor has been performed, which limits the level of switching transients. On contrary, regression based controlled switching methodology for energization of a shunt reactor has been presented by Rajjotte and his co-workers [84]. In this methodology, opening/closing timings of CB is optimized using effective training and testing module. Recently, Lee *et. al* [85] presented a new controlled switching strategy for energization/de-energization of a shunt reactor based on maximum V_{GAP} and minimum arcing time, respectively. However, the effect of MOT scatter of the CB has not been considered in the said work.

1.4.3 Power transformer

Liberalization of the power system network brings many private players in the field with renewable sources. This results in frequent switching of the power transformer. However, random energization of power transformer under no-load condition draws a high amount of inrush current from the source [50], [51], [60]. Subsequently, this high inrush current creates thermal and dielectric stresses on the winding of the transformer and TVD at the load side terminals of the transformer. These stresses may create a turn-to-turn fault in the power transformer [86]. Based on the SCCL of the source, this TVD takes a long time to regain its rated value [59]. The generated inrush causes maloperation of the differential relay of the transformer. In order to avoid the false tripping due to transformer inrush current, researchers have proposed various algorithms based on heuristic search [56], [87]. Although heuristic search provides better accuracy, selection of parameter is not an easy task. Moreover, it is to be noted that the magnitude of inrush current depends on the resistance of the winding, level of residual flux, magnetization characteristic of the core, and phase angle of the applied voltage. In practice, three kinds of switching strategies as discussed below are used for mitigation of inrush current during controlled energization of an unloaded power transformer.

(i) In the first method, energization of an unloaded power transformer is carried out at gap voltage peak without considering the level of residual flux. However, this is a compromised solution.

(ii) The second strategy is to energize the transformer when the magnitude of the residual flux is same as the prospective flux. Here, the level of residual flux is estimated by integrating the load side voltage.

(iii) The recent practice in Asia Pacific region is to perform controlled de-energization before the controlled energization of a transformer. This controlled de-energization brings the lowest possible value of the residual flux.

Based on controlled strategy (i), Table 1.2 shows summary of controlled energization and de-energization targets for different configurations of the power transformer [4], [15], [65]. The sequence of controlled closing is determined considering anticlockwise phase sequence. Here, the gap voltage of phase-A is considered as a reference and the level of residual flux has been neglected. Moreover, methodologies that eliminate the effect of residual flux have been reported in literature [54] and [61]. In [54], the zero level of residual flux at core has been obtained using low voltage ultra-frequency source. The demagnetization of core has been achieved by increasing the frequency of reversal of the source. Similarly, in [61], demagnetizing

of transformer core has been attended by using low voltage dc source. However, both of these methodologies require detail study of the response of the inductor for a dc source [61].

Table 1.2 Summary of controlled energization and de-energization targets for different configurations of the power transformer.

Sr. No	Power apparatus	Connection configuration	Phase-A	Phase-B	Phase-C
Controlled energization targets (radian)					
1	Power transformer	Yg-Yg	π/2	7× π/6	5× π/6
		Yg-Δ	π/2	π	π
		Y-Δ	π/3	π/3	5× π/6
		Δ-Yg, Δ-Y, Δ-Δ	π/3	π/3	5× π/6
Controlled de-energization targets (radian)					
2	Power transformer	Yg-Yg	π/2	7× π/6	5× π/6
		Yg-Δ	π/2	π	2× π/3
		Y-Δ	π/2	π	π
		Δ-Yg, Δ-Y, Δ-Δ	π/2	π	π

Based on strategy (ii), controlled energization of the no-load transformer has been carried out after considering the level of residual field in the core of the transformer [50], [51]. In [50], the proposed technique works on core equalization principle, which suggests that the net sum of flux in the core is zero for three limb core where one of the windings is connected in delta configuration. Here, the level of residual flux in the core has been judged by integrating load side voltages. Further, after energization of the first phase, the dynamic residual flux in other two phases attain half of the value and in opposite direction with respect to first energized phase. Hence, these two phases are energized after one forth cycle time of the first phase. It is known as rapid energization strategy. However, this technique requires detailed information about complete transient behaviour of the particular transformer. In addition, error in the estimation of the level of residual flux may create high level of inrush during the energization of the power transformer. On contrary, in [51], delay closing technique has been proposed and the same has been tested considering parameters such as operating time scatter of the CB, prestrike of CB, and errors in the measurement of the residual flux. Though this technique produces good results, complete elimination of inrush current is not possible particularly for a transformer that has different configurations. Further, implementation of the proposed delay closing technique of the CB in real field is also a challenging task.

In case of controlled strategy (iii), the basic aim is to minimize the level of inrush current and subsequent TVD during no-load energization. In this case, it is ensured that built up rate of dielectric strength of CB during de-energization will not allow formation of restrike and the level of residual flux in the core is locked [58]. Here, controlled de-energization has been performed

prior to controlled energization [54]. This controlled de-energization locks the level of residual flux and brings it to the lowest possible level. However, it is required to memorize the last pole of the CB to be de-energized because the same should be closed first during next controlled energization of the power transformer.

1.4.4 Shunt capacitor

In actual power system, the shunt capacitor is used to improve voltage profile under full load condition. It neutralizes the effect of lagging reactive power due to line reactance. Further, the switching of capacitor banks is carried out automatically or manually based on full load and light load conditions. This requires frequent switching of shunt capacitors. The main aim is to minimize the level of switching transients during energization and de-energization of the capacitor bank. In this regard, the controlled opening and closing minimizes the level of switching transients such as inrush current and stresses due to overvoltage [4], [64], [88]. Table 1.3 shows summary of controlled energization and de-energization targets for different configurations of the shunt capacitor [4], [15], [65]. In this summary, different configurations such as Yg, Y, and Δ have been considered. Here, the sequence of controlled closing is determined considering anticlockwise phase sequence and gap voltage of phase-A as a reference.

Table 1.3 Controlled energization and de-energization targets for different configurations of the shunt capacitor.

Sr. No	Power apparatus	Connection configuration	Phase-A	Phase-B	Phase-C
Controlled energization targets (radian)					
1	Shunt capacitor	Yg	0	2× π/3	π/3
		Δ	π/6	2× π/3	π/6
		Y	π/6	2× π/3	π/6
Controlled de-energization targets (radian)					
2	Shunt capacitor	Yg	π/2	7× π/6	5× π/6
		Δ	π/2	π	π
		Y	π/2	π	π

In [64], the author has proposed controlled switching technique for shunt capacitor considering mechanical and operating time delay of CB. However, the mechanical operating time variations of the CB may cause high inrush current during energization of the shunt capacitor. In case of back to back charging of shunt capacitor bank, this may create false tripping in the network. At the same time, in [88], energization of a shunt capacitor has been proposed using pre-insertion inductor. Comparative evaluation between pre-insertion inductor with PIR has been carried out during energization of a shunt capacitor. This comparative evaluation suggests that though pre-insertion inductor is cost effective compared to PIR, the performance

of PIR in terms of minimization of the level of switching transient during energization of a shunt capacitor is better than pre-insertion inductor. Further, in both the aforementioned techniques, it is recommended to provide adaptive compensation to counterbalance the effect of operating time variations of the CB.

It has been observed from the literature survey that very less numbers of papers have been reported for controlled switching of a shunt capacitor. It is observed that network configuration and MOT variations of the CB play a vital role for the implementation of the CS. Here, there is a scope for development of controlled switching technique utilizing adaptive compensation to minimize the MOT variations of the CB.

1.5 Different factor affecting the performance of controlled switching

1.5.1 Impact of CB characteristic

In order to make the successful implementation of the CS for transmission lines and different power system apparatus, a CB plays an important role. The accuracy of controlled switching depends on variations in the MOT of the CB. Further, the permissible limit for the variation in MOT of the CB is decided by thermal and dielectric characteristics of CB. The consistent operating time of the CB is essential to achieve the exact optimal target [25], [74], [89]. Mainly, systematic and statistical variations cause inconsistent MOT of the CB [73]. Based on the criteria reported in [25], [74], and [89], the suitability of the CB for the application of controlled switching has been checked by performing some special type tests. However, inaccurate measurement of MOT variation of CB causes trouble in the implementation of controlled switching. Therefore, determination of the optimal targets for different configurations of the power apparatus and MOT scatter of the CB are still burning issues [74], [75].

1.5.2 Diversified targets for different load configurations

Table 1.1 to Table 1.3 show different controlled closing and controlled opening targets for transmission line and different power apparatus such as shunt reactor, power transformer, and shunt capacitor [4]. Due to wide variations in the behaviour of different power system apparatus, optimal targets may vary from zero to peak of the V_{GAP} [89]. At the same time, variations in MOT add further difficulty in the implementation of CS. In case of reclosing of compensated transmission line having different configurations, the analysis of line side voltages and V_{GAP} is of prime importance to determine the optimal controlled reclosing target.

1.5.3 One-and-half-breaker and non-switchable breaker schemes

In order to minimize the effect of statistical and systematic variations of the CB, utilization of a hybrid combination of PIR-CB and CSD has been suggested in the proposed

work. In Asia–Pacific region, most of the EHV and UHV substations are equipped with One-and-Half-Breaker (OHB) scheme [3], [73]. The single-line-diagram of OHB scheme and line with non-switchable reactor scheme are shown in Fig. 1.9 (a) and (b), respectively.

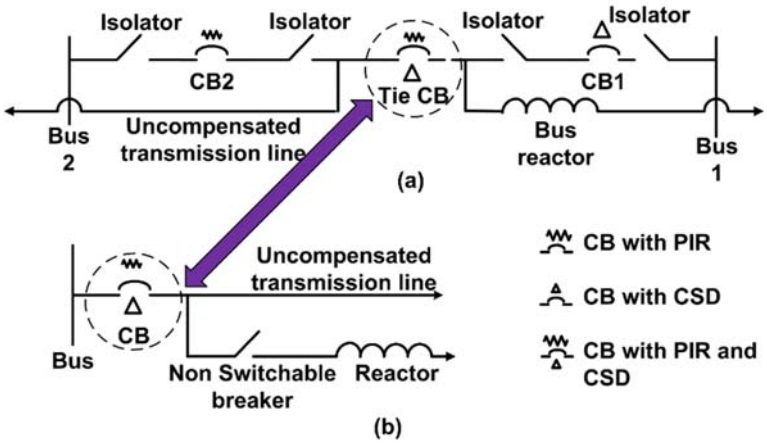

Fig. 1.9 Representation of (a) OHB scheme and (b) Non-switchable breaker scheme.

It has been observed from Fig. 1.9 (a) that three modes of operations are possible for OHB scheme, which are as given below.

(i) CS of bus reactor using CB with CSD located at Bus-1

(ii) PIR-CB (Bus-2) is used for the uncontrolled switching of the transmission lines

(iii) Tie-CB has both PIR-CB and CSD.

In the first case, CSD is used for controlled switching of bus reactor whereas PIR CB is used for uncontrolled switching of transmission line for the second case. In the third case, tie-CB provides flexibility such that the bus reactor is used as the line reactor and it converts the uncompensated line into shunt reactor compensated transmission line. Further, the tie-CB has a hybrid combination of CSD and PIR-CB in which PIR is used for switching of the transmission line and CSD has been utilized for switching of shunt reactor.

At tie-CB, the hybrid combination of PIR-CB with CSD is readily available in this scheme without any additional efforts [23]. Moreover, in the non-switchable breaker scheme, CB also contains this hybrid combination for the switching of either transmission line or shunt reactor. The details of PIR-CB have been discussed in the next section.

1.6 Concept of PIR

PIR consists of a resistor stack and two switches. Throughout the thesis, the full assembly together is termed as PIR. Depending upon the position of bypass switch with respect to main

contacts of CB (interrupter), two types of PIR configurations, namely series PIR and parallel PIR, are commonly used [7], [11], [13]. Fig. 1.10 (a) and (b) show both connection configurations of PIR. The series PIR configuration is usually employed due to low cost and less space requirement [7]. Nevertheless, the electrical behaviour of both configurations remains the same. It has been reported in the literature that the usage of PIR for suppression of switching overvoltage is presented in terms of Switching Suppress Factor (SSF), which is given by eq. (1.1) [1].

$$SSF = \left(Z_C \Big/ R + Z_C \right) \tag{1.1}$$

Where, R indicates the value of PIR and Z_C represents surge impedance of the transmission line. For series PIR configuration, the electrical making occurs primarily between interrupter followed by the contacts of PIR switch, which bypasses the resistor after MIT is over. Subsequently, EIT is defined as the duration from the instant when prestrike happens between interrupter till the PIR switch electrically closes. Normally, PIR is designed based on MIT.

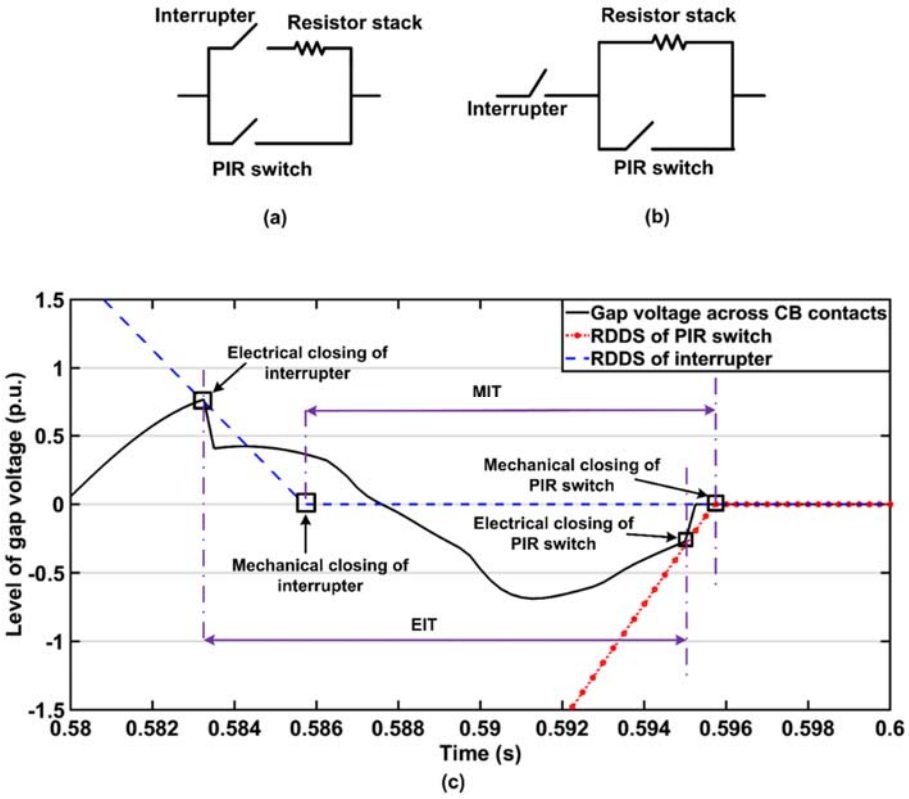

Fig. 1.10 Assembly of (a) parallel PIR, (b) series PIR, and (c) concept of the electrical and mechanical closing of PIR-CB.

However, depending upon the magnitude of gap voltages and Rate of Decay of Dielectric

Strength (RDDS) of interrupter and PIR switch, EIT varies for different operating conditions. The value of EIT of PIR depends on parameters such as the magnitude, shape, and polarity of the gap voltage as well as on the values of RDDS of interrupter and PIR switch. In order to demonstrate the concepts of EIT and MOT of the PIR-CB, a simulation study has been carried out. Here, energization of a transmission line has been performed at random instant. Fig. 1.10 (c) shows the results of this study. The typical value of RDDS for interrupter and PIR switch (considered in this study for a 400 kV breaker) is 100 kV/ms and 130 kV/ms, respectively [7]. It is to be noted that EIT for the PIR-CB may change during the operation keeping MIT constant. However, designing of PIR-CB has been carried out considering constant MIT. In the presented work, hybrid combination of CSD with PIR-CB is utilized to minimize the effect of MOT scatter of the CB.

1.7 Motivation and research gap

From the aforementioned discussion, it is has been cleared that the close coordination between the characteristic of transmission line/power apparatus and CB performance is essential for successful implementation of controlled switching [62]. However, it is challenging to bring this close coordination in actual practice due to practical limitations such as MOT scatter of CB, different configurations of the load side equipment, and non-availability of the accurate measuring devices at the substation site [17], [62]. Moreover, it is to be noted that CB is a mechanical device. Therefore, the controlled opening/closing targets (electrical targets) are attained from the mechanical opening/closing targets. However, the MOT of the CB changes due to systematic variations such as dc voltage, ambient temperature, hydraulic/air pressure of the CB, and the aging effect [55]. It is possible to counterbalance these systematic variations of the CB by CSD using auto compensating curve techniques [55]. Conversely, the statistical variations such as the difference in Rate of Rise of Dielectric Strength (RRDS) & RDDS, and pitting on contacts cannot be compensated. Nevertheless, these statistical variations cause MOT scatter of the CB, which in turn affects the controlled switching application during energization/re-energization of transmission lines and power apparatus. The minimization of the effect of MOT scatter of the CB is one of the challenging area for the research.

Based on the literature review following research gaps have been identified in the area of application of controlled switching for transmission line, power transformer, and shunt reactor.

(i) Transmission line:

- During controlled energization and re-energization of UCTL and SCTL, effect of MOT scatter of the CB (±1 ms) has not been considered in the reported literature

[9], [24], [79], [80], [90].

- The reported optimal targets for energization and re-energization of UCTL and SCTL are zero crossing instant of V_{GAP}. However, due to the non-repetitive nature of V_{GAP}, it is difficult to predict and attain the optimal reclosing target [79], [80].
- At EHV and UHV levels, the general practice is to operate three-phase auto recloser during temporary Single-Line-to-Ground (SLG) faults for SCTL. In this case, other two healthy phases face unnecessary outages, which reduces the overall reliability of the network.

(ii) Shunt reactor:

- Uncontrolled energization of a shunt reactor draws high amount of charging current, which contains asymmetric dc component. This causes saturation of instrument transformers as well as it takes a long time for the decaying, which in turn increases the chances of maloperation of the protective relay [37], [63], [91].
- The shunt reactor requires a particular controlled switching strategy. At the same time, MOT scatter of the CB causes adverse effect, which increases complexity in realtime implementation of the CS.

(iii) Power Transformer:

- Uncontrolled energization of power transformer draws large amount of inrush current (almost around 7 p.u.) [47]. The controlled switching strategy is utilized to reduce such high inrush current.
- The effect of MOT scatter of the CB prevents successful implementation of controlled switching and limits the reduction of inrush current to 4.0 p.u.[55] Moreover, this inrush contains large amount of harmonics, which further degrades the power quality.
- The high inrush current develops thermal stress in the winding and TVD. Particularly, in case of a weak grid system, this TVD causes a disturbance in the behaviour of other power apparatus connected on the same circuit.
- The behaviour of flux linkages during energization of magnetically and electrically coupled transformers is different. In this case, the effect of MOT scatter generates different level of inrush current.

1.8 Objectives of the proposed research work

Based on the abovementioned research gaps, following objectives of the proposed research work have been determined.

(i) Transmission line:

- To develop a controlled switching technique for minimization of switching surges during energization and re-energization of UCTL and SCTL utilizing source side voltage.
- To develop a technique, which minimizes the effect of MOT scatter of the CB during implementation of CS for UCTL and SCTL.
- To design a scheme for controlled closing/reclosing of SCTL utilizing line side voltage considering effect of MOT scatter of the CB of the order of ± 1 ms and with different levels of compensation.
- To develop a novel controlled Single Phase Auto Reclosing (SPAR) technique for SCTL, which reduces unnecessary outages and improves the reliability and efficiency of the power system network. The validation of the proposed controlled SPAR technique is carried out with MOT scatter of the CB (± 1 ms). This technique should be capable to limit the level of switching surges.

(ii) Shunt reactor

- To develop a controlled switching technique for energization of shunt reactor having different connection configurations for minimization of asymmetric dc component of the charging current. The proposed technique should be tested considering MOT scatter of the CB of the order of ± 1 ms.

(iii) Power transformer

- To develop a controlled energization technique of an unloaded power transformer for minimization of the level of inrush current and TVD. The developed technique should be capable of limiting the level of inrush during energization of both magnetically and electrically coupled power transformer considering MOT scatter of the CB (± 1 ms).

1.9 Contributions of the research work

In order to fulfill aforementioned objectives, an attempt has been made. Following are the contributions of the presented work.

1.9.1 Controlled switching of UCTL and SCTL utilizing local end supply side voltages

Normally, the controlled energization/re-energization of UCTL and SCTL has been carried out at zero crossing instant of V_{GAP}. In case of energization of a fully discharged transmission line (either UCTL or SCTL), it is easy to obtain the aforementioned optimal closing target due to the absence of trapped charges (line side voltages) on the line. Therefore, energization of fully discharged UCTL/SCTL has been carried out at zero crossing instant of supply side voltage. On contrary, it is difficult to determine optimal closing target during energization of a partially discharged transmission line (reclosing). In this case, it is essential to analyze the polarity and nature of the line side voltages during the dead time of the CB. In the presented research work, a new methodology has been proposed, which does not require the precise measurement of line side voltages during energization of a partially discharged UCTL and SCTL. Moreover, the technique is tested and validated for non-faulted and faulted situations. In faulted conditions, the fault is sustained for 100 ms, 150 ms, and 200 ms, and the dead time of CB is of the order of 300 ms has been considered. In case of SCTL, analysis of the proposed methodology considering different level of compensations has also been included. In order to validate a wide range of applicability of the proposed methodology, effect of different factors such as weather conditions, different SCCLs of the sources, effect of presence/absence of SA, and change in closing phase sequence are considered. In the proposed work, the developed technique has been evaluated for critical situation such as effect of MOT scatter of the CB for both UCTL and SCTL.

1.9.2 Controlled switching of SCTL by analyzing line side voltages

In this approach, a controlled closing/reclosing of SCTL has been achieved by analyzing line side voltages. It has been observed that the line side voltages, generated due to the presence of trapped charges on line, are oscillatory in nature. Therefore, the gap voltage also becomes oscillatory. Subsequently, the zero crossing instant of V_{GAP} is non-repetitive in nature. Because of that, it is required to identify other reclosing targets during re-energization of SCTL. In order to validate the developed CS technique, modelling of a 400 kV existing Indian power system network containing SCTL has been developed in PSCAD/EMTDC software package. In this model, the spacing between two conductors, the distance between phase to the ground conductor and ground clearance are designed as per Indian electricity rules. In this technique, the optimum

reclosing targets have been achieved based on the estimated phasor magnitude and angle of the line side voltages. Various cases of closing and reclosing of SCTL have been generated from the developed simulation model by varying load angle, source impedance, level of compensation, length of line, type of fault, and duration of fault. The validation of the proposed technique has been carried out utilizing the generated test cases, which contains both fault conditions as well as non-faulted situation. Further, the validation of the proposed technique has also been performed considering the impact of SA, the effect of MOT scatter, and the influence of different SCCL of grid sources. It can be concluded from the obtained result that the level of switching surge has been reduced due to implementation of the proposed technique. Furthermore, the effect of MOT scatter of CB is significantly reduced. The proposed methodology is also able to discriminate between temporary and permanent fault.

1.9.3 Controlled single phase auto reclosing of SCTL

At EHV and UHV level, possibilities of occurrence of temporary SLG fault are very high. Therefore, in order to maintain continuity of supply through healthy phases, a new controlled switching strategy has been proposed by developing SPAR scheme for SCTL. In the presented work, DFT analysis of the line side voltage (faulted phase) has been performed during the dead time of CB. Thereafter, the optimal reclosing target has been obtained using V_{GAP} and the 2nd harmonic component of $V_{L.}$ The performance of the proposed SPAR technique has been evaluated in terms of statistical analysis of switching surge across the length of line for three different compensation levels of SCTL. Moreover, the assessment of the proposed technique has been carried out considering the effect of SA, the incidence of different grid sources, and impact of MOT scatter of the CB. It is observed that the presented technique is able to minimize the level of switching surge up to 1.5 p.u. during different SLG fault condition.

1.9.4 Controlled energization of a shunt reactor

A novel technique for controlled energization of a shunt reactor has been proposed. The controlled energization has been performed at a specific point on the wave, which minimizes the level of the asymmetric dc component of the charging current. Here, the detailed modeling of shunt reactor has been carried out with different connection configurations such as Yg, Y, and Δ. Further, to minimize the level of asymmetric dc component of charging current during energization of a shunt reactor, mathematical analysis has been carried out, which determines optimal MIT, value, and insertion instant of the PIR-CB. These mathematically obtained values have been validated by performing a simulation study on the developed model in PSCAD/EMTDC software package. Moreover, the effect of MOT scatter of the CB is also included in the simulation study. It is to be noted that the proposed methodology mitigates the

effect of MOT scatter of the CB during energization of the shunt reactor. Moreover, the results obtained from the real field implementation of the proposed technique, for the energization of 180 MVAr and 240 MVAr shunt reactors (765 kV), evidently validate the wide range of applicability of the proposed technique.

1.9.5 Controlled energization of a power transformer

A new technique for controlled energization of a power transformer has been proposed. Here, controlled energization of a power transformer is carried out at peak of the gap voltage. Further, the effect of different SCCL of the sources on the level of inrush current is also considered. However, due to the effect of MOT scatter, the inrush current attains almost 4 p.u. value during controlled energization of a power transformer. Subsequently, in order to minimize the effect of MOT scatter of the CB, usage of hybrid combination of PIR-CB and CSD has been proposed. The modeling of magnetically and electrically coupled power transformers have been carried out using PSCAD/EMTDC software. In order to validate the performance of the developed scheme, various cases of energization of the power transformer have been generated by utilizing the developed simulation model. Moreover, it is to be noted that the response of dynamic fluxes varies differently during controlled energization of the electrically coupled and magnetically coupled power transformers. Therefore, the proposed algorithm is also tested and validated on the field data acquired from electrically (1500 MVA, Yg/Y/Δ: (765 kV)/(400 kV)/(33 kV)) and magnetically (500 MVA, Yg/Yg/Δ: (400 kV)/(220 kV)/(11 kV)) coupled power transformers. It has been observed from simulation as well as field results that the suggested approach restricts the level of inrush current within 1 p.u. limit. Different practical factors such as MOT scatter of the CB, level of residual flux, and energy dissipated in PIR have also been considered. At the end, the proposed methodology has been compared with the conventional controlled switching methodology in terms of the level of inrush current and TVD. Unlike the conventional controlled switching methodology, the proposed methodology minimizes the effect of MOT scatter of the CB in terms of level of inrush current in a more improved way during energization of an unloaded power transformer.

1.10 Organization of thesis

The thesis is organized in seven chapters.

Chapter-1: In this chapter, an introduction to uncontrolled switching of transmission lines and different power apparatus has been thoroughly discussed. This discussion includes the effects and issues of uncontrolled switching of transmission lines and power apparatus. Afterwards, the phenomena of controlled closing and opening have been explained with its

advantages along with other technical issues. Based on literature review, the controlled energization and de-energization targets for transmission lines and different configurations of various power apparatus have been presented. The chapter also presents introduction of OHB schemes, which is located at most of the substations at EHV and UHV level in Asia Pacific region. At the time application of controlled switching, the effect of CB co-ordination and difficulties in determining optimal closing/reclosing targets for different power apparatus are also explained.

Chapter-2: This chapter presents newly developed controlled switching technique for UCTL and SCTL using supply side voltage measurements. The development of simulation models for UCTL and SCTL using PSCAD/EMTDC software package has been explained meticulously. Simultaneously, the modeling of a hybrid combination of PIR-CB and CSD has also been included in the discussion. The detailed analysis of derivation of optimal value and MIT of PIR has been presented. At the end, the assessment of the proposed technique considering MOT scatter of the CB, absence/presence of SA, and different SCCL of grid sources has been discussed thoroughly.

Chapter-3: This chapter includes a new controlled switching technique that minimizes the level of switching surge during energization and re-energization of SCTL using a hybrid combination of PIR-CB and CSD. The proposed methodology requires line side voltage measurements during the dead time of the CB. The modeling of an existing Indian 400 kV, 400-km long SCTL using PSCAD/EMTDC software package has been explained meticulously. Moreover, the detailed analysis about the performance of the proposed technique considering variation in the length of the line, level of compensation, type of fault, duration of fault, fault inception angle, short circuit capacity of source and inclusion/removal of SA has been included. At the end, comparative evaluation of the proposed methodology with the reported methodology has also been incorporated.

Chapter-4: A new controlled SPAR technique based on hybrid combination of CSD and PIR-CB has been discussed in this chapter. Detailed modeling of simulation model considering an existing 400 kV, SCTL using PSCAD/EMTDC software package has been elaborated. Further, the performance of the proposed technique considering variation in parameters such as line length, compensation level, fault duration, fault inception angle, fault location, effect of SA, and influence of different grid sources has been deliberated. At last, a comparison between the proposed technique and reported technique has been carried out.

Chapter-5: This chapter discusses a new optimized controlled switching strategy to minimize the level of the asymmetric dc component of the charging current during energization

of a shunt reactor. Moreover, in depth mathematical analysis for getting an optimize insertion instant, value, and EIT of PIR has been presented. Moreover, the assessment of the performance of the proposed methodology by generating large numbers of simulation cases in PSCAD/EMTDC software package has been discussed. Furthermore, performance of the proposed technique considering different EITs, effect of MOT scatter, and the value of PIR has been incorporated. Finally, authenticity of the suggested technique has been verified on field results acquired by energizing 240 MVAr and 180 MVAr shunt reactors at 765 kV level.

Chapter-6: This chapter presents evaluation of controlled energization technique during energization of an unloaded power transformer using hybrid combination of CSD and PIR-CB. Effect of parameters such as statistical scatter of mechanical operating time, tolerance of the auxiliary contact used as a feedback element, and variation in MIT & EIT of the PIR-CB during controlled energization of an unloaded power transformer has been explained. Moreover, the assessment of the proposed methodology considering magnetically coupled and electrically coupled power transformers has been incorporated. The details about modeling of the complete system including power source, PIR-CB, and magnetically & electrically coupled power transformers using PSCAD/EMTDC software package have also been discussed in this chapter. Lastly, comparison between the PIR-CB based proposed methodology with the conventional methodology has been highlighted in this chapter.

Chapter-7: The final chapter includes the conclusion of the presented research work and contribution made by the author. It also includes some suggestions for the future scope of the presented research work.

Chapter 2

Controlled switching technique for UCTL and SCTL based on local end supply side voltages

2.1 Introduction

In this chapter, new controlled switching technique is proposed to minimize the level of switching surge during energization of fully discharged and partially discharged UCTL and SCTL considering local end supply side voltages. As discussed in section 1.4.1 that the nature of V_{GAP} is oscillatory and non-repetitive in case of energization of a partially discharged SCTL [1], [4], [15]. Hence, it is very difficult to predict the forthcoming zero crossing instant, which is considered as an optimal controlled switching target. Therefore, it is required to determine optimal controlled energization targets other than V_{GAP}. Moreover, in order to derive the optimal controlled closing targets for energization of a partially discharged line, it is essential to observe the nature of line side voltages during the dead time of CB. In case of UCTL and SCTL, the polarity of the trapped charge during dead time of the CB is unidirectional and bidirectional, respectively. In the real field, Capacitive Coupling Voltage Transformer (CCVT)/magnetic Potential Transformer (PT) is used for line side voltage measurement. However, it is difficult to tune the instrument transformer to replicate line side voltages accurately. Therefore, in presented work, the controlled energization targets for fully discharged and partially discharged UCTL & SCTL are obtained using supply side voltage measurement instead of line side voltage measurement.

2.2 Factors responsible for generation of high switching surge

Generally, energization of fully discharged transmission lines and re-energization (auto recloser) of transmission lines establish switching surges. In section 1.2.1 and 1.5, various factors responsible for generation of a high level of switching surges along with basic terminology related to controlled switching in conjunction with PIR has been explained thoroughly. Fig. 2.1 (a) and (b) show the single-line-diagram of UCTL and SCTL (with shunt reactor connected at both ends) used in the simulation study of the presented work. Further, in case of SCTL (shunt reactor connected at one end of the line (source side)), the reactor (X_{L2}) from Fig. 2.1 (b) is removed and based on the compensation level, the magnitude of 'X_{L1}' has been calculated. Here, the level of switching surge is measured at the remote end of the line (Bus2). In Fig. 2.1, Z_{SA} and Z_{SB} represents source impedance at Bus1 and Bus2, respectively.

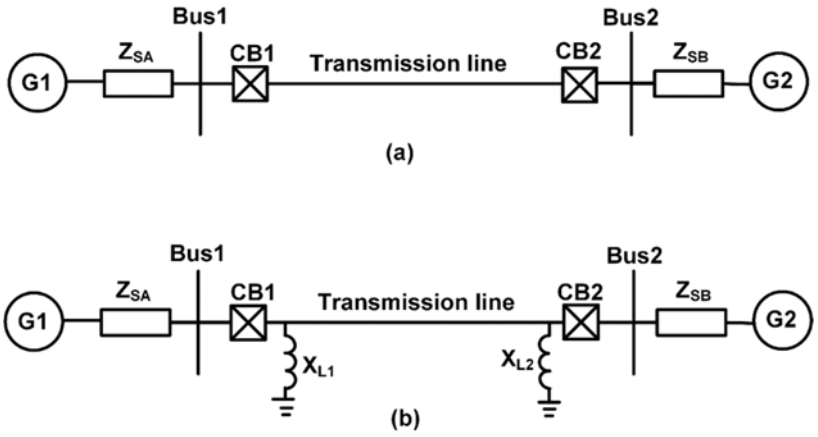

Fig. 2.1 Single line diagram of (a) UCTL and (b) SCTL.

For energization of fully discharged UCTL/SCTL (Case-1), the normal controlled switching practice is to energize the line at source side voltage zero. However, for remaining cases, the same philosophy cannot be applied. In context to re-energization of partially discharged line (Case-2), the conditions such as no-fault, short time temporary fault (fault sustains for very short duration compared to protection dead time of 300 ms), long time temporary fault (fault clears just prior to the end of protection dead time) and permanent fault resulting into lockout are considered. In case of UCTL, exponentially decaying line side voltages (trapped charge) are observed because of energy stored in the stray capacitance of the line. On the other hand, for SCTL, the presence of shunt reactor connected either at one end or at both ends of the line creates L-C oscillations with a frequency less than the fundamental frequency. In practice, either PT or CCVT is used for measurement of line side voltages. However, it is reported in the literature that PTs are rarely used in practice for voltages more than 100 kV due to techno-economic constraints [24]. At the same time, it has been mentioned in IEC-61869-3 that the accuracy offered by PT is maintained up to optimal level if the variation in voltages is of the order of 80%-120% and 25%-100% for measuring class and protective class PT, respectively. As the oscillating line side voltage crosses the above-mentioned limit (usually attains a peak value more than 1.2 p.u.), it would be difficult to accurately replicate the oscillating line side voltages using PT [92]. During the protection dead time, the magnetic circuit of PT gets saturated due to exponentially decaying line side voltages [24]. Hence, the PT does not replicate the line side voltage accurately. On the other hand, in case of SCTL, it is troublesome to replicate the line side voltages by PT due to the presence of non-power frequency components. In case of CCVT, the trapped charge will not decay rapidly due to large capacitance offered by it. The decaying rate of trapped charge also depends upon the configuration of line,

type of switching duty and reclosing on permanent/temporary faults. Furthermore, in case of single or double line-to-ground faults, mutual coupling along with asymmetric nature of the fault current may cause a high level of unsymmetrical overvoltages on non-faulty phases [93], [94]. Fig. 2.2 (a) and (b) shows the simulation results in terms of the response of CCVT during de-energization of a partially discharged UCTL and SCTL, respectively. The response of CCVT captured from the real field using Disturbance Recorder (DR) during de-energization of a partially discharged UCTL is shown in Fig. 2.2 (c). The sequence of de-energization for both the lines is also shown in Fig. 2.2 (a) and (b). It has been observed from Fig. 2.2 (a) that the waveform of trapped charge reaches zero value after 2-3 cycles. However, in the actual field, it decays exponentially. As shown in Fig. 2.2 (a), the response of CCVT obtained from simulation study has been mapped with the field results as shown in Fig. 2.2 (c). Comparison of both these figures clearly indicates the exactness of the response of CCVT obtained from the simulation study and the real field. Therefore, for cases 2, 3, and 4, the precise measurement and interpolation of line side voltages are crucial for accurate evaluation of controlled switching targets.

2.2.1 Controlled switching of transmission lines having PIR breaker

The representation of the OHB scheme and line with non-switchable reactor scheme is shown in Fig. 1.9 (a) and (b), respectively. As shown in Fig. 1.9 (a), CSD has been provided with PIR-CB on tie bay for controlled de-energization of the reactor to minimize the probability of reignition [74]. Conversely, the following conditions are considered for a transmission line with non- switchable reactor (Fig. 1.9 (b)).

(i) The transmission line can be used as uncompensated line by opening dis-connector of the shunt reactor (UCTL mode).

(ii) The transmission line can be used with compensation by connecting a shunt reactor (SCTL mode).

(iii) The transmission line is disconnected by opening its dis-connector and the line reactor is used as the bus reactor for reactive power compensation.

For condition (iii), in order to minimize the possibility of reignition with the PIR-CB of the line, the CSD has been provided for controlled de-energization of the reactor. Conversely, for conditions (i) & (ii), the CSD is usually bypassed. As discussed in the previous section, to mitigate secondary surge further, the controlled energization of the transmission line with PIR-CB is performed with the same CSD having different settings for conditions (i) and (ii) [73].

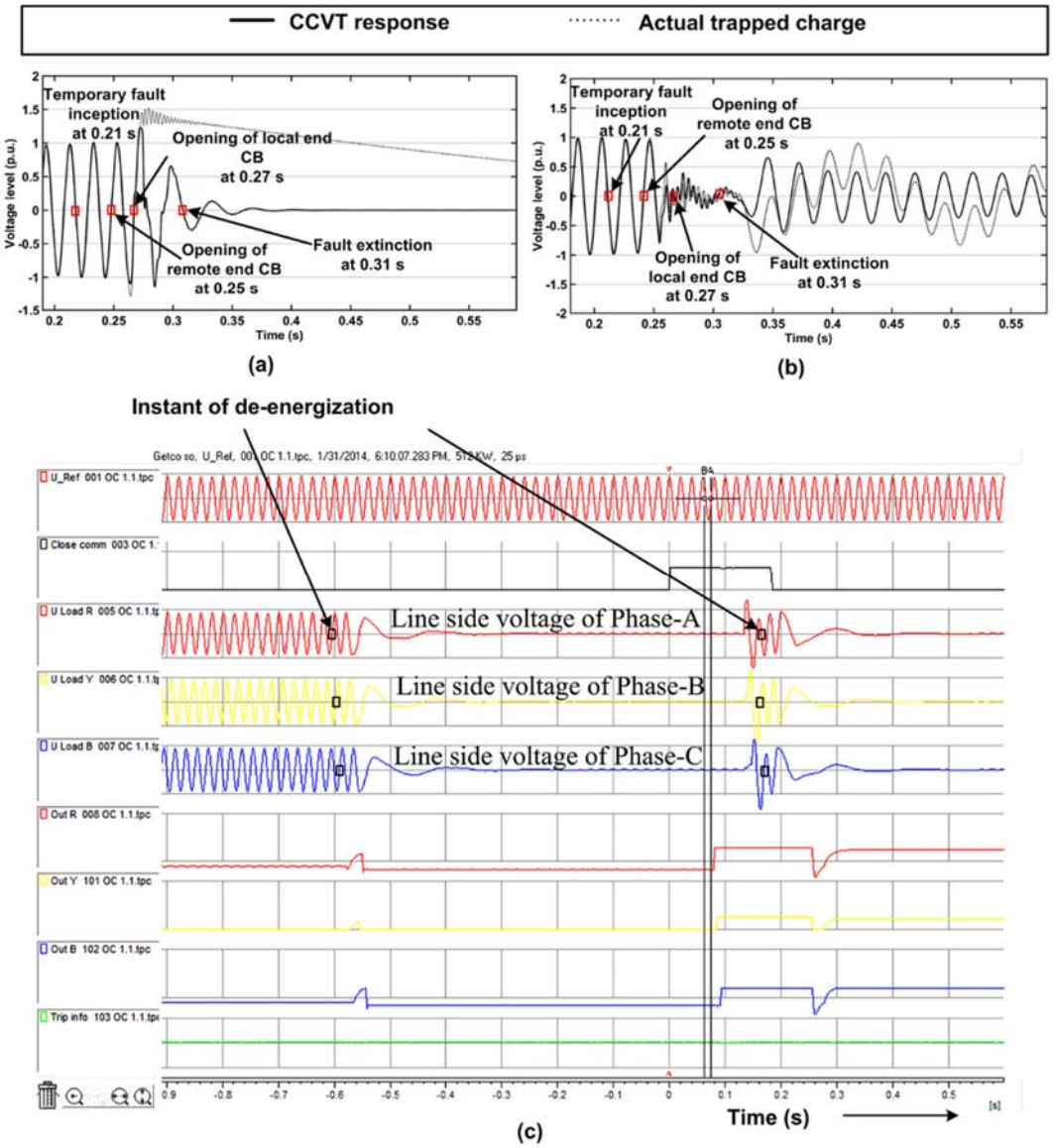

Fig. 2.2 Response of CCVT, simulation results during de-energization of partially discharged (a) UCTL, (b) SCTL, and (c) field results during partially discharged UCTL.

2.2.2 Behaviour of PIR during energization of transmission lines

PIR consists of a resistor stack and two switches. The full assembly together is termed as PIR throughout the thesis. Depending upon the position of bypass switch with respect to main contacts of CB (interrupter), two types of PIR configurations, namely series PIR and parallel PIR, are commonly used. However, the series PIR configuration is usually employed due to low cost and less space requirement [7].

In this presented work, the series PIR configuration is used to perform all simulation cases. Subsequently, the proposed methodology will be equally applicable to parallel PIR configuration as the electrical behaviour for both configurations remains the same. It has been

reported in the literature that the usage of PIR suppresses the switching overvoltage by a factor of $Z_C/(R+Z_C)$ at the remote end of the line [1], [2]. Here, '*R*' indicates the value of PIR and *'Z_C'* represents surge impedance of the transmission line.

For series PIR configuration, the electrical making occurs primarily between interrupter followed by the contacts of PIR switch, which bypasses the resistor after MIT is over. Subsequently, EIT is defined as the duration from the instant when prestrike happens between interrupter till the PIR switch electrically closes. Normally, PIR is designed based on MIT. However, depending upon the magnitude of gap voltages and RDDS of PIR switch, EIT varies for different operating conditions [7]. It depends on the magnitude, shape, and polarity of the gap voltage across the contacts of CB as well as on the values of RDDS of interrupter and PIR switch. Fig. 2.3 demonstrates the dependency of EIT on RDDS of interrupter and PIR switch. The typical value of RDDS for interrupter and PIR switch, considered in this study for a 400 kV breaker, is 100 kV/ms and 130 kV/ms, respectively [7]. Fig. 2.3 shows the simulation results in terms of 10% change in the value of RDDS for both interrupter and PIR switch on EIT.

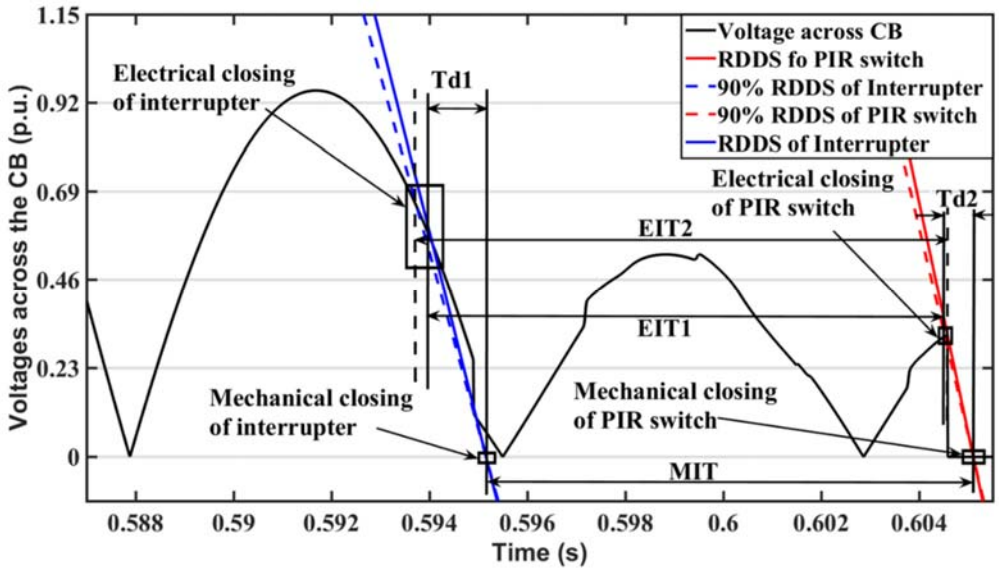

Fig. 2.3 Effect of change in the value of RDDS of interrupter and PIR switch on EIT.

It is observed from Fig. 2.3 that EIT varies due to change in prestrike instants while MIT remains constant. Moreover, though there is a 10% change in the RDDS of interrupter and PIR switch, the prestrike instants are varied in a narrow band for PIR switch and interrupter. Moreover, it is to be noted from Fig. 2.3 that the time lapse between electrical closing and mechanical closing for interrupter and PIR-switch is 1.3 ms ('Td1') and 0.3 ms ('Td2'), respectively. This improves the performance of application of controlled switching.

2.3 Modelling of power system network

2.3.1 Modelling of the transmission line

The modeling of a 400 kV, 50 Hz UCTL and SCTL with SIR less than 0.5 is done using PSCAD/EMTDC software package [83]. Aforementioned Fig. 2.1 (a) and (b) shows a single-line-diagram of UCTL and SCTL, respectively with shunt reactor connected at both ends of the line. The sampling frequency of 4 kHz has been used for a fundamental frequency of 50 Hz [95], [96]. Moreover, 369 kV switching class SAs are employed at both ends of the line for suppression of switching overvoltages [97]. The transmission line has been modeled by the frequency dependent phase model, available in PSCAD, as it is commonly used for transient overvoltage study [83].

The parameters of the transmission line and base source are given in Appendix-A1. Furthermore, as per Indian Electricity rules, ground clearance of the conductor and the spacing between phase conductors for rated line voltage (kV) are calculated using (2.1) and (2.2), respectively [90].

$$\text{Ground clearance}\quad (CL_G) = [5.2 + \{(kV - 33)/33\} \times 0.3] \tag{2.1}$$

$$\text{Specing between phase conductors}\quad (CL_P) = [3.7 + \{(kV - 33)/33\} \times 0.3] \tag{2.2}$$

Moreover, the surge impedance (Z_C) of the transmission line is calculated using (2.3).

$$Z_C = \sqrt{\frac{R + j\omega L}{G + j\omega C}} \tag{2.3}$$

Where, ω is the angular velocity (rad/s) and *R, G, L* and *C* represents resistance (Ω/km), conductance (mho/km), inductance (H/km) and capacitance (F/km) of the line, respectively. In case of SCTL, the impedance of the shunt reactor (X_{lr}) and the impedance (X_n) of Neutral Grounding Reactor (NGR) is calculated using (2.4) and (2.5), respectively.

$$X_{lr} = \frac{1}{\eta \times \beta_c} \tag{2.4}$$

Where, η and β_c represents the amount of compensation and the positive sequence susceptance of the transmission line, respectively.

$$X_n = \frac{1}{3} \times \left\{ \omega \times (C_0 - C_1) + \frac{1}{X_{11}} \right\}^{-1} - X_{11} \tag{2.5}$$

Where, C_0 and C_1 is the zero and positive sequence capacitance of the line, respectively, whereas X_{11} is the positive sequence impedance of the shunt reactor [98].

2.3.2 Assessment of PIR parameters

In order to determine the optimal value of PIR and MIT, a simulation study has been carried out on a power transmission network, as shown in Fig. 2.1 (a & b), using PSCAD/EMTDC software package [83]. In this presented work, all the simulations are performed by installing SAs at both ends of the line. During energization of a partially discharged UCTL using PIR-CB, the level of switching surge mainly depends on the following parameters:

(i) Value of the Pre-Insertion Resistor (PIR)

(ii) MIT of the PIR

(iii) Insertion instant of PIR.

In order to analyze the effect of an individual parameter on the level of the switching surge, the variation in the level of switching surge against different values of one of the parameter has been observed, keeping the other two parameters constant. In this manner, the level of switching surge against different values of PIR has been determined, maintaining the insertion instant and MIT of PIR constant. Based on literature reported on PIR-CB, the value of MIT equals to the time of half cycle (i.e. 10 ms considering the fundamental frequency of 50Hz) is taken [6], [7]. A simulation study during energization of a partially discharged 200-km long UCTL has been carried out. This study has been carried out using following insertion instants of PIR.

(i) Half of the peak of the supply side voltage

(ii) Peak value of the supply side voltage

In this study, the variation in the level of the switching surges (primary and secondary surges as discussed in section-1.4.1) against the different values of PIR (Ratio of the value of PIR ('*R*') against surge impedance of the transmission line ('*Zc*')) has been observed. The range of variation in the ratio of '*R/Zc*' is considered as 0.04 - 1.7. Fig. 2.4 (a) and (b) show the simulation results. The PIR insertion target for Fig. 2.4 (a) and (b) is half of the peak value and the peak value of the supply voltage considering non-faulted condition. It has been observed

from Fig. 2.4 (a) and (b) that the level of primary surge is higher than the secondary surge till inter-section point 'a'. At this point, the value of *R/Zc* is around 0.77. Thereafter, the value of primary surge reduces, whereas the secondary surge remains almost constant up to point 'b' and then increases.

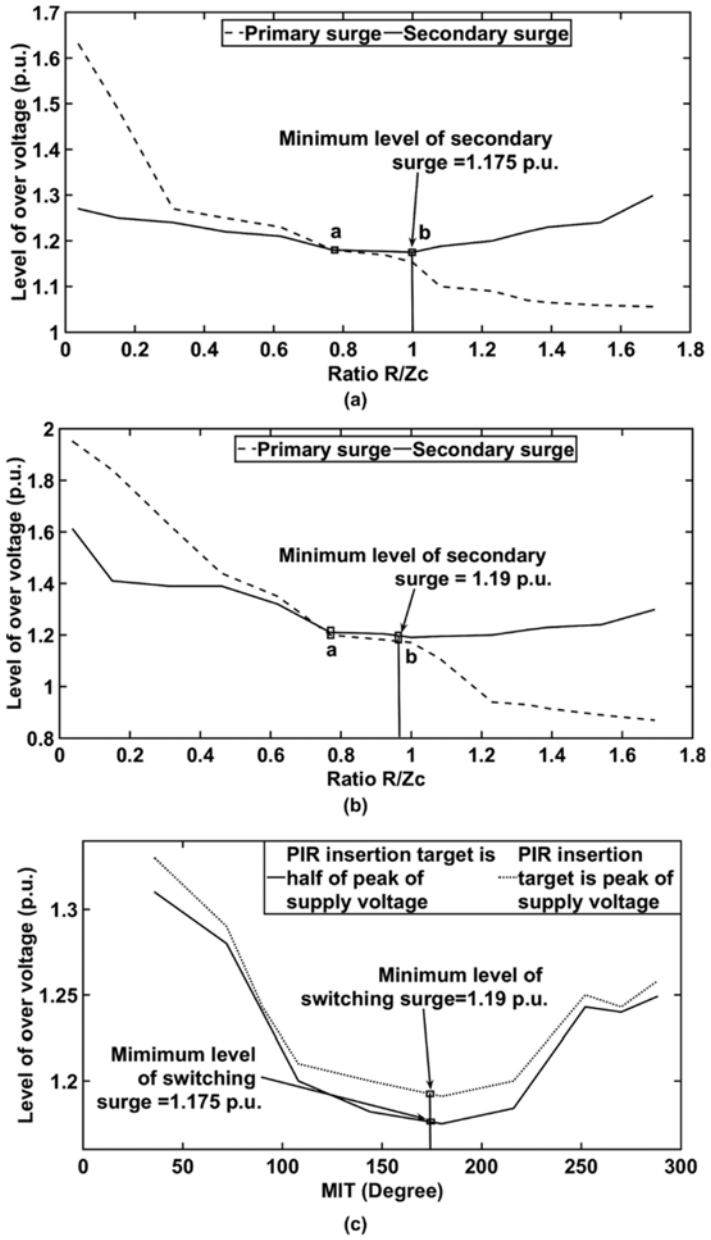

Fig. 2.4 Variation in level of switching surge against different values of PIR for insertion instant of PIR (a) at half of the peak value, (b) at the peak value of the supply side voltage, and (c) variation in level of switching surge against different values of MIT.

Hence, the minimum value of the secondary surge is obtained when the value of *R/Zc* = 1. It is to be noted from Fig. 2.4 (a) and (b) that the minimum value of secondary surge is lower

in case when the closing target is half of the peak of the supply voltage compared to the closing target as the peak of the supply voltage. In order to further verify the optimal value of MIT, a simulation study during energization of a partially discharged 200-km long UCTL has been carried out considering non-faulted cases using the optimal value of PIR (R/Zc = 1). In this study, the variation in the level of switching surge (either primary or secondary whichever is higher) against different values of MIT (36^0 - 288^0) using both above-mentioned closing targets, has been obtained. Fig. 2.4 (c) shows the simulation results of this study. It has been observed from Fig. 2.4 (c) that the minimum level of switching surge is obtained, when the value of MIT = 180^0 for both aforementioned closing targets.

2.3.3 Derivation of optimal controlled switching targets

The existing controlled switching methodology is based on targeting the making instant when the gap voltage across the CB contacts is minimum. In this regard, it is essential to accurately replicate the line side voltages. However, in this presented work, a new controlled switching methodology is presented taking reference of source side voltages and just the polarity of line side voltage at the time of de-energization of the line. In order to employ point on wave switching, seven testing targets, as shown in Fig. 2.5 (a), have been considered on the source side voltage waveform. These targets are termed as the "reference targets".

By utilizing these targets, the proposed controlled switching methodology minimizes the switching overvoltage during energization of UCTL and SCTL by optimizing the electrical insertion instant of PIR (electrical closing instant of interrupter). It has been reported in the literature that the level of switching surges, during energization of a partially discharged UCTL and SCTL, can be minimized by limiting the value of gap voltage across the contacts of CB at the time of closing [15], [74]. In order to determine the optimal closing targets for UCTL and SCTL, a simulation study of line side voltages during protection dead time of a partially discharged UCTL and SCTL has been carried out. Fig. 2.5 (b) and (c) shows the waveform of supply voltage and trapped charge (line side voltage) for a 200-long UCTL in case of no-fault and temporary short time SLG fault condition, respectively. It has been observed from Fig. 2.5 (b) and (c) that the magnitude of the trapped charge is almost equal to half of the peak value of the supply voltage at the end of protection dead time. Utilizing this fact, half of the peak value of supply voltage is taken as the optimal closing target for UCTL. These are indicated as reference target '1' and '5' (considering both the polarity of the trapped charge) in Fig. 2.5 (a). In order to determine the optimal closing targets for SCTL, a simulation study has been carried

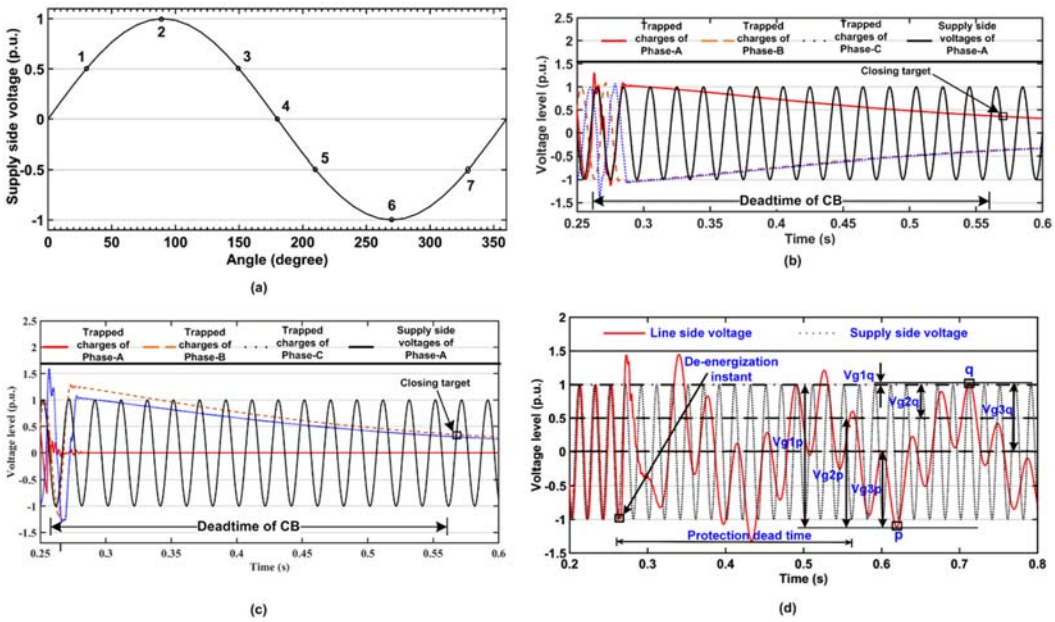

Fig. 2.5 (a) Reference targets, (b) effect of trapped charge decay for 200 km long UCTL in case of non-faulted situation, (c) short time single-line-to-ground fault situation, and (d) conceptual representation to determine the optimal closing target for SCTL.

out considering oscillating nature of line side voltages. Utilizing this fact, three supply side closing targets, as given below, have been evaluated.

(i) Positive peak of the supply voltage (Vmax).

(ii) Half of the positive peak of the supply voltage (Vmax/2).

(iii) Supply voltage zero (Vzero).

Out of the above-mentioned targets, the optimal closing target is that target for which the gap voltage does not attain the extreme level for any polarity of the line side voltages. Hence, in order to determine the level of switching overvoltages, a simulation study during energization of a partially discharged SCTL considering non-faulted and different faulted conditions has been performed with aforesaid targets. It has been observed that the switching overvoltages are maintained well within the limit. Fig. 2.5 (d) shows the simulation results for the following two extreme cases of line side voltages.

(i) When the line side voltage attains negative peak (point ‘p’)

(ii) When the line side voltage attains positive peak (point ‘q’)

In this case, the gap voltage is the difference between supply side and line side voltages. With reference to point ‘p’, it has been observed from Fig. 2.5 (d) that the gap voltage for the aforementioned three closing targets (Vmax, Vmax/2, and Vzero) is Vg1p, Vg2p, and Vg3p,

respectively. Similarly, for the second extreme case of line side voltage (point 'q'), the gap voltage for the same three reference targets is Vg1q, Vg2q, and Vg3q, respectively. It is clear from Fig. 2.5 (d) that the level of gap voltage changes widely for two closing targets (Vg1p & Vg1q and Vg2p & Vg2q), whereas the level of gap voltage, developed considering the supply voltage zero as a closing target (Vg3p and Vg3q), remains unchanged irrespective of change in polarity of the line side voltage. It can be well appreciated that the supply voltage zero should be the best suitable target, which maintains the gap voltage within moderate limit. Table 2.1 shows the level of the gap voltages for different closing targets.

Table 2.1 Level of gap voltage for different closing targets of SCTL

Sr. No	Scenario at the instant of closing		Gap voltage (p.u.)	Level of gap voltage (p.u.)
	Supply side voltage (p.u.)	Line side voltages (p.u.)		
1	Vmax	Negative peak (point 'p')	Vg1p	2.22
2	Vmax/2	Negative peak (point 'p')	Vg2p	1.72
3	Vzero	Negative peak (point 'p')	Vg3p	1.22
4	Vmax	Positive peak (point 'q')	Vg1q	0.22
5	Vmax/2	Positive peak (point 'q')	Vg2q	0.72
6	Vzero	Positive peak (point 'q')	Vg3q	1.22

It is to be noted from Table 2.1 that the level of gap voltage changes widely for closing targets Vg1p & Vg1q and Vg2p & Vg2q, whereas it stays constant for Vg3p & Vg3q. In the proposed methodology, the supply voltage zero is taken as an optimal closing target for SCTL (target '0' in Fig. 2.5 (a)). Subsequently, the proposed methodology does not depend on the effect of the polarity of the oscillating line side voltage.

2.4 Proposed technique

Fig. 2.6 (a) shows the flowchart of the proposed technique. The proposed technique does not require precise measurement of line side voltage during protection dead time. It utilizes rising tip side half of the peak value of the supply voltage as a closing target for UCTL and the supply voltage zero as a closing target for SCTL. In Fig. 2.6 (a), the half of the peak value of the supply voltage on rising tip side is indicated as target "A", whereas the supply voltage zero is indicated as target "B". As shown in Fig. 2.6 (a), the configuration of the transmission line (un-compensated (UCTL)/compensated (SCTL)) is given as input to the proposed methodology. The process starts upon detection of breaker status changeover from close to open. At the time of de-energization, the polarity of the individual phase of line side voltage has been stored by CSD. This is required for UCTL as the direction of the trapped charge remains unaltered during the protection dead time. Therefore, in the proposed methodology, the reclosing operation for UCTL

has been performed on the same polarity of the source voltage.

Fig. 2.6 (b) shows conceptual layout of CSD for the storage of polarity. The CSD is capable to acquire current and voltage data from the actual field through CT and CCVT. However, the proposed scheme requires voltage data only. Accordingly, as shown in Fig. 2.6 (b), the CSD acquires line side voltage data through instrument transformers continuously. It is to be noted that the voltage signal is fed directly to the data storage and evaluation module of CSD using Analog to Digital Converter (ADC), whereas current signal fed to this module through current-to-voltage (I-V converter) converter and ADC. The data storage module of CSD stores the acquired data using non-volatile memory.

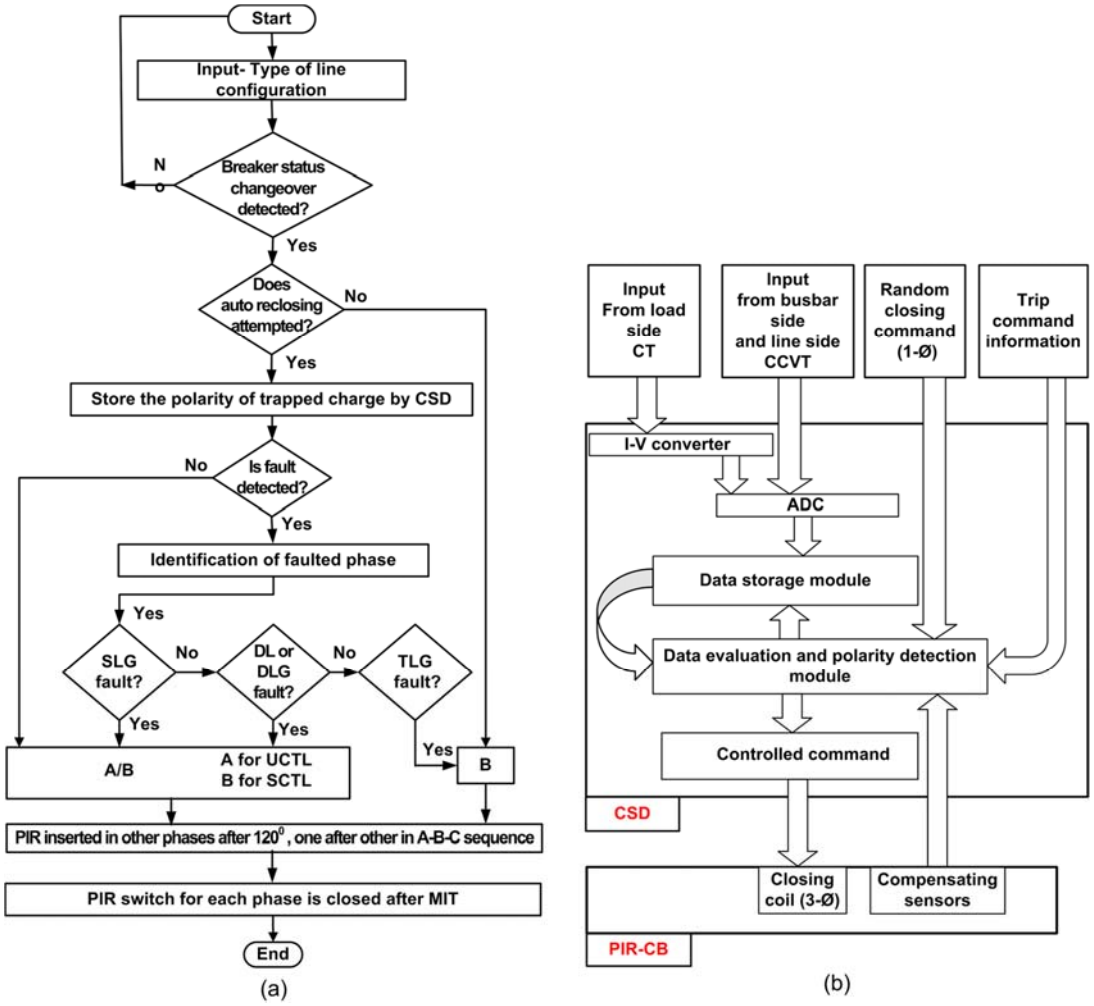

Fig. 2.6 (a) Flowchart of the proposed methodology and (b) conceptual layout of CSD.

When the random closing command is raised either by manual mode or through Supervisory Control and Data Acquisition (SCADA), it is converted into controlled closing command by introducing intentional delay. This delay is calculated based on voltage & current

data acquired from the actual field and type of load to be switched. Moreover, based on the type of load to be switched such as transmission line, transformer, shunt-reactor, and shunt capacitor, evaluation of the optimum switching targets will be carried out by the data evaluation and polarity detection module of CSD.

For this purpose, different settings are provided. Various tasks performed by data evaluation and polarity detection module are as under.

(i) It analyses the voltage and current signals acquired from the real field.

(ii) It evaluates mechanical operating time of the CB for last operation by collecting the feedback from an auxiliary contact of the CB.

(iii) It detects zero crossing of busbar side and line side voltages for individual phases. This will be used for evaluating optimum output command for individual poles of the CB after considering operating time of CB. This is known as adaptive operating time functionality and it is based on the auto-compensating curve fitting technique.

(iv) Variation in different parameters such as ambient temperature, dc supply voltage, and hydraulic/air pressure of the CB is responsible for change in the MOT of the CB. This else otherwise, would result into incorrect determination of the actual switching targets. Required compensation factor in operating time of individual poles of CB (both close and open) has been evaluated based on data collected from compensating sensors. Hence, this module calculates an intentional time delay after the initiation of input close command considering all the above-mentioned parameters.

(v) The instant, when the tripping command has been given to CB, the trip command information module activates the data evaluation and polarity detection module. Thereafter, the data evaluation and polarity detection module starts acquiring the line side voltage data from data storage module for a time period of 2-4 cycles. In case of opening operation of the CB, the change in line side voltage has been identified by data evaluation and polarity detection module using abrupt change detection algorithm [99]. There are numbers of abrupt change detection algorithms developed by manufacturers [100]. Discussion of these algorithms is out of scope of this chapter. Subsequently, the polarity of the line side voltage for individual phases have been identified and the optimal closing targets for next energization operation are also determined [100]. The non-auto-recloser is as

good as energization of the fully discharged transmission line. Utilizing this fact, the PIR should be inserted at supply voltage zero ("B") for both types of configurations of the transmission line (UCTL/CTL). Generally, auto-reclosing is performed only for SLG fault. However, in order to verify the effectiveness of the proposed methodology, faults other than SLG fault are also considered. It is to be noted that the proposed methodology for non-faulted condition utilizes the same closing targets, which are used for faulted conditions. In case of non-faulted condition, the first phase to re-close is the phase, which attains reference target A or B, prior to other two phases after the protection dead time. Upon detection of a fault, phase/phases involved in the fault will be identified by the faulted phase classifier algorithm [99].

After re-closing the first phase, the trapped charge of reclosed phase as well as other phase/phases shifts towards the polarity of first reclosing phase. In case of SLG fault, among two non-faulted phases, the phase that attains closing target "A/B" earlier shall be closed first. In case of line-to-line (DL)/double-line-to-ground (DLG) fault, the healthy phase should be re-closed first at the target "A/B" in the proposed flowchart. The targeting in case of triple-line (TL)/triple-line-to-ground (TLG) faults on UCTL/SCTL is performed in the same manner as it is used during energization of a fully discharged line (non-auto recloser case denoted by target "B" in the flowchart). Moreover, for all cases (including faulted or non-faulted condition with or without recloser), the remaining two phases should be energized in A-B-C phase sequence after 120°, one after other. The literature reported on the energization of partially discharged UCTL and SCTL suggests that the level of switching surge generated in case of stagger pole closing of CB is found lower than simultaneous pole closing of CB [77].

Table 2.2 Summary of simulation cases generated for UCTL & SCTL.

Length of line (km)	Level of compensation (%)	Type of fault	Polarity of trapped charge	Fault resistance (Ω)	Duration of fault (ms)	Load angle (δ)	Fault distance (% of line length)	Fault inception angle (degree)	Total cases
UCTL									
200 (1)	Not Applicable	A-G, A-B, A-B -G, A-B -C-G (4)	+ ve, -ve (2)	0.0001, 100 (2)	100, 250 (2)	-30^0 (1)	0, 50, 100 (3)	0^0, 90^0, 135^0 (3)	288 cases
SCTL									
450 (1)	30,50,70 (3)	A-G, A-B, A-B -G, A-B -C-G (4)	+ ve, -ve (2)	0.0001, 100 (2)	100, 250 (2)	-30^0 (1)	0, 50, 100 (3)	0^0, 90^0, 135^0 (3)	864 cases

In staggered closing, each phase of the breaker is closed one after another, generally in A-B-C sequence. The stagger pole operation of CB reduces the level of switching surges by preventing the interaction among the phases, where switching surge on one phase induces additional surge at the wrong time on another phase. In case of simultaneous three-phase reclosing, these additional induced surges create the highest overvoltage [4]. Hence, in proposed methodology, the concept of staggered pole operation of the CB has been utilized.

2.5 Simulation cases

In order to evaluate performance of the proposed algorithm, wide variation in system conditions, operating parameters and type of fault have been considered. The simulations also include critical cases like terminal fault (zero km from Bus1) and out of phase closing. Here, out of phase closing is carried out by inserting PIR at an instant when the polarity of the supply side voltage is opposite to the polarity of line side voltage. This leads to generation of the maximum level of the secondary surge. Table 2.2 shows summary of simulation cases generated with variation in operating and system parameters. In this context, line length (1) × type of fault (4) × polarity of trapped charge (2) × fault resistance (2) × duration of fault (2) × load angle (1) × fault distance (3) × fault inception angle (3) = 288 simulation cases have been generated. Afterwards, these cases are tested for all seven reference targets as specified in Fig. 5 (a). Therefore, an overall dataset of 2,016 (288 × 7) fault cases has been investigated for UCTL in this study. Similarly, utilizing all the above-mentioned cases along with three different values of the compensation level (30%, 50%, and 70%), 6,048 (2,016 × 3) cases have been generated for SCTL. Moreover, two types of SCTL configurations are considered (i) shunt reactors are connected at both ends of the line and (ii) shunt reactor is connected at one end of the line. Therefore, a total of 12,096 (6,048 × 2) simulation cases have been simulated for SCTL.

2.6 Results and discussion

2.6.1 Proposed controlled switching methodology for UCTL and SCTL

In real scenario, there may be a possibility of nuisance tripping during no-fault condition. This effect is considered in simulations by varying the polarity of trapped charge (positive and negative) with constant line length (200-km) and load angle (30^0). Furthermore, these (2×1×1) cases are tested on 7 reference targets in context to insertion instant of PIR. Therefore, a total of 14 cases (2 × 7), involving auto recloser during no-fault condition, have been investigated in this study for UCTL. Similarly, 14 × 3 (three compensation levels) = 42 cases of auto recloser during no-fault condition have been studied for SCTL.

Subsequently, a simulation study has been carried out during energization of a partially

discharged UCTL and SCTL using PIR-CB. The simulation study has been performed on SCTL considering aforementioned three levels of compensation for non-faulted and different faulted conditions such as SLG, DL, DLG, and TLG faults. Fig. 2.7 (a) shows the overvoltage in terms of the level of secondary surge for 200-km long UCTL. Moreover, Fig. 2.7 (b), (c), and (d) show the same effect for 450-km long SCTL with 30 %, 50 %, and 70 % compensation level, respectively.

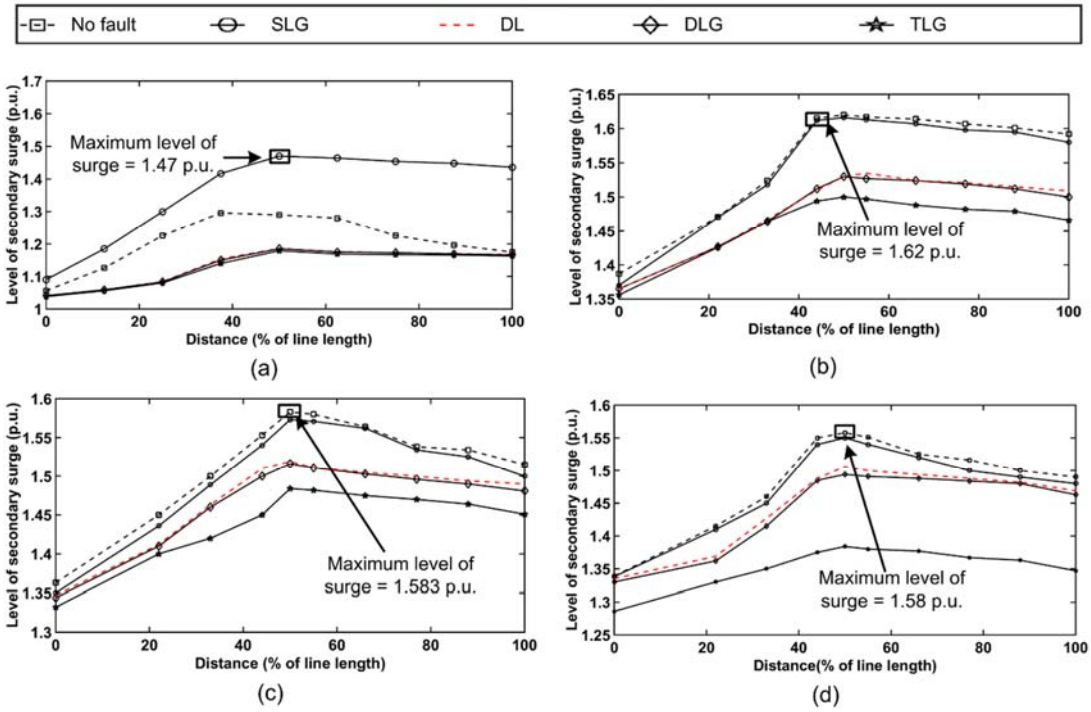

Fig. 2.7 Over voltages along the length of (a) 200-km long UCTL (b) 30%, (c) 50%, and (d) 70% compensated 450-km long SCTL.

This comparison is in terms of the maximum secondary surge generated at the remote end (Bus-2) of UCTL and SCTL with SA. It is to be noted from Fig. 2.7 that the level of switching surge increases from sending end to receiving end and becomes maximum at the mid-point of the line. Thereafter, it decreases slowly towards the receiving end. In case of energization of a partially discharged UCTL (Fig. 2.7 (a)), the highest level of switching surge (1.47 p.u.) is observed during short time temporary (100 ms) SLG fault compared to non-faulted and different faulted situations. On other hand, it is clear from Fig. 2.7 (b)-(d) that the highest level of the secondary surge is observed during no-fault situation with 30% compensation level compared to other faulted conditions. Moreover, the level of secondary surge is always higher in case of SLG fault compared to other faults. In case of SLG fault, the level of secondary surge is highest (1.62 p.u.) for 30% compensation level.

2.6.2 Effect of MOT scatter of the CB

The latest generation of CBs have mechanical and dielectric characteristics, which can attain the making target with the accuracy of ±1ms [4]. In order to evaluate performance of the proposed methodology, a simulation study has been carried out. During this study, energization of a partially discharged UCTL and SCTL is performed considering the combined effect of the MOT and RDDS scatter of the CB. Various switching scenarios are used for comparing switching overvoltage mitigation performance of PIR-CB with non-PIR-CB.

The MOT of CB changes due to statistical and systematic variations. The systematic variations in MOT occur due to external parameters such as variation in the ambient temperature, dc battery supply voltage, and aging effect (after the time of installation). Based on appropriate testing in laboratories, it has been observed that the controlled switching relays can compensate aforementioned systematic variation in operating time using suitable compensation curves. On the other hand, the statistical variations in operating time of the CB cannot be compensated. In this presented work, an overall variation of ±1 ms is considered. A simulation study during energization of a partially discharged 200-km long UCTL and 450-km long SCTL has been carried out using the proposed methodology (which contains both CSD and PIR-CB) and the usual PIR methodology. In this study, various conditions such as no-fault, SLG fault, DLG fault, DL fault, and TL/TLG fault have been analyzed. The MOT scatter due to statistical variations of the CB of the order of ±1 ms has been considered. During this study, three different levels of compensation for SCTL (30%, 50%, and 70%) have been considered. Moreover, the level of switching surge is monitored at the far end of the transmission line. The simulation results for UCTL are shown in Fig. 2.8 (a), whereas Fig. 2.8 (b)-(d) show the simulation results for SCTL. It is to be noted from Fig. 2.8 (a) that the maximum level of switching surge given by the usual PIR methodology and the proposed methodology is of the order of 1.9 p.u. and 1.34 p.u., respectively, during no-fault condition. However, during faulted (SLG fault) condition, the maximum level of switching surge is around 1.76 p.u. and 1.54 p.u. for the usual PIR methodology and the proposed methodology, respectively. Conversely, as observed from Fig. 2.8 (b)-(d), the maximum level of switching surge given by the proposed methodology is always lower than the usual PIR methodology for faulted/no-fault situations. The above discussion clearly indicates superiority of the proposed scheme over the usual PIR methodology in terms of reduction in the level of switching surge.

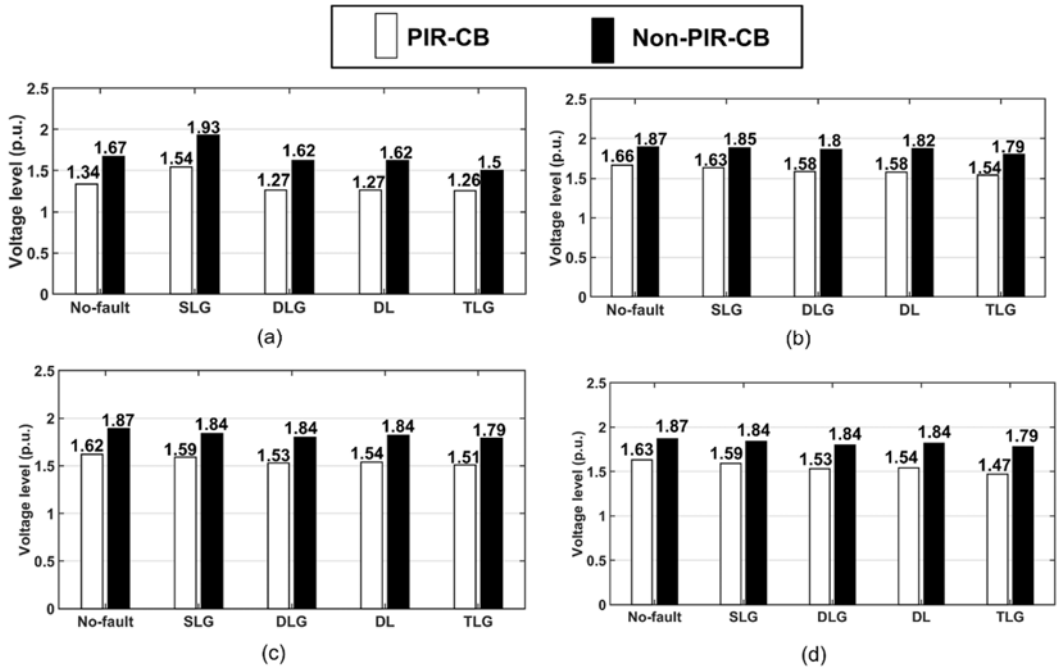

Fig. 2.8 Comparative evaluation of the proposed methodology and usual PIR (stand-alone) methodology during energization of a partially discharged (a) UCTL, (b) 30%, (c) 50%, and (d) 70% compensated SCTL.

2.6.3 Effect of strong and weak source

In order to evaluate performance of the proposed algorithm in context to grid strength, three different sources having different parameters, as shown in Table 2.3, have been considered. In this case, a simulation study during energization of a partially discharged 200-km long UCTL and 450-km long SCTL has been carried out for the proposed methodology (which contains both CSD and PIR-CB) and the usual PIR methodology. For all these cases, the same numbers of faulted and non-faulted cases, as mentioned in previous sub-section, have been generated.

Table 2.3 Performance of the proposed methodology against varying short circuit capacity of the source.

Parameters	Length of line (km)	S1 (Strong source)	S2 (Weak source-1)	S3 (Weak source-2)
Short circuit level (kA)	---	40	28	11
Positive sequence impedance (Ω)	---	0.4115+ j 3.546	1.5 × S1	4 ×S1
Zero sequence impedance (Ω)	---	2.822 + j 10.08	1.5 × S1	4×S1
Level of switching surge (p.u.) for UCTL	200	1.47	1.47	1.46
Level of switching surge (p.u.) for SCTL	450	1.62	1.6	1.58

In this study, the dataset of 288 faulted cases and 02 non-faulted cases for UCTL and 864 faulted cases and 06 non-faulted cases for SCTL have been investigated for all three sources. It has been observed from Table 2.3 that the variation in secondary surge is negligible against change in short circuit level or grid strength.

2.6.4 Effect of weather conditions and line insulation

It has been reported in literature that the magnitude of trapped charges changes due to effect of weather conditions and line insulation. In order to evaluate performance of the proposed methodology, a simulation study during energization of a partially discharged 200-km long UCTL has been carried out considering variation in the decaying rate of the trapped charges in no-fault condition. In this study, at the time of energization of a partially charged UCTL, two extreme levels (i.e. 0.8 p.u. and 0.2 p.u.) of trapped charges at the end of protection dead time are considered. The simulation results of the study are shown in Fig. 2.9. It has been observed from Fig. 2.9 that the level of switching surge remains immune to the variation in the magnitude of the trapped charge due to weather conditions and line insulation.

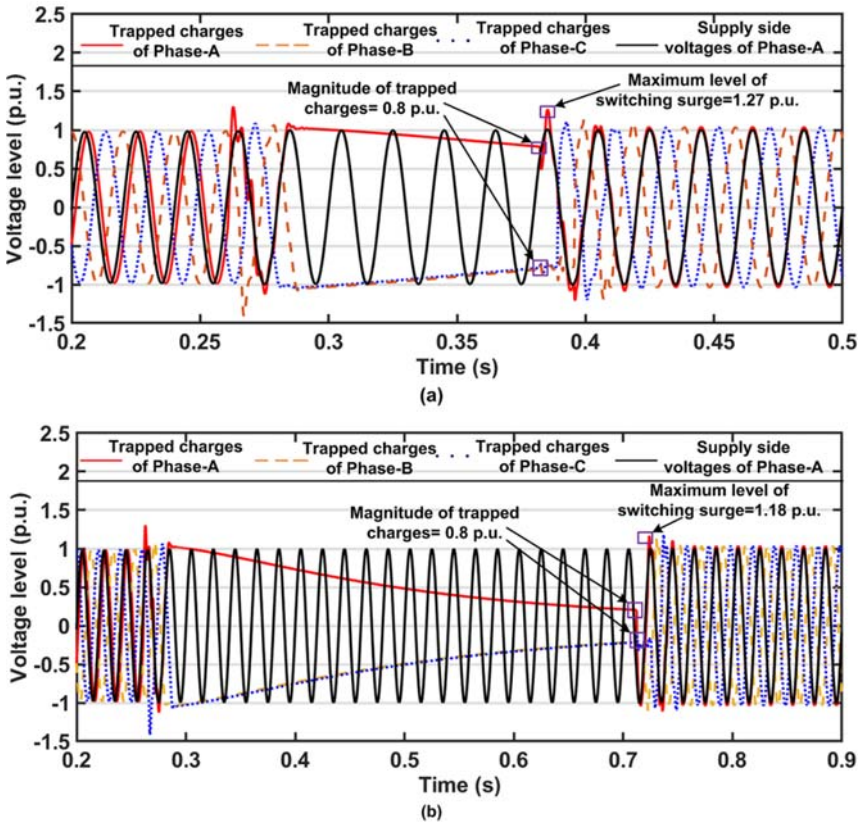

Fig. 2.9 Effect of different magnitude of the trapped charges (a) 0.8 p.u. and (b) 0.2 p.u. on the level of switching surge during energization of a partially discharged UCTL considering no-fault condition.

Moreover, Table 2.4 shows the summary of switching surge developed during energization of a partial discharged UCTL due to variation in the weather conditions. It is observed from Table 2.4 that the level of switching surge remains below 1.3 p.u. for both aforementioned cases.

Table 2.4 Performance of the proposed methodology considering change in decaying rate of trapped charges.

Sr. No	Level of trapped charge (p.u.)	Maximum level of switching surge (p.u.)
1	0.8	1.27
2	0.2	1.18

2.6.5 Effect of SA

In order to evaluate performance of the proposed methodology considering presence and absence of SA at both the ends of the line, a simulation study during energization of a partially discharged 200-km long UCTL and 450-km long SCTL has been carried out. Table 2.2 shows summary of various cases generated for the abovementioned situation. The simulation results are shown in Table 2.5. It has been observed from Table 2.5 that the difference in the level of switching surge with and without considering the effect of SA is minor.

Table 2.5 Simulation results with and without considering the effect of SA.

Sr. No	Type of transmission line	Condition (Fault)	Maximum level of switching surge (p.u.)		
			With SA	No-SA	Difference
1	UCTL	No-fault	1.51	1.52	0.02
		SLG fault	1.53	1.57	0.04
		DL fault	1.46	1.47	001
		DLG fault	1.46	1.46	0
		TLG fault	1.41	1.43	0.02
2	SCTL with 30% compensation	No-fault	1.56	1.57	0.01
		SLG fault	1.57	1.59	0.02
		DL fault	1.51	1.52	0.01
		DLG fault	1.5	1.5	0
		TLG fault	1.48	1.48	0
3	SCTL with 50% compensation	No-fault	1.49	1.49	0
		SLG fault	1.5	1.51	0.01
		DL fault	1.49	1.50	0.01
		DLG fault	1.48	1.48	0
		TLG fault	1.45	1.45	0
4	SCTL with 70% compensation	No-fault	1.35	1.35	0
		SLG fault	1.48	1.48	0
		DL fault	1.47	1.47	0
		DLG fault	1.46	1.46	0
		TLG fault	1.35	1.35	0

2.6.6 Effect of change in closing sequence

For staggered pole operation of CB, the closing phase sequence A-C-B has been reported in the literature [15] instead of proposed closing sequence (i.e. A-B-C). Comparative evaluation of both the aforementioned phase sequences in terms of level of switching surge has been carried out. In this study, energization of a partially discharged 200-km long UCTL and 450-km long SCTL has been carried out. Data sets, as shown in Table 2.2 for UCTL and SCTL, have been utilized. The simulation results are shown in Table 2.6. The switching surge is measured at the remote end of the line. It is to be noted from Table 2.6 that negligible variation in the level of switching surge is obtained during energization of partially discharged UCTL and SCTL, due to the change in phase sequence. Therefore, it can be said that the proposed methodology works satisfactory for both (A-B-C and A-C-B) closing phase sequences of the CB.

Table 2.6 Performance of the proposed methodology against change in closing sequence of the CB.

Sr. No	Type of transmission line	Condition (Fault)	Maximum level of switching surge (p.u.)		
			Closing sequence A-B-C	Closing sequence A-C-B	Difference
1	UCTL	No-fault	1.34	1.35	0.01
		SLG fault	1.54	1.61	0.07
		DL fault	1.27	1.31	0.04
		DLG fault	1.27	1.3	0.03
		TLG fault	1.26	1.3	0.04
2	SCTL with 30% compensation	No-fault	1.66	1.71	0.05
		SLG fault	1.63	1.69	0.06
		DL fault	1.58	1.62	0.04
		DLG fault	1.59	1.62	0.03
		TLG fault	1.55	1.60	0.05
3	SCTL with 50% compensation	No-fault	1.62	1.66	0.04
		SLG fault	1.59	1.62	0.03
		DL fault	1.53	1.54	0.01
		DLG fault	1.54	1.54	0
		TLG fault	1.51	1.53	0.02
4	SCTL with 70% compensation	No-fault	1.6	1.64	0.04
		SLG fault	1.57	1.59	0.02
		DL fault	1.53	1.56	0.03
		DLG fault	1.54	1.56	0.02
		TLG fault	1.47	1.52	0.05

2.6.7 Effect of change in fault inception and load angles

In the presented work, the impact of variation in fault inception and load angles have been analyzed on the developed CS technique for energization of partially discharged UCTL. Table 2.2 of the thesis shows summary of the parameters varied to generate simulation cases. In this table, it has been shown that the value of load angle is set as -30^0, whereas the fault inception angles have been considered as 0^0, 90^0, and 135^0. The results obtained in terms of switching

surge (p.u.) due to the variation in fault inception and load angles are plotted in Fig. 2.10 and Fig. 2.11, respectively. The results obtained for variation in fault inception angels 0^0 and 135^0 during energization of a partially discharged UCTL is shown in Fig. 2.10 (a) and (b), respectively. Conversely, the results obtained for load angle variation -30^0 and -10^0 are shown in Fig. 2.11 (a) and (b), respectively. It has been observed from Fig. 2.10 (a) and (b) that due to the variation in fault inception angle, the value of switching surge is varying in very narrow band. At the same time, with respect to Fig. 2.11 (a) and (b), it could be said that due to the variation in load angle, the level switching surge remains unaffected.

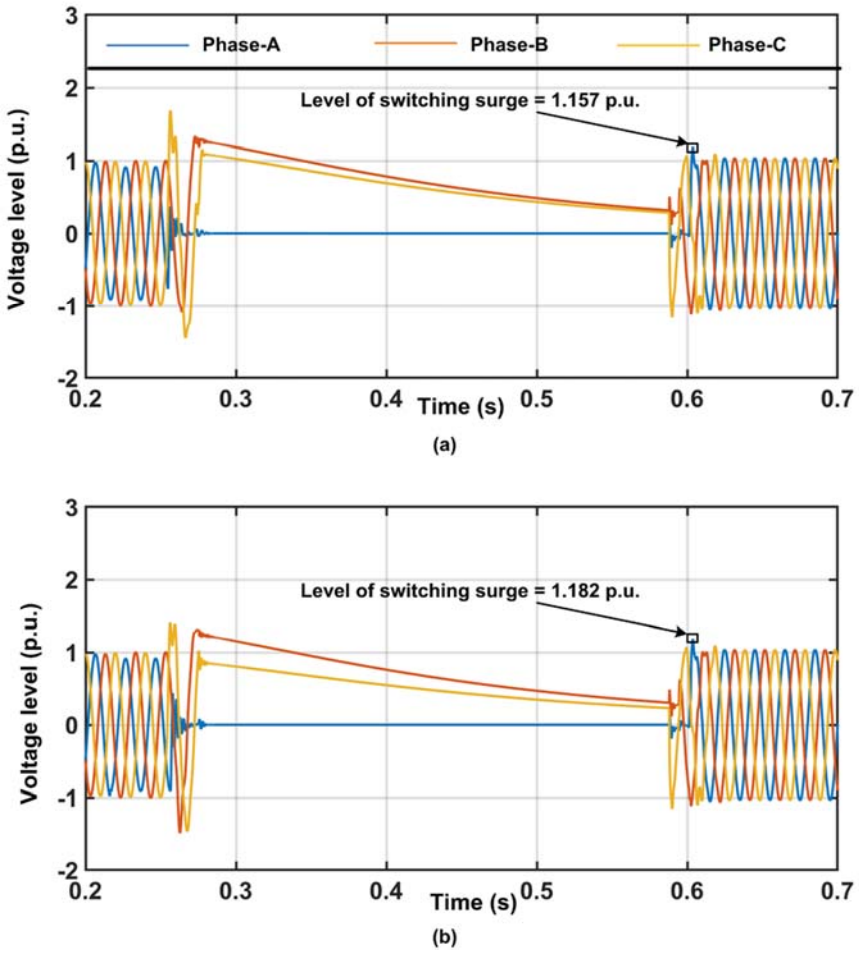

Fig. 2.10 Effect of fault inception angle during energization of a partially discharged UCTL for (a) 0^0 and (b) 135^0

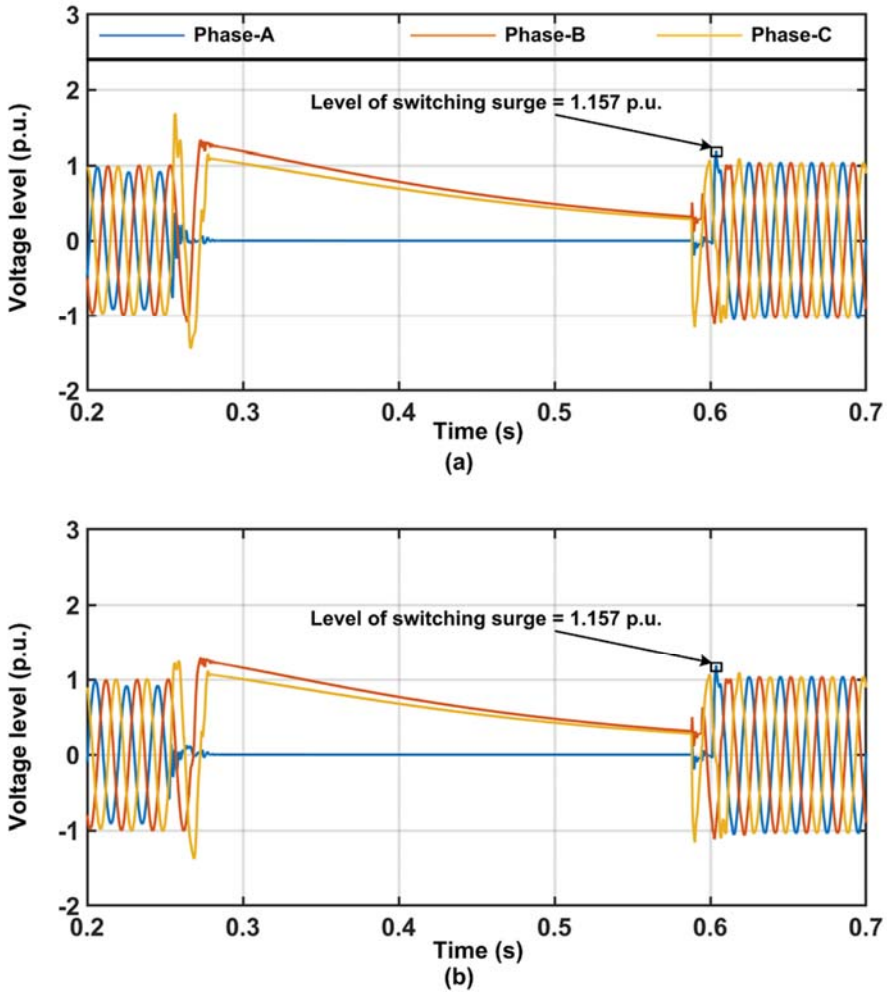

Fig. 2.11 Effect of load angle during energization of a partially discharged UCTL (a) -10^0 and (b) -30^0

2.7 Summary

This chapter presents a new methodology, which effectively mitigates the switching surge during energization/re-energization of UCTL and SCTL with the help of CSD with PIR-CB. Compared to the existing controlled switching strategy (both for UCTL/SCTL) that requires line side voltage signatures, the proposed methodology does not necessitate the same for SCTL and requires only the polarity of line side voltages at the time of de-energization for UCTL. The performance of the proposed methodology has been evaluated by generating diversified cases on 400 kV UCTL and SCTL using PSCAD/EMTDC software package. These cases were generated by varying parameters such as polarity of trapped charge, fault location, type of fault, fault resistance, and fault inception angle. The simulation results clearly indicate that the proposed methodology is able to further mitigate the switching surge of the order of 33% and 20% for UCTL and SCTL, respectively. The comparative evaluation of the proposed methodology with the usual PIR methodology indicates its effectiveness during statistical

variations of CB of the order of ±1 ms. The response of the proposed methodology remains immune to the effect of various parameters such as type of source, weather conditions, insulation resistance, closing phase sequence (A-C-B), and presence/absence of SA.

Chapter 3

Controlled switching of SCTL using line side voltages

3.1 Introduction

In this chapter, controlled switching technique for energization/re-energization of SCTL is discussed. As explained in section 1.5.3, the combination of CSD and PIR-CB is readily available in OHB scheme at UHV/EHV levels. Therefore, a new controlled switching strategy using CSD with PIR-CB is presented for mitigation of the level of switching surge during energization/re-energization of SCTL. It is observed that V_L attains oscillatory waveform during the dead time of CB in case of re-energization of SCTL. Subsequently, V_{GAP} also attains oscillatory nature, which makes zero crossing instant non-repetitive in nature. Therefore, it is difficult to predict and implement zero crossing instant of V_{GAP} as CS target. The controlled switching targets other than V_{GAP} can be derived by the suggested scheme. Verification of the presented scheme has been done by modelling an existing 400 kV Indian sub-station network in PSCAD/EMTDC environment. The parameters such as ground clearance, distance between two phase conductors, type of conductors, and distance between phase conductors to top ground wire have been determined based on Indian electricity rules. The developed technique requires line side voltage measurement during the dead time of CB. In addition, it can also be extended for discriminating permanent fault with temporary fault.

3.2 Network configuration

The proposed technique uses the combination of CSD with PIR-CB. This combination is readily available in EHV/UHV substations equipped with OHB and non-switchable breaker schemes [101]. The single-line-diagram of an existing 400 kV Sub-Station (S/S), located at Dehgam, Gujarat, India, containing the said type of combination is shown in Fig. 3.1. As shown in Fig. 3.1, seven transmission lines are connected to 400 kV bus located at Dehgam S/S. Among all the lines, 315 km long SCTL connected between Dehgam and Nagda S/S is considered in this study. The 50 MVAr shunt reactors are installed on this line at both ends. The line is designed with Aluminum Conductor Steel Reinforced (ACSR) twin conductor. The enlarged portion of Fig. 3.1 shows the actual connection configuration of the line connected between Dehgam and Nagda S/S. As observed from Fig. 3.1 the CSD is used for switching of shunt reactor whereas PIR-CB is kept for switching of the transmission line. Subsequently, the tie-line

CB that contains both CSD and PIR is utilized for switching of shunt reactor and UCTL.

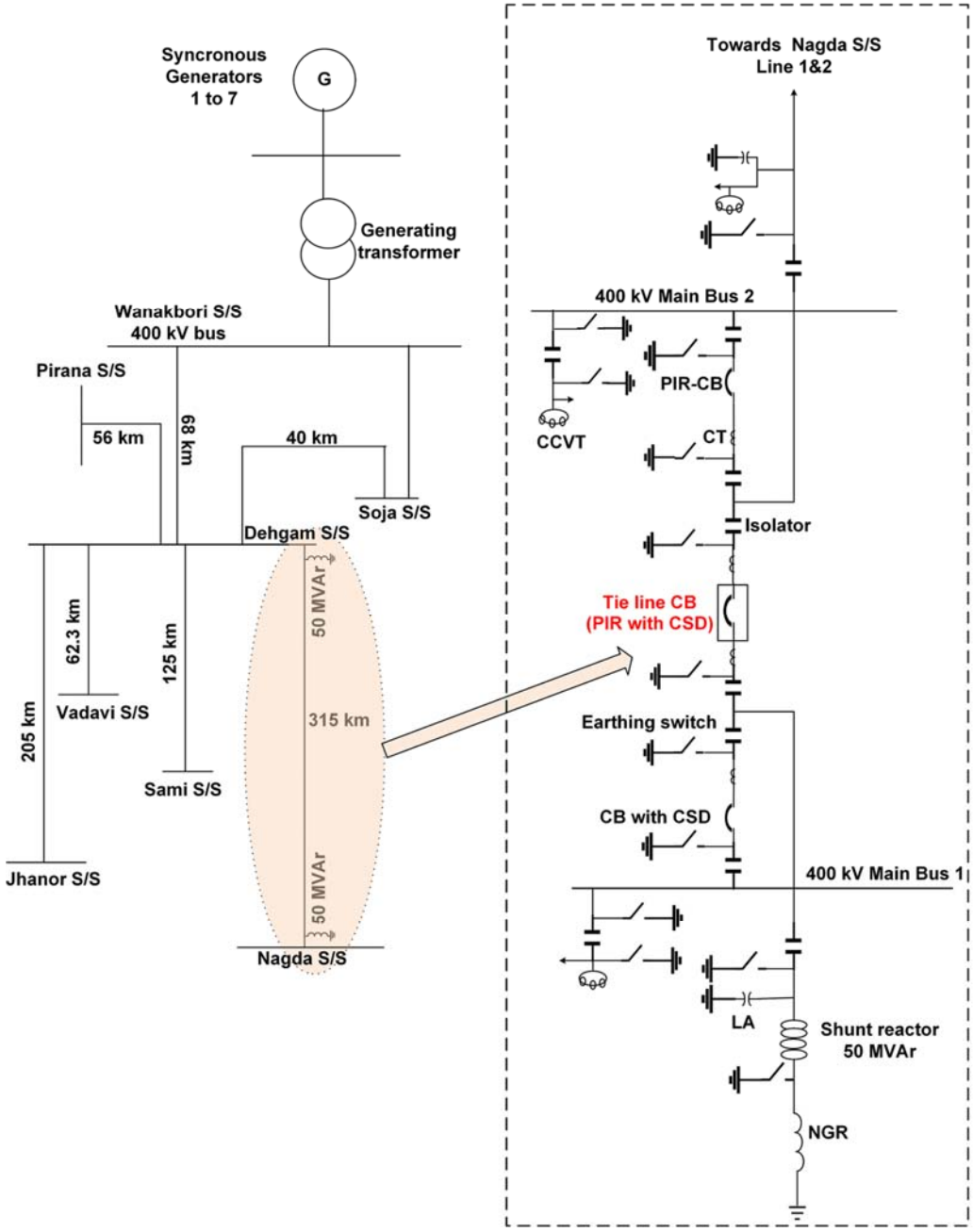

Fig. 3.1 Single-line-diagram of a 400 kV existing S/S in India.

3.2.1 Proposed algorithm

Fig. 3.2 shows the flowchart of the proposed algorithm. As shown in Fig. 3.2, the

proposed algorithm is activated with the detection of the changeover status of the CB. If the CB is detected open than the auto-reclosing attempt of the SCTL is checked. The non-recloser operation indicates energization of fully discharged SCTL. Therefore, the optimal closing target is zero crossing instant of the supply side voltage. This closing target is defined as Target-B in the proposed algorithm. In case of auto-reclosing, the line side voltages of all the three-phases are acquired during the dead time of CB (300 ms).

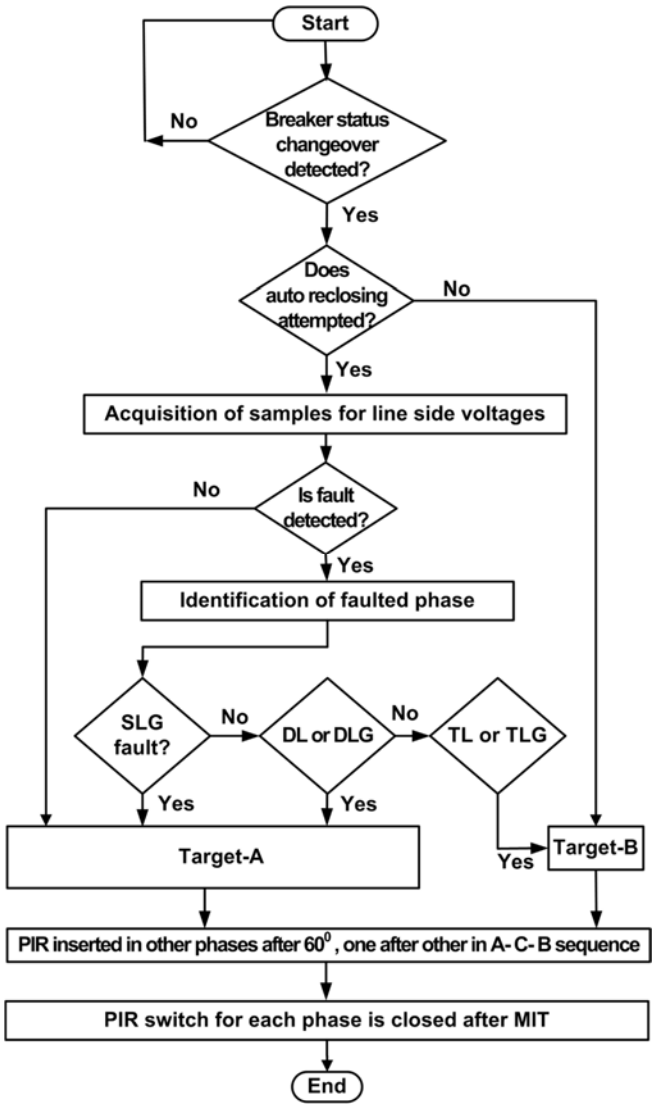

Fig. 3.2 Flowchart of the proposed algorithm

In this situation, it is necessary to detect the fault and faulted phase before reclosing attempt is performed. Here, task of discriminating faulted situation from normal condition as well as faulted phase identification is achieved with the help of fault detection and phase identification algorithm reported in [99]. The proposed algorithm can also be extended for

discrimination between temporary fault and permanent fault. The detailed procedure is given in section 3.4.4. During SLG, DL, and DLG faults, the energization of a partially discharged SCTL (reclosing) is done at closing Target-A. At the same time, for TL and TLG faults, energization of the SCTL has been carried out at Target-B. On the other hand, in case of no-fault situation (i.e. CB opens due to malopearation of the relay), energization of the partially discharged SCTL has been performed at Target-A.

These two targets (A and B) are insertion targets for PIR-CB. Therefore, after attaining these insertion targets, the PIR has been removed from the circuit after MIT in A-C-B sequence. In the proposed algorithm, energization of a partially discharged and fully discharged transmission line is carried out at Target-A and Target-B, respectively. The process of determination of the optimal closing target (Target-A) is explained in the following sub-section.

3.2.2 Derivation of optimal closing Target-A

Fig. 3.3 (a) shows variation in line side voltage during de-energization (dead time of CB) of SCTL with 30% compensation level. The stepwise procedure for derivation of the proposed Target-A is given in Fig. 3.3 (b). As observed from Fig. 3.3 (b), the proposed technique utilizes instantaneous values of acquired line side voltages for achieving optimal closing Target-A. The proposed technique is based on a calculation of phasor values of line side voltages ($V[n]$) of all three-phases i.e. V_A, V_B, and V_C. These phasors values are obtained using a Discrete Fourier Transform (DFT) algorithm as per eq.(3.1).

$$V[n] = \sum_{t=0}^{N-1} v(t)\, e^{-j2\pi nt/N} \tag{3.1}$$

Where N is the number of samples in a window (80), n is the order of the harmonics, *V[n]* is the frequency domain output voltage signal in terms of Cartesian coordinate, *v(t)* is the instantaneous value of acquired voltage signal and *t* is the time instant. In the proposed technique, the DFT analysis has been carried out up to 7th harmonic components. Therefore, eq.(3.2) gives phasor values of the input line side voltages for 0 to 7th order harmonic components.

$$V[n] = \left[V_A[n],\ V_B[n],\ V_C[n]\right]^T \tag{3.2}$$

Where, n = 0 to 7 and V_A, V_B and V_C are the phasors values of voltage for A, B, and C phases, respectively. Afterwards, as per eq.(3.3), the addition of all three-phase phasor voltages has been performed with respect to its order of harmonics.

$$V_{ABC}[n] = V_A[n] + V_B[n] + V_C[n] \tag{3.3}$$

The signal obtained from eq. (3.3) has been further utilized to achieve the resultant signal (V_{Total}) as given in eq. (3.4).

$$V_{Total} = \left(V_{ABC}[0]\right) + \left(\sum_{m=1}^{m=7} \left|V_{ABC}[n]\right| \times \sin(m\theta + \varphi_{ABC}[n]) \right) \tag{3.4}$$

Where, $V_{ABC}[0]$ is the value of addition of three-phase dc components. Further, $|V_{ABC}[n]|$ and $\varphi_{ABC}[n]$ are magnitude and angle of addition of three-phase fundamental to 7th order harmonic components, respectively. Moreover, $\theta = \omega \times t$ in which ω is the angular velocity of fundamental component of voltage in rad/sec.

It has been observed from past-published literature that the level of switching surge during energization of a partially discharged SCTL can be minimized by limiting gap voltage (V_{GAP}) across the contacts of CB [16], [74]. However, in case of SCTL, zero crossing instant of V_{GAP} does not repeat after fixed time interval. Therefore, it is difficult to predict the next zero crossing instant of V_{GAP} after the dead time of the CB. In this regard, an attempt has been made by presenting a new controlled reclosing strategy that limits the level of switching surge during reclosing of the SCTL. Here, the reference signal (V_{Total}) repeats its zero crossing after fixed interval. Hence, it is easy to predict the next zero crossing instant of the reference signal. Subsequently, it can be easily implemented in the real field.

In order to determine the optimal closing Target-A during de-energization of a partially discharged SCTL, a simulation study has been carried out. Fig. 3.3 (c) and (d) show the simulation results in terms of gap voltages across phase-A ($V_{GAP(A)}$) and V_{Total}. It has been observed from Fig. 3.3 (c) and (d) that the zero crossing of $V_{GAP(A)}$ and V_{Total} occurs almost at the same instant for SCTL having 30% and 70% compensation, respectively. Therefore, the first zero crossing instant of the V_{Total} after dead time of the CB is considered as optimal closing target (Target-A). In addition, in case of TL and TLG faults, the trapped charges on SCTL are almost zero. Therefore, energization of SCTL after the dead time of CB is as good as energization of fully discharged SCTL. Utilizing this fact, this energization has been performed considering zero crossing instant of supply side voltage, which is same as gap voltage zero instant. This closing target is considered as Target-B.

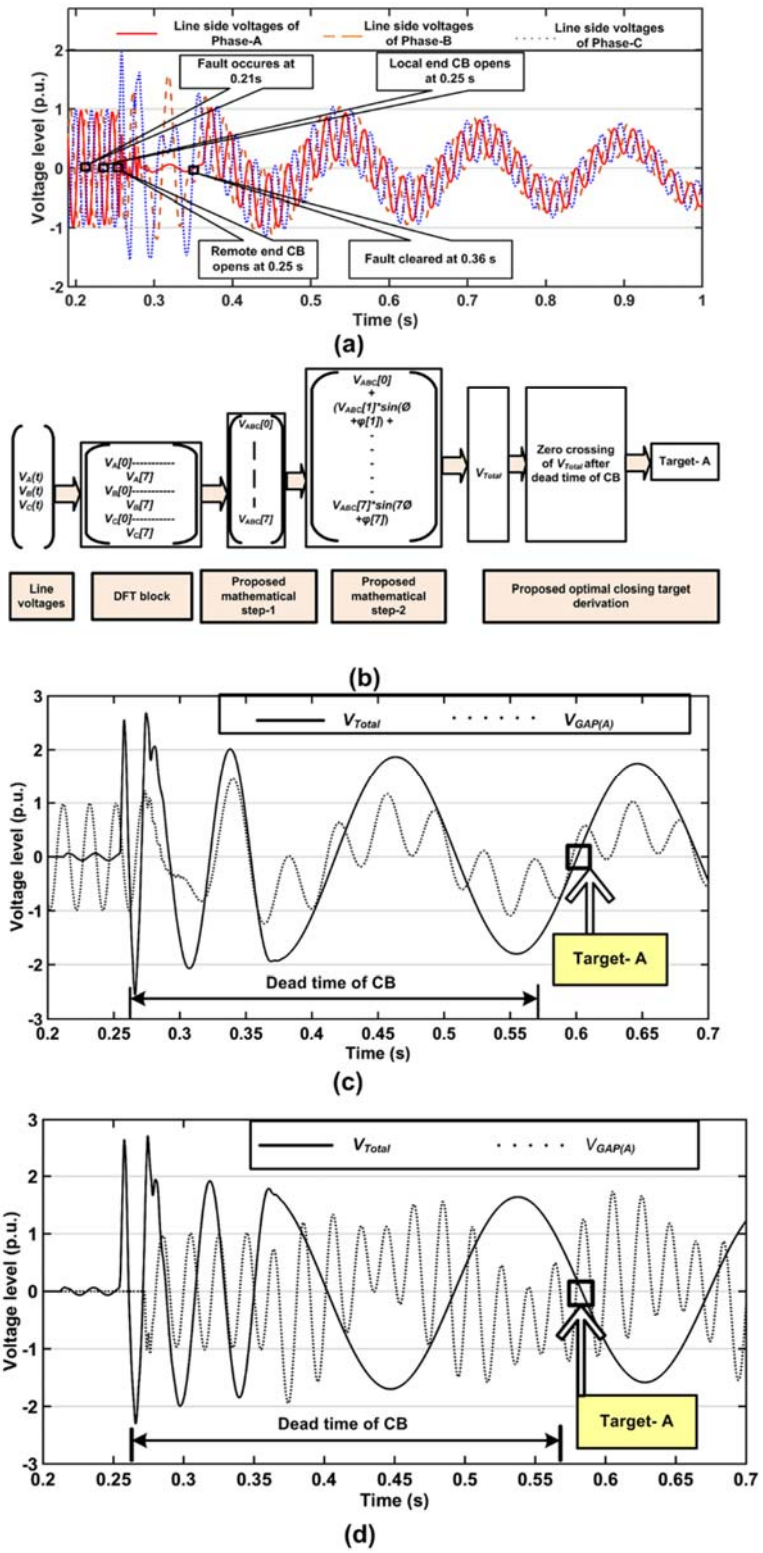

Fig. 3.3 (a) Variation in the level of line side voltage during dead time of CB, (b) stepwise procedure for derivation of the proposed target, (c) derivation of optimal closing Target-A for 30%, and (d) 70% compensated SCTL .

3.3 Simulation and modelling

3.3.1 Modelling of the network

In order to validate the proposed technique, a simulation model of an Indian 400 kV network containing Dehgam S/S and Nagda S/S (as shown in Fig. 3.1) has been developed in the PSCAD/EMTDC environment. Fig. 3.4 (a) shows the single-line-diagram of the developed simulation model. In this model, Dehgam S/S is considered as source-end (local end) and Nagda S/S is treated as remote end (load end). It has been observed from Fig. 3.4 (a) that both sub-stations are equipped with OHB schemes having CSD and PIR at tie line CB. In this model, the SCTL has been developed using frequency dependent phase model of PSCAD/EMTDC software package [83]. Furthermore, 369 kV switching class SAs have been designed and located at both ends of the line [97]. Moreover, as per Indian Electricity rules [90], the ground clearance, spacing between ground & phase conductors, and spacing between two phase conductors are determined for SCTL. In the presented technique, samples of voltage signals have been acquired at a sampling frequency of 4 kHz with a fundamental frequency of 50 Hz [95], [96]. Likewise, the switching surge has been measured at remote end (i.e. at Nagda S/S). The values of shunt reactors and NGRs are calculated as per the equations given in [98]. The parameters of source and line along with parameters of conductor configuration are mentioned in Appendix A2.

3.3.2 Modelling of PIR

In order to determine the optimal value of PIR and its MIT, a simulation study has been carried out for UCTL according to the procedure reported in [76]. Generally, the level of switching surge during energization of a partially discharged UCTL/SCTL depends on (i) the value of the resistance (R) offered by PIR, (ii) MIT of the PIR and (iii) insertion instant of PIR. In order to identify independent effect of any one parameter on the level of switching surge, the other two parameters are kept at fixed value.

3.3.2.1 Calculation of R

Normally, the value of MIT is of the order of half cycle (in this case it is 180^0 = 10 ms for a fundamental frequency of 50Hz) [2], [7]. As mentioned earlier, the optimal value of PIR (R) has been determined by observing the variation in the level of switching surge against different values of PIR (in terms of the ratio of the value of PIR (R) to the surge impedance of the line (Zc)). Here, variation in the ratio of R/Z_C is considered from 0 to 1.4 [76].

In order to develop model of PIR-CB, it is required to calculate the optimal value of R and its MIT. To achieve this task, a simulation study has been carried out by utilizing

parameters/data of UCTL as reported in [90]. During this study, energization of a partially discharged UCTL has been performed in A-C-B sequence considering no-fault situation (as it creates highest level of switching surge compared to faulted situations). At the same time, in order to verify the level of switching surge, PIR is inserted at two different instants (i) at peak of the source voltage when the polarity of source side voltage is opposite to the polarity of the trapped charge (Target-1) (ii) at supply voltage zero (Target-2). The simulation results in terms of level of switching surge against different ratio of R/Z_C are shown in Fig. 3.4 (b).

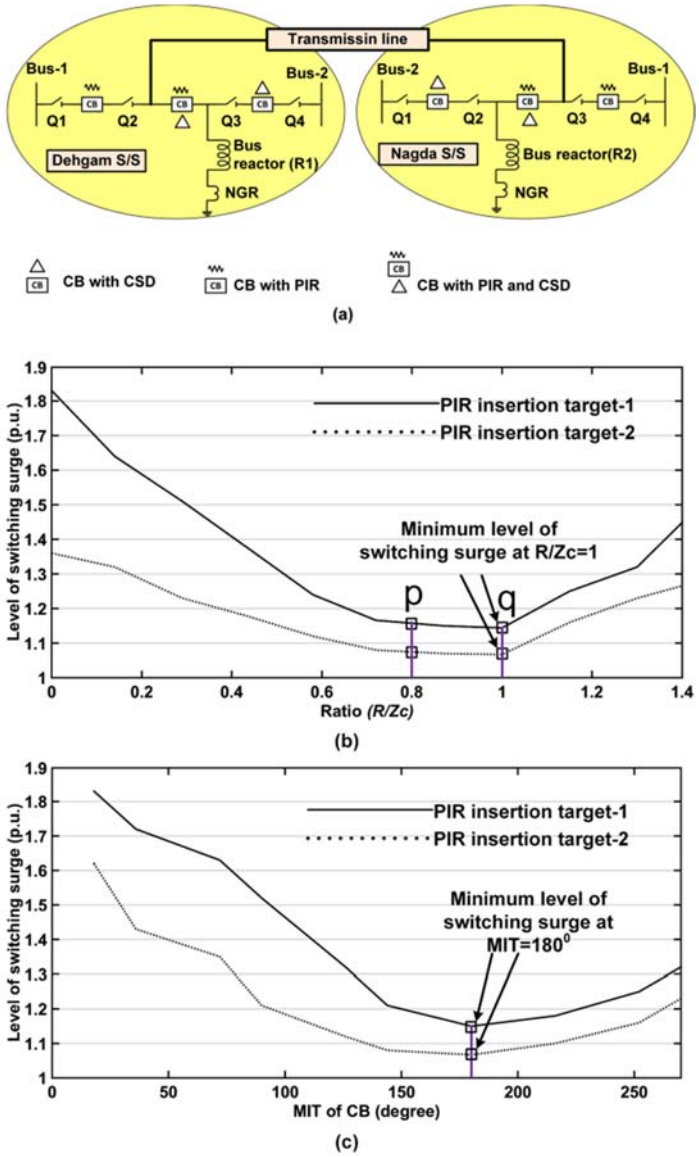

Fig. 3.4 (a) Developed simulation model of power system network, (b) level of switching surge for different value of PIR, and (c) level of switching surge for different value of MIT.

It has been observed from Fig. 3.4 (b) that the level of switching surge reduces up to

point ‘p’ (R/Z_C is around 0.8). Thereafter, it remains almost constant up to point ‘q’ (R/Z_C is 1.0). Hence, the minimum value of the switching surge is obtained when the value of R/Z_C = 1.0 for both insertion targets. In this modal, this relation is utilized for calculation of R for PIR-CB.

3.3.2.2 Calculation of MIT

In order to achieve optimal value of MIT, the value of PIR and its insertion instant are kept constant during the above simulation work (in this case, the value of R/Z_C = 1.0). In this study, variation in the level of switching surge against different values of MIT (from 18^0 to 288^0) during abovementioned two different closing targets has been observed. Fig. 3.4 (a) Developed simulation model of power system network, (b) level of switching surge for different value of PIR, and (c) level of switching surge for different value of MIT. Fig. 3.4 (c) shows the simulation results in terms of level of switching surge against different values of MIT. It has been observed from Fig. 3.4 (c) that the minimum level of switching surge is obtained when the value of MIT is 180^0. Moreover, it is to be noted from Fig. 3.4 (b) and (c) that the level of switching surge is lower in case when the closing is performed at Target-2 compared to Target-1.

3.3.2.3 Optimal insertion instant

In order to determine the optimal insertion instant of PIR, the value of PIR and MIT are kept at fixed values. In the proposed work, the optimal values of PIR and MIT, obtained from the above mentioned simulation work, have been utilized. The procedure of obtaining optimal target (Target-A) has been thoroughly described in section 3.2.2.

3.3.3 Concept of controlled switching device

The proposed methodology attains optimal making target using CSD that converts randomly closing command into controlled closing command. It uses different modules to perform various tasks. Fig. 3.5 (a) shows the conceptual layout of CSD [74]. As shown Fig. 3.5 (a), the entire CSD is divided into three main parts (i) input unit (ii) output unit and (iii) central unit.

3.3.3.1 Input unit

This unit includes measurement module, feedback module, and command module. The measurement module collects the samples of three-phase voltages and currents from line side and busbar side. The function of feedback module is to acquire feedback from compensating sensors. The feedback signal provides data of MOT of last operation, dc voltage, and air/hydraulic pressure of CB along with ambient temperature. These parameters are further utilized for calculation of MOT for next operation. The command module receives random

closing/opening command raised by SCADA or manual operation. The received random command is further given to the central unit, which converts it into controlled command. However, in case of emergency, the received random command can be avoided with the help of bypass module.

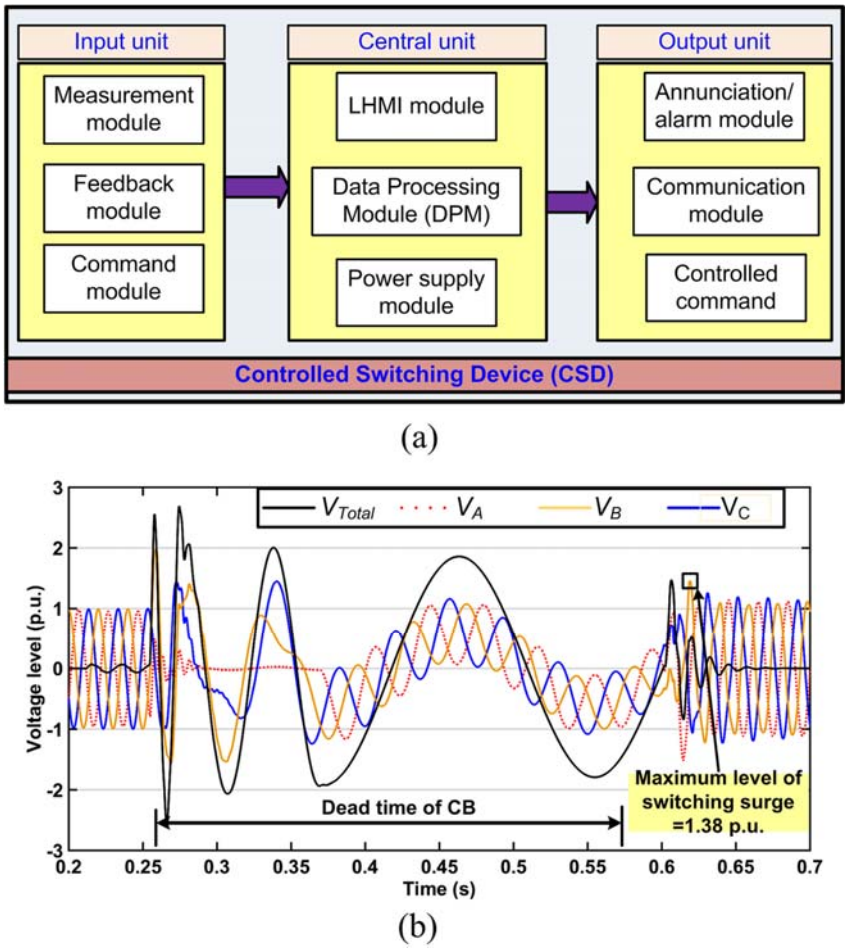

Fig. 3.5 (a) Conceptual layout of CSD and (b) implementation of the proposed methodology during SLG fault for SCTL with 30% compensation level.

3.3.3.2 Central unit

This unit includes Data Processing Module (DPM), Local Human Machine Interference (LHMI) module, and Power supply module. The function of DPM is to process received random command and captured voltage signals (with help of measurement module) as per the presented algorithm. At the end of the proposed algorithm, a controlled closing target (Target-A or Target-B)) is generated. Further, these data are also stored in a non-volatile memory, which is a part of DPM. The LHMI module is used to modify/alter the settings of the device. The power supply module is utilized to supply different dc voltages to various modules.

3.3.3.3 Output unit

This unit includes a command module, annunciation/alarm module, and a communication module. The command module transfers the controlled command from CSD to the CB for proper operation of CB according to the derived target. Here, in case of any abnormality/emergency, the annunciation/alarm module provides an alarm. Moreover, in order to communicate with different Intelligent Electronic Devises (IEDs) located in the control room of S/S, the communication module is provided. This module supports protocols such as IEC 61850-8-1, IEC 61850-9-2LE and Hyper Text Transfer Protocol (HTTP) over Ethernet. Furthermore, the Ethernet based communication system uses RJ-45 or fibre optic multimode L-C connector. At the end, the events are captured/recorded using DR using the communication module.

3.3.4 Simulation cases

In order to evaluate performance of the proposed methodology, large numbers of simulation cases have been generated. Table 3.1 shows the summary of simulation cases generated by changing different operating and systematic parameters such as type of connection configuration of shunt reactor, length of line, level of compensation, fault location, fault duration, fault inception angle, types of fault, fault resistance, and load angle.

Table 3.1 Summary of simulation cases generated for SCTL

Event	Parameter variation	Number of cases	Total cases generated
Fault condition	Length of line (km): 315 and 400	(2)	2×2×3×4×2×3×3×2×3=5184
	Type of connection configuration: Double ended and single ended	(2)	
	Level of compensation: 30%, 50%, and 70%	(3)	
	Types of fault: A-G, A-B, A-B-G, and A-B-C-G	(4)	
	Fault resistance (Ω): 0.01 and 100	(2)	
	Fault duration (ms): 100, 150, and 220	(3)	
	Fault location(% of line length): 0, 50, and 100	(3)	
	Load angle: 100 and 300	(2)	
	Fault inception angle: 00, 900, and 1350	(3)	
Number faulted cases generated			5184
No-fault condition	Length of line (km): 315 and 400	(2)	2×2×3=12
	Type of connection configuration: Double ended and single ended	(2)	
	Level of compensation: 30%, 50%, and 70%	(3)	
Number of no-fault cases generated			12
Overall cases generated			5196

It has been observed from Table 3.1 that 5184 cases have been generated for fault condition whereas 12 cases have been simulated for no-fault situation. Hence, a total of 5196 (5184+12) cases as a whole, have been investigated in this presented work.

3.4 Evaluation of the proposed technique

Performance of the proposed methodology has been evaluated by considering different level of compensation, presence/absence of week source and the effect of SA. The results obtained for various cases are discussed in the following sub-sections.

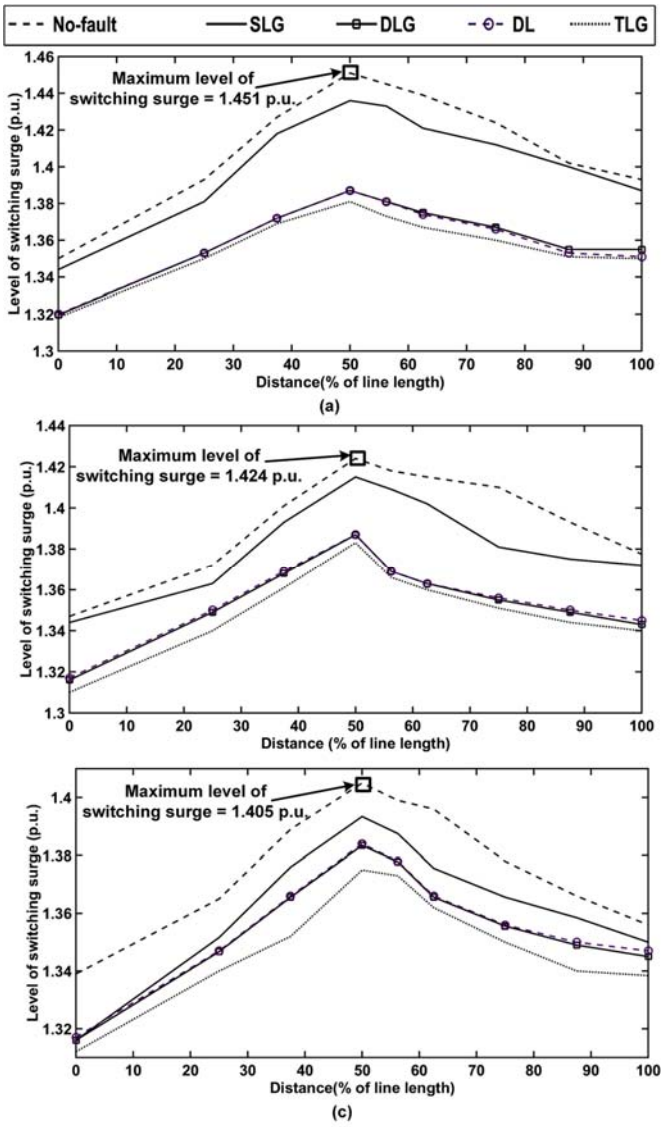

Fig. 3.6 Level of switching surge for with (a) 30%, (b) 50%, and (c) 70% compensated 400-km long partially discharged SCTL.

3.4.1 Effect of compensation level

In order to evaluate response of the proposed scheme on different level of compensation, energization of a partially discharged SCTL is carried out for 30%, 50% and 70% of compensation level during faulted and no-fault conditions. Fig. 3.6 (a), (b), and (c) shows the

results obtained in terms of overvoltage profile across length of the line for 30%, 50% and 70% compensation level, respectively. It is to be noted from Fig. 3.6 (a) - (c) that the level of switching surge increases from sending end (0% of line length) to receiving end (100% of line length) and, becomes maximum at the mid-point of the line. Thereafter, it decreases gradually from the mid-point to the receiving end. It has been further noticed from Fig. 3.6 (a) - (c) that the highest level of the switching surge (1.45 p.u.) is observed during no-fault situation with 30% compensation level at the mid-point of the line. However, at remote end, its value is 1.39 p.u. Furthermore, it has been observed that the level of switching surge is always higher in case of SLG fault as compared to other types of faults.

3.4.2 Influence of SA

In order to evaluate performance of the proposed methodology considering presence and absence of SA at both the ends of the line, a simulation study has been carried out. The performance of the proposed scheme has been evaluated on various cases as mentioned in. Table 3.2 shows the simulation results given by the proposed scheme in terms of level of switching surge at the remote end during the presence and absence of SA in the line. It has been observed from Table 3.2 that there is a marginal change in the level of switching surge during energization of a partially discharged SCTL for various cases of with and without considering SA.

Table 3.2 Performance of the proposed methodology considering the effect of SA at remote end of line

Different conditions	Level of switching surge (p.u.)		
	With SA	Without-SA	Difference in the level of switching surge (p.u.)
No fault	1.393	1.425	0.032
Faulted	1.387	1.416	0.029

3.4.3 Effect of grid strength

In order to evaluate performance of the proposed algorithm in context to grid strength, three different sources (S1, S2, and S3) having different parameters, as shown in Table 3.3, have been considered. For all these cases, the same numbers of faulted and non-faulted cases, as mentioned in previous sub-section, have been generated. The dataset, as mentioned in Table 3.1, have been investigated for all three sources. It has been observed from Table 3.3 that the variation in the level of switching surge is negligible even with varying short circuit level or grid strength.

Table 3.3 Performance of the proposed methodology against different short circuit capacity of the source.

Parameters	Length of line (km)	S1 (Strong source)	S2 (Weak source-1)	S3 (Weak source-2)
Short circuit level (kA)	---	40	28	11
Positive sequence impedance Ω)	---	0.4115+ j 3.546	1.5 × S1	4 ×S1
Zero sequence impedance Ω)	---	2.822 + j 10.08	1.5 × S1	4×S1
Maximum level of switching surge (p.u.) for non-faulted situations	400	1.393	1.39	1.39
Maximum level of switching surge (p.u.) for faulted situations	400	1.387	1.386	1.385
Short circuit level (kA)	---	40	28	11
Positive sequence impedance Ω)	---	0.4115+ j 3.546	1.5 × S1	4 ×S1
Zero sequence impedance Ω)	---	2.822 + j 10.08	1.5 × S1	4×S1
Maximum level of switching surge (p.u.) for non-faulted situations	400	1.393	1.39	1.39
Maximum level of switching surge (p.u.) for faulted situations	400	1.387	1.386	1.385

3.4.4 Discrimination between temporary and permanent fault

Discrimination between temporary and permanent fault can be identified by the proposed technique with the help of measurement of line side voltages. By analysing the nature of V_{Total} in terms of time taken to complete one cycle during fault and after the fault clearly distinguishes permanent fault with temporary fault. In order to prove authenticity of this concept, the simulation study has been carried out by considering two compensation levels (i.e. 30% and 70%). In this study, following sequence has been performed.

- Occurrence of a SLG fault at 0.21 s.
- Opening of remote end CB after two cycles (i.e. at 0.25 s).
- Opening of local end CB after one cycle of the opening of remote end CB (i.e. at 0.27 s).
- Then the fault is cleared after 150 ms (i.e. at 0.36 s). In this situation, most of the trapped charge of the faulted phase has been drained to earth due to SLG fault whereas rest two phases are healthy. Around 0.37 s, the trapped charge of faulted phase attains almost same magnitude compared to other two healthy phases. Subsequently, it will start oscillating with other two phases.

Fig. 3.7 (a) and (b) show the simulation results of the study. It is to be noted from Fig. 3.7 (a) and (b) that the time taken by V_{Total} to complete one cycle is almost 100 ms in case of permanent fault. This is indicated by Zone-1 in both the figures. Conversely, in case of transient

fault (after the clearance of fault), the time taken by V_{Total} is around 200 ms. This is indicated by Zone-2 in both the figures. In order to further verify the said concept, several simulations, in terms of permanent and temporary fault with varying parameters, have been performed. shows the time taken by V_{Total} to complete one cycle. It has been observed from that discrimination between permanent and temporary fault can be carried out with the help of time taken by V_{Total}. Here, different temporary fault conditions such as fault sustains for 100 ms, 150 ms , and 200 ms are considered. It has been observed from that the discrimination between temporary and permanent fault can be achieved by analyzing waveform of $V_{Total.}$

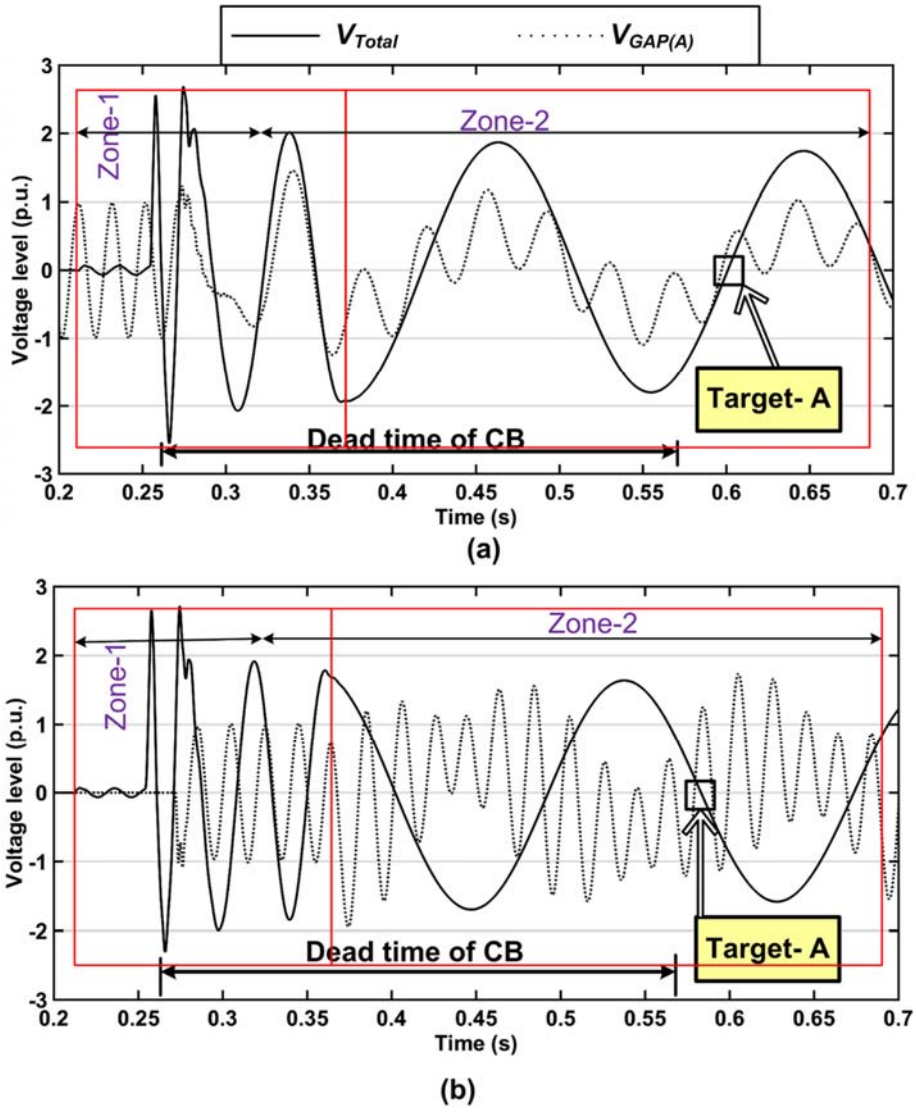

Fig. 3.7 Fault discrimination between temporary and permanent fault using proposed methodology for (a) 30%, (b) 70% compensated SCTL.

3.5 Comparative evaluation of the proposed methodology with CSD only

The quality factor is defined as the ratio of power stored to power dissipated in R-L series

circuit. Subsequently, in case of shunt reactor and NGR, it is the ratio of inductive reactance to resistance of the circuit. It has been observed that the value of resistance (R_s) is very less compared to inductive reactance (X_{11}) for shunt reactor and NGR [98], [102].

The design of shunt reactor and NGR has been carried out using equation (3.5) and (3.6), respectively [98], [102].

$$X_{11} = \left(1/(\eta \times \beta c)\right) \tag{3.5}$$

$$H = 0.002 \times Q \tag{3.6}$$

Where, X_{11} represents positive sequence reactance of the shunt reactor. η and βc stands for level of compensation and positive sequence susceptance of the transmission line, respectively. Further, H and Q represents power loss and rating of NGR, respectively. Additionally, it has been reported in [102] that the power loss in shunt reactor and NGR is only 0.2% of its total ratting.

Table 3.4 Time taken by V_{Total} to complete one cycle during permanent and temporary fault.

k (%)	Type of fault with fault resistance (R_f in Ω)	Time up to which fault sustains (T_f in ms)	Time taken by V_{Total} to complete one cycle	
			during permanent fault (ms)	in case of temporary fault (ms)
30	SLG with R_f=0.001	100	118	186
		150	126	184
		200	118	192
	SLG with R_f=100	100	92	186
		150	93	186
		200	91	187
50	SLG with R_f=0.001	100	118	186
		150	126	184
		200	118	192
	SLG with R_f=100	100	92	186
		150	93	186
		200	91	187
70	SLG with R_f=0.001	100	116	191
		150	117	192
		200	116	191
	SLG with R_f=100	100	91	192
		150	92	192
		200	91	191
k is the compensation level				

Hence, the value of resistance is very low compared to reactance of shunt reactor and NGR. Additionally, it has been reported in [102] that the resistance of the NGR is negligible

with respect to its reactance. The data of NGR, as obtained from real field (one of the substation in India), are depicted in Appendix A2.

Comparative evaluation of the proposed methodology in terms of switching surge with the methodology suggested in [80] is depicted in Table 3.5.. It is to be noted from Table 3.5 that the level of switching surge attained by the proposed methodology is lower than the value obtained by the methodology suggested in [80]. Further, at low level of compensation of SCTL, the proposed methodology gives better result as the methodology suggested in [80] may not be able to achieve optimal reclosing target for SCTL.

Table 3.5 Comparison between proposed methodology and methodology reported in [80]

Sr. No.	Length of line (km)	k (%)	R_s (Ω/ phase)	X_{11} (Ω/ phase)	Quality factor	Switching surge (p.u.) given by	
						Scheme reported in [80]	Proposed scheme
1	315	30	9.35	4675.94	500	It is not possible to achieve optimal closing target.	1.33
2		50	5.61	2805.56	500	1.59	1.32
3		70	3.51	2003.98	570.65	1.35	1.3
4	400	30	7.24	3618.37	499.77	Comparison is not possible due non-availability of reported data.	1.4
5		50	4.34	2171.02	500.23		1.38
6		70	3.11	1550.73	498.50		1.36
k is the compensation level							

3.6 Comparison of the proposed technique with the existing technique

The latest generation of CBs available in market have mechanical and dielectric characteristics that can attain the closing target with an accuracy of ±1ms. The MOT of the CB changes due to statistical and systematic variations. The systematic variations in MOT have been observed due to external parameters such as variation in the ambient temperature, dc battery supply voltage, and aging effect (after the time of installation).While testing in laboratories, the systematic variation in operating time can be compensated in the controlled switching relays using suitable compensation curves. On the other hand, it would not be possible to compensate statistical variation in operating time of the CB.

In this presented work, an overall variation of ±1 ms due to the statistical variation in MOT & RDDS of the CB is considered. In order to evaluate performance of the proposed methodology, a simulation study has been carried out. During this study, energization of a partially discharged 400-km long SCTL is carried out using the proposed methodology (which contains combination of CSD and PIR-CB) and the controlled switching methodology reported

in [42]. For both techniques, various conditions such as no-fault, SLG fault, DLG fault, DL fault, and TLG fault have been analysed. Here, three different levels of compensation for SCTL (30%, 50%, and 70%) have been considered. Moreover, the level of switching surge is monitored at the remote end of the transmission line.

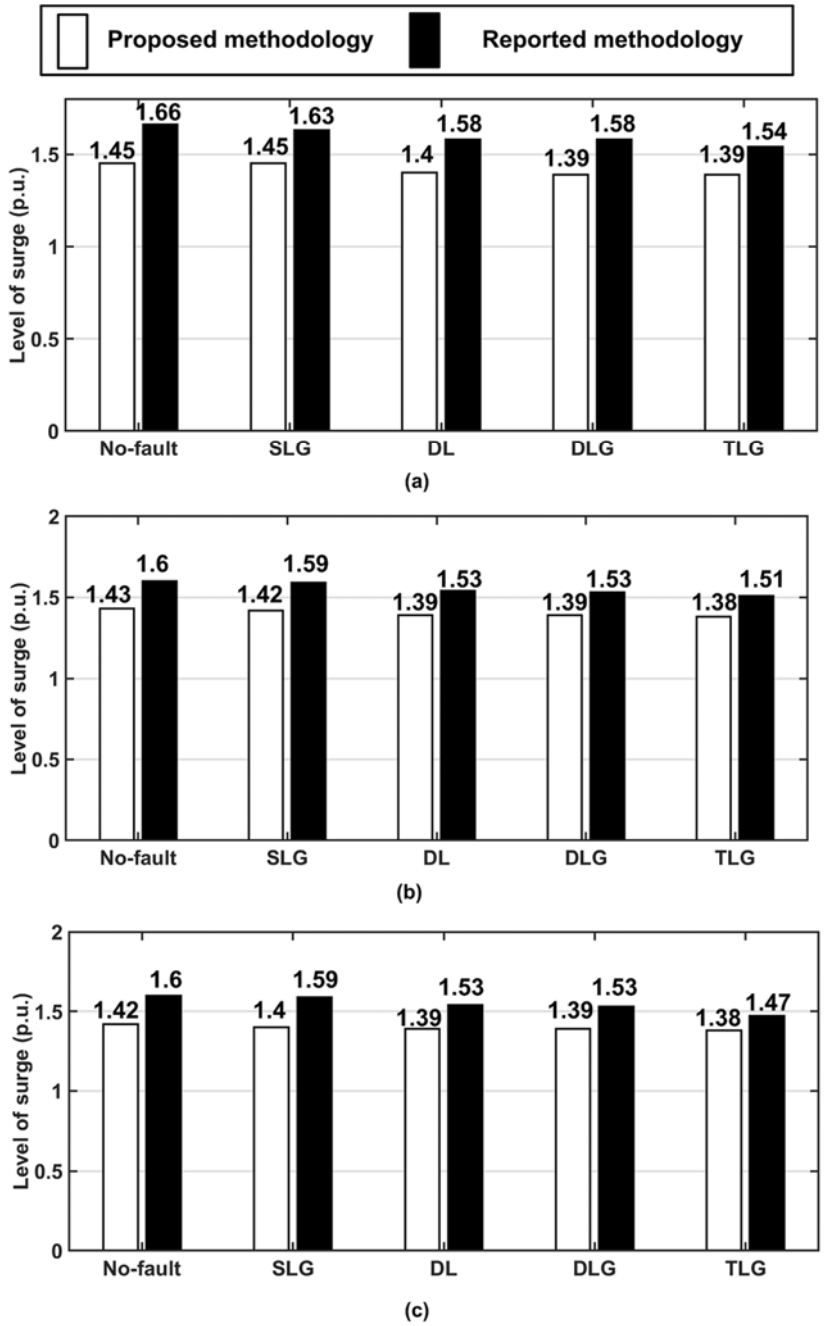

Fig. 3.8 Comparison of proposed methodology with the existing methodology for (a) 30%, (b) 50%, and (c) 70% compensated SCTL.

Fig. 3.8 shows comparative evaluation of the proposed methodology with the methodology reported in [42] during energization of a partially discharged 400-km long SCTL.

It is to be noted from Fig. 3.8 (a) that the maximum level of switching surge given by the reported controlled switching methodology and the proposed methodology is of the order of 1.66 p.u., and 1.45 p.u., respectively, during no-fault condition. On the other hand, during faulted (SLG fault) condition, the maximum level of switching surge is around 1.63 p.u. and 1.45 p.u. for reported controlled switching methodology and the proposed methodology, respectively.

Table 3.6 comparison of the proposed methodology with methodology reported in [42]

Sr. No	Proposed methodology	Methodology reported in [42]
1	The optimal reclosing target is determined based on line side voltage signature.	This methodology has considered supply side voltage zero crossing instant as an optimal reclosing target for SCTL without measuring line side voltages.
2	Based on past-published literature on reclosing of SCTL, zero crossing/minimum level of gap voltage (V_{GAP}) has been utilized as an optimal reclosing target. However, due to non-repeatable nature of V_{GAP}, it is difficult to predict reclosing target. On the other hand, the proposed methodology has suggested a new methodology in which V_{Total} has been used as a reclosing target for SCTL. This is derived by performing DFT of the line side voltages during the dead time of CB. Due to its repetitive nature, it is easy to predict the forth coming zero crossing instant. It is to be noted that V_{GAP} minimum and zero crossing of V_{Total} occurs almost at the same instant.	In this methodology, zero crossing instant of local end supply side voltages has been used as the optimal controlled reclosing target. Though this optimal target is repetitive in nature, it is not sure that zero crossing instant of supply voltage and V_{GAP} minimum occur at the same instant. Therefore, this methodology yields a compromised solution.
3	Utilization of this methodology reduces the level of switching surge compared to the methodology suggested in [21].	This methodology has utilized supply side voltage to determine optimal reclosing target for SCTL. However, utilization of supply voltage further increases the level of the switching surge.
4	Additionally, the proposed methodology is capable to differentiate between permanent fault and temporary fault. This is helpful to avoid damage to the power system equipment by blocking the operation of auto-reclosing attempt of the circuit breaker in case of permanent fault.	This methodology is not able to distinguish between permanent fault and temporary fault.

Similarly, it has been observed from Fig. 3.8 (b) and (c) that the maximum level of switching surge given by the proposed methodology is always lower than the reported controlled switching methodology during faulted/no-fault situations. The above discussion clearly indicates superiority of the proposed scheme over the reported controlled switching methodology in terms of reduction in the level of switching surge. The detailed comparison between the proposed methodology and methodology reported in [42] is shown in Table 3.6

3.7 Summary

This chapter presents a new methodology, which effectively mitigates the switching surge during energization/re-energization of a 400-km long SCTL with the help of CSD and

PIR-CB. The modelling of SCTL has been carried out considering the existing real field scenario in India. The performance of the proposed methodology has been evaluated by generating diversified cases on an existing 400 kV, 400-km long SCTL using PSCAD/EMTDC software package. These cases are generated by varying parameters such as length of the line, fault location, type of fault, fault resistance, level of compensation and fault inception angle. The simulation results clearly indicate that the proposed methodology is able to further mitigate the switching surge of the order of 30% compared to the existing methodology for SCTL. The comparative evaluation of the proposed methodology with reported methodology indicates its effectiveness particularly when the effect of MOT scatter of the CB (of the order of ±1 ms) is taken into account. At the same time, the response of the proposed methodology remains immune to the effect of various parameters such as presence/absence of SA and source strength. The philosophy presented here can also be extended for discrimination between permanent fault and temporary fault.

Chapter 4

Controlled Single Phase Reclosing Technique for SCTL

4.1 Introduction

In order to increase reliability, performance and efficiency of power system network, most of EHV and UHV transmission lines are equipped with single phase auto reclosing facility. In case of a SLG fault on the line, only faulted phase of the CB opens while maintaining continuous power supply for other two healthy phases. Utilizing this fact, a new controlled SPAR technique for SCTL is proposed in this chapter. The suggested technique is based on hybrid combination of CSD and PIR-CB, which is available without any additional investment in the substation designed at EHV level and above in Asia Pacific region. Further, the performance assessment of the proposed methodology has been carried out by modelling an existing 400 kV, SCTL in PSCAD/EMTDC software package. Unlike utilizing oscillatory and non-repetitive nature zero crossing instant of V_{GAP} as an optimal controlled reclosing target for SCTL, the proposed technique utilizes optimal reclosing targets other than V_{GAP}. In order to obtain other optimal reclosing targets, the proposed technique performs DFT analysis of the acquired line side voltage of faulted phase during the dead time of CB.

4.2 Proposed approach

4.2.1 Network configuration

At EHV and UHV levels, most of the substations are equipped with one-and-half-breaker and non-switchable breaker schemes [3]. The layout of one of the existing Indian 400 kV Sub-Station (S/S) is shown in Fig. 4.1. As shown in Fig. 4.1, the electrical power in S/S-Soja is supplied from two power generating stations namely (i) Ukai (G1) (ii) Wanakbori (G2). Then the power is transmitted to different S/S using four transmission lines. Out of these four lines, 290 km long line connected between S/S-Soja and S/S-Indore is SCTL. The 50 MVAr shunt reactors are connected at both ends of the said line. Further, aluminum conductor steel reinforced twin conductor is used to transmit the power. For ease of understanding, the actual connections of the said line are shown in zoomed portion of Fig. 4.1. As shown in zoomed portion of Fig. 4.1, CSD is used for switching of shunt reactor at one bay (end) whereas PIR-CB is kept for switching of the line at other bay [103]. Subsequently, the tie-line CB that contains both CSD and PIR is utilized for switching of shunt reactor and uncompensated transmission line. Furthermore, one-and-half-breaker scheme provides flexibility for the usage of bus reactor as line reactor by switching the CB at appropriate bay [103].

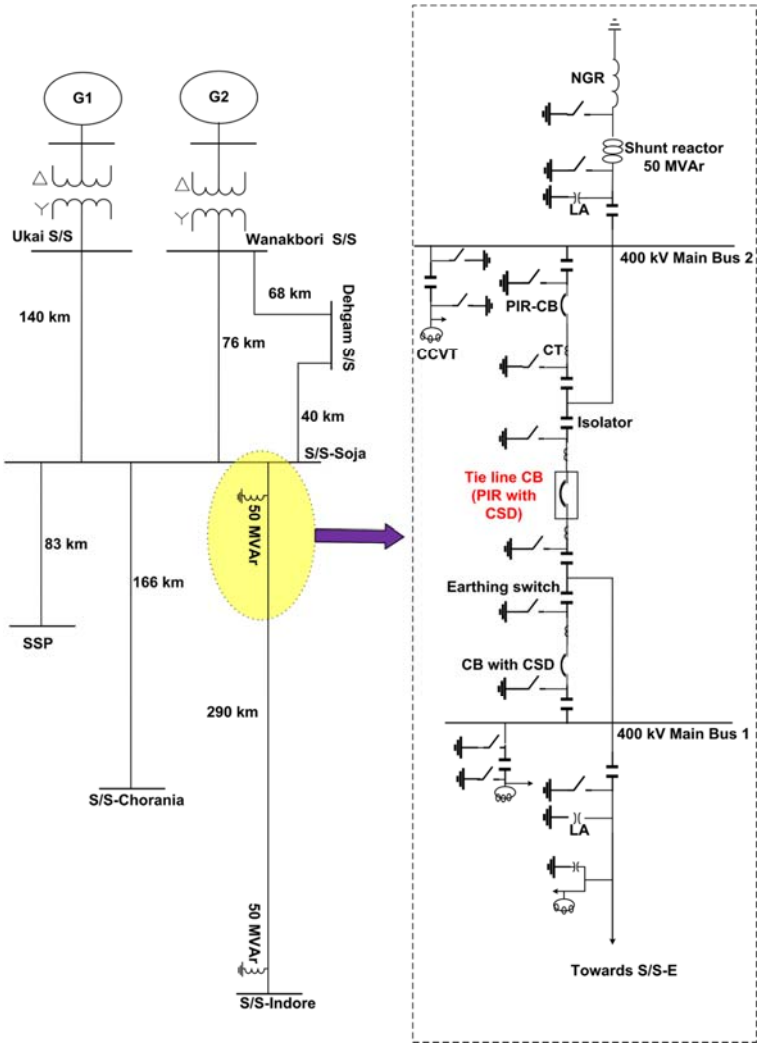

Fig. 4.1 Layout of an existing Indian 400 kV S/S

4.2.2 Proposed algorithm

The flowchart of the proposed technique is shown Fig. 4.2. The proposed algorithm activates once the breaker status changeover has been identified. Thereafter, it is required to check whether SPAR is attempted or not. The SPAR attempt is decided based on nature of the fault (permanent or temporary). In case of permanent fault, the proposed algorithm will go back to reset position. On contrary, SPAR is attempted in case of a temporary fault. In order to identify the optimum reclosing target, V_L and V_{GAP} of faulted phases are acquired and analyzed during dead time of CB (300 ms). Initially, DFT of V_L is performed up to 7^{th} harmonics at a fundamental frequency of 50 Hz.

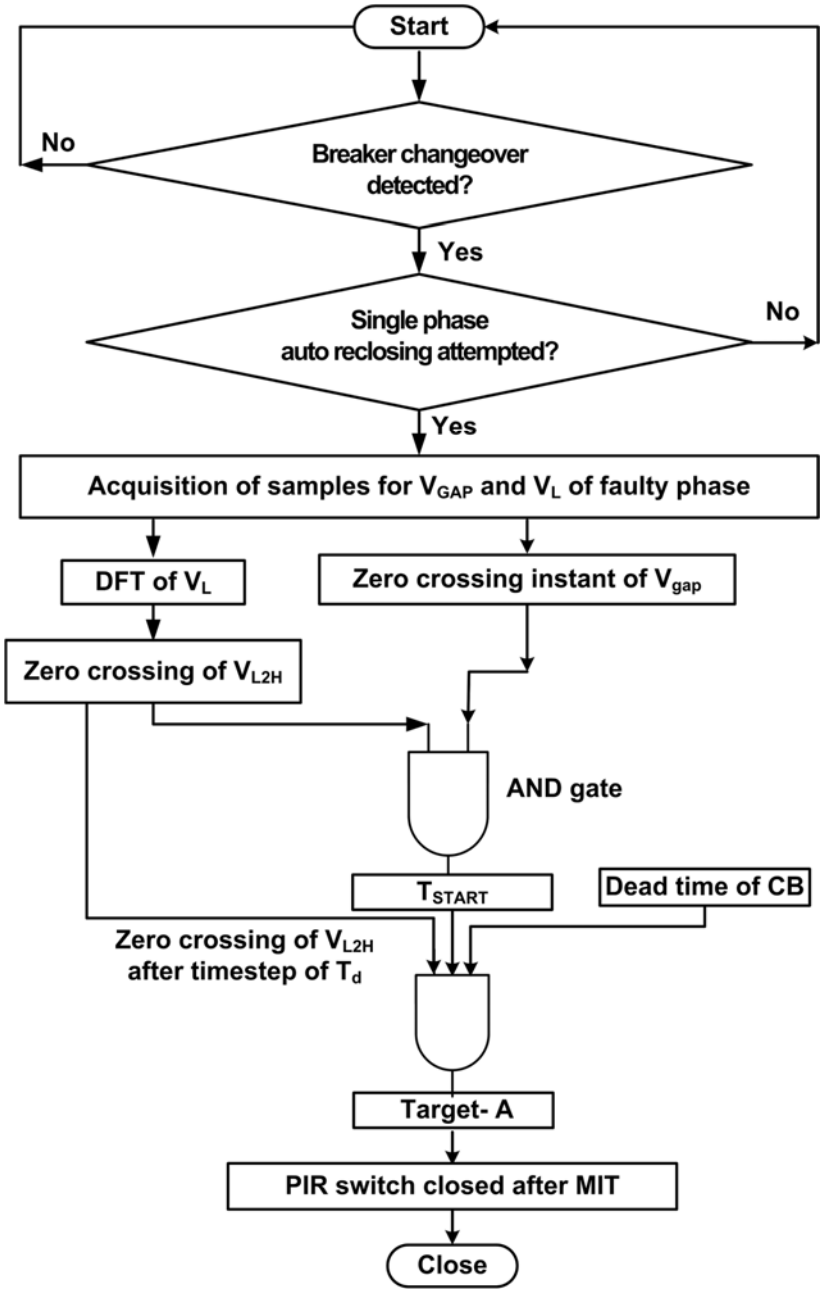

Fig. 4.2 Flow chart of the proposed technique.

Out of all seven harmonic components, the zero crossing instant of the 2nd harmonic is monitored. The instant at which zero crossing of V_{GAP} and 2nd harmonic component of V_L (V_{L2H}) occurs simultaneously is defined as T_{START}. After attaining T_{START}, the time span required to complete two full cycles of V_{L2H} is observed. This span is expressed as optimum delay period (T_d). It has been observed that zero crossing instant of V_{GAP} and V_{L2H} is almost overlapped in a time step of T_d irrespective of level of compensation. Further, it has been reported in [74], [104] that the switching surges during reclosing of the line can be minimized by limiting V_{GAP} at the closing instant. Utilizing this fact in the proposed scheme, the Target-A is defined as zero crossing instant of V_{L2H} in time step of T_d after completion of dead time of the circuit breaker. It

is to be noted that this target (Target-A) is optimum insertion instant of PIR. Subsequently, the PIR has been removed from the circuit by closing PIR switch after optimum MIT of the circuit breaker. The stepwise mathematical procedure to obtain the optimum closing target (Target-A) is explained in the following sub-section.

4.2.3 Evaluation of optimum reclosing target

In order to obtain optimum reclosing target for SCTL, V_L and V_{GAP} are analysed during dead time of CB. Fig. 4.3 (a) shows oscillating nature of V_L for SCTL with 25% compensation. Moreover, stepwise mathematical procedure to obtain the optimum reclosing target for SCTL (Target-A) is shown in Fig. 4.3 (b).

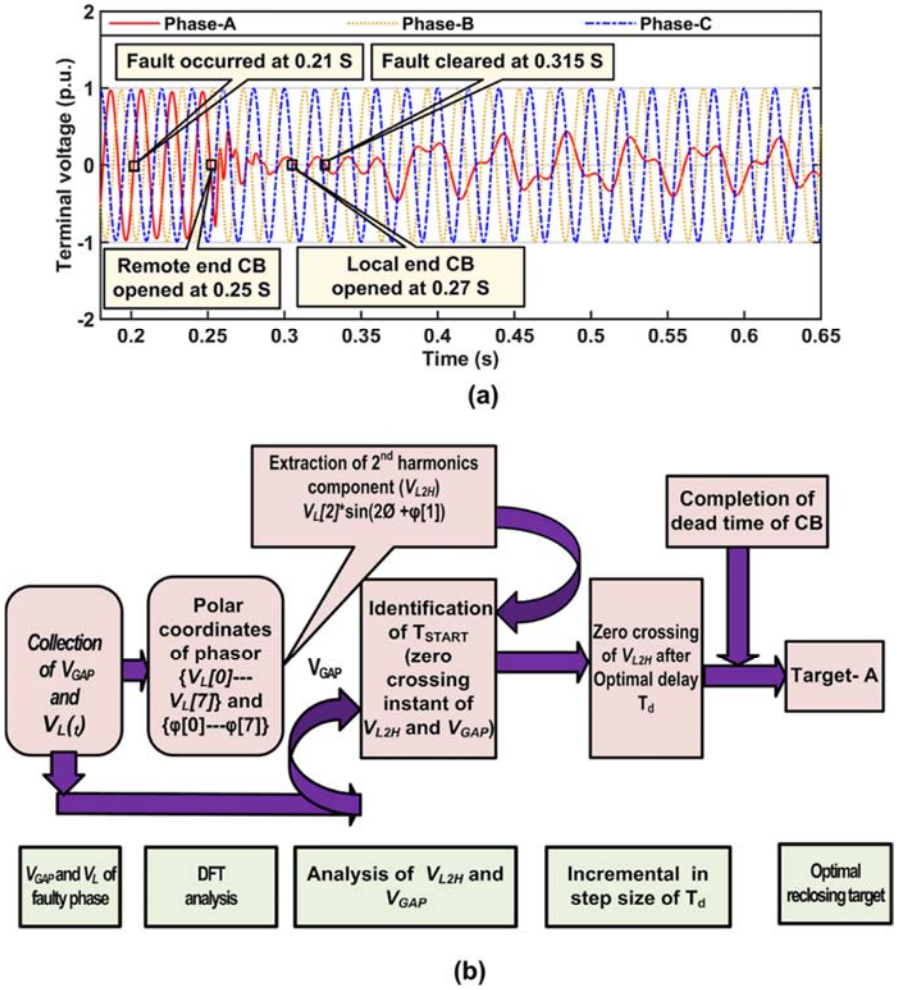

Fig. 4.3 Variation in line side voltages during dead time of the CB for 25% compensated SCTL and (b) stepwise mathematical procedure for derivation of the proposed target.

Initially, one cycle post fault samples of V_L and V_{GAP} are acquired from the S/S using instrument transformers. Afterwards, phasors ($V[k]$) of faulted phase line voltage (in this case, it is phase-A) up to 7th harmonic components are calculated using DFT algorithm according to eq.

(4.1).

$$V[k] = \sum_{t=0}^{N-1} v(t)\, e^{-j2\pi kt/N} \tag{4.1}$$

Where k is the order of the harmonics, $V[k]$ is frequency domain output in Cartesian coordinate form, $v(t)$ is the instantaneous value of signal, N is total numbers of samples in the cycle (i.e. 80 samples), and t is the time instant. Thereafter, values of different harmonic components are arranged columnwise using transposed property of matrix as per eq.(4.2)

$$V[k] = \left[V_A[k]\right]^T \tag{4.2}$$

Where, k = 0 to 7. Also, V_A [1 to 7] represents phasors components of faulted phase voltage. Then, the 2nd harmonic component (V_{L2H}) of faulted phase voltage is separated. Thereafter, the optimal SPAR target is obtained using the same procedure as mentioned in section 4.2.2.

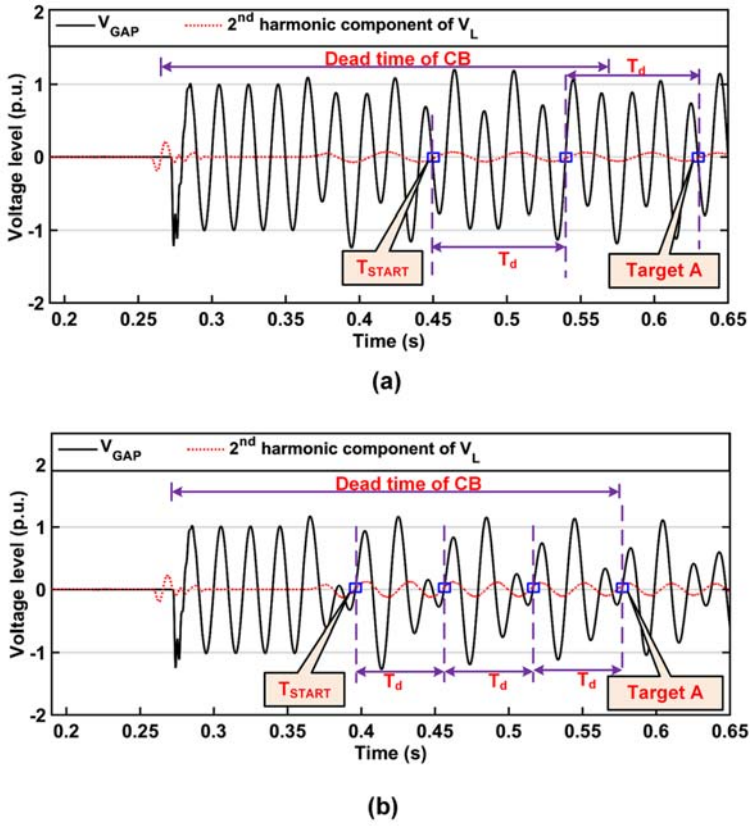

Fig. 4.4 (a) Assessment of optimum controlled SPAR target for (a) 25% and (b) 75% compensated SCTL.

In order to obtain the optimum reclosing Target-A, a simulation study has been performed. Fig. 4.4 (a) and (b) show the results in terms of V_{GAP} and V_{L2H} of faulted phase. It is noted from Fig. 4.4 (a) and (b) that zero crossing of gap voltages for phase-A (V_{GAP}) and V_{L2H} of faulted phase occurs almost at the same instant for SCTL having 25% and 75% compensation levels. Therefore, considering time step of T_d after dead time of CB, the first zero crossing instant of V_{L2H} of faulted phase is proposed as optimum SPAR target. It is observed from Fig. 4.4 (a) and (b) that V_{GAP} attains minimum value irrespective of level of compensation at Target- A. Hence, Target-A is considered as an optimum SPAR target for SCTL.

4.3 Modelling of simulation model

4.3.1 Assessment of network

A simulation model of an existing Indian 400 kV power system network has been developed in the PSCAD/EMTDC environment. Fig. 4.1 shows the single-line-diagram of the developed simulation model. In this model, S/S Soja and S/S-Indore is treated as source end (local end) and remote end (load end), respectively. The said two substations are employed with one-and-half-breaker scheme, which contains hybrid combination of CSD and PIR (it is readily available in tie line CB). In the proposed work, frequency dependent phase model of PSCAD/EMTDC software package is used for modelling of SCTL [83]. Furthermore, at both ends of SCTL, 369 kV SAs are installed [97]. Moreover, the spacing between two phase conductors, spacing between ground & phase conductors, and ground clearance are taken from Indian Electricity rules [90]. The samples are acquired at a sampling frequency of 4 kHz [95], [96]. In the proposed work, the switching surge has been observed at remote end. Moreover, shunt reactors (having different levels of compensation) and NGRs are designed based on the equations given in [98]. The details of parameters of various equipment are given in Appendix A2.

4.3.2 Assessment of parameters for PIR

The selection of value of PIR (R) and its MIT are important aspects of the proposed work. These parameters are obtained based on a simulation study and using the same procedure as reported in [76]. Generally, the switching surge during reclosing of uncompensated and shunt compensated transmission lines depends on (i) R (ii) MIT and (iii) insertion instant of PIR. Subsequently, the individual effect of any parameter on the switching surge can be judged by keeping the other two parameters constant.

4.3.2.1 Evolution of the value of PIR (R)

Based on literature reported in [2], [7], [21], the observed value of MIT is around half

cycle time (in this case it is 180^0 = 10 ms for a fundamental frequency of 50Hz). In order to obtain the optimum *R*, the level of switching surge against different values of *R* has been observed. In this case, different values of *R* is plotted in terms of the ratio of *R* to the characteristic impedance of the line (Z_C) and this ratio (R/Z_C) varies from 0 to 1.4 [76].

Based on process reported in [21], the optimal value of *R* and MIT of PIR has been obtained by performing a simulation study. In this study, reclosing of uncompensated transmission line has been performed in A-C-B sequence considering no-fault situation (as it creates the highest level of switching surge compared to faulted situations) [9]. Here, the parameters of uncompensated transmission line is selected according to the procedure given in [90]. These parameters are depicted in Appendix A2.

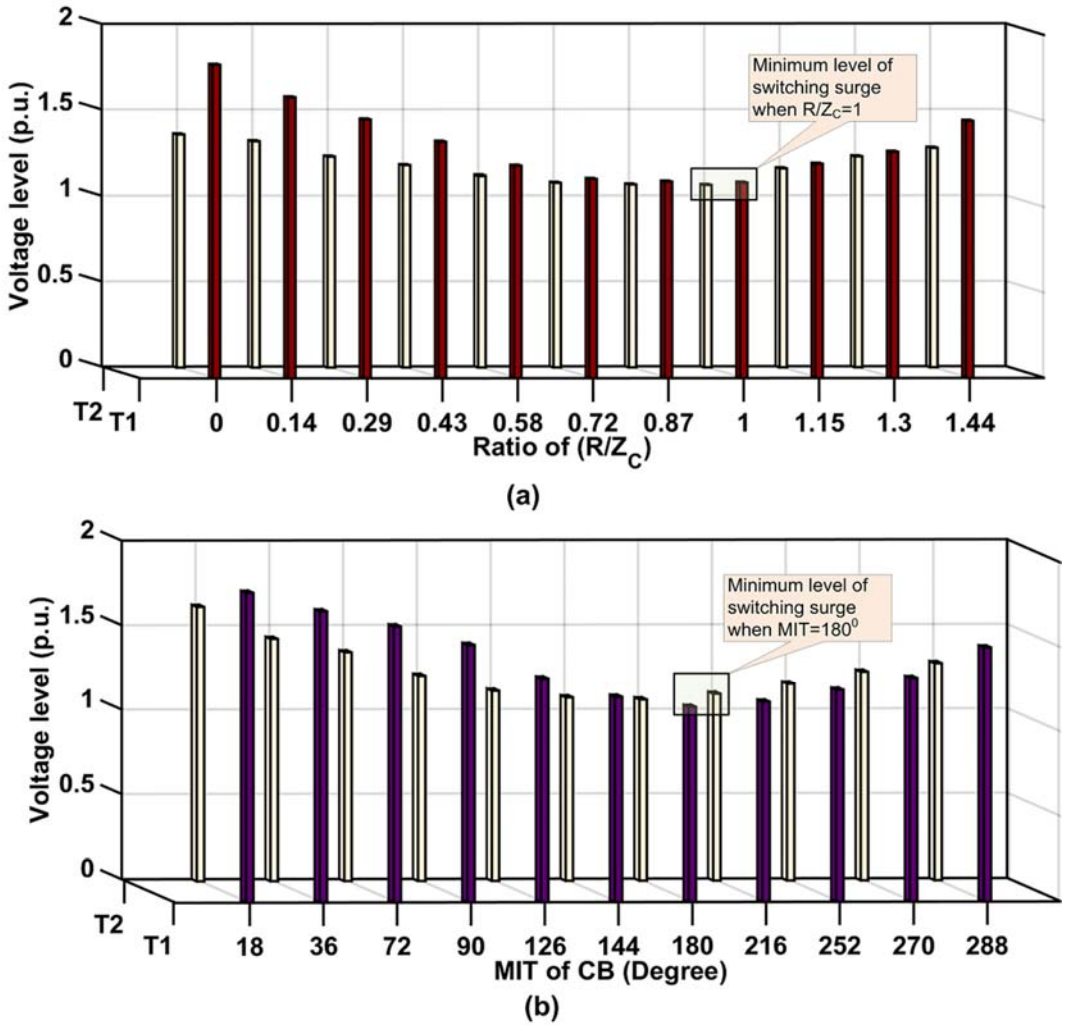

Fig. 4.5 (a) Switching surge level against *R* and (b) MIT.

In order to validate the simulation results, the level of switching surge against *R* has been

obtained for two different PIR insertion instants as described below.

(i) Worse target: It is shown as Target-1 (i.e. peak of the source voltage when the voltage polarity of source side and line side are opposite to each other).

(ii) Compromised target: It is shown as Target-2 (i.e. supply voltage zero).

The simulation results are shown in Fig. 4.5 (a). It has been observed from Fig. 4.5 (a) that the level of switching surge reduces gradually till R/Z_C is around 0.8. Thereafter, it changes marginally up to 1.0 and then increases. Further, the pattern of switching surge remains same for both the aforementioned insertion targets and the switching surge attains minimum magnitude, when R/Z_C = 1.0. Therefore, this value is considered as the optimum value for PIR-CB.

4.3.2.2 Optimum MIT of PIR

The same procedure, as adopted for determining the value of R, can be used for obtaining the optimum value of MIT. Therefore, a simulation study has been performed in which the values of R and insertion instant of PIR are kept constant. In this study, for both aforementioned closing targets, MIT changes from 18^0 to 288^0 and the level of switching surge against different MIT (from 18^0 to 288^0) has been plotted. Fig. 4.5 (b) indicates the simulation results. It is to be noted from Fig. 4.5 (b) that the lowest level of switching surge is achieved when MIT equals to 180^0. Moreover, it has been further observed from Fig. 4.5 (a) and (b) that the switching surge attains higher magnitude for closing Target-1 compare to closing Target-2.

4.3.2.3 Optimum insertion instant of PIR

In order to obtain the optimum insertion instant of PIR, the value of PIR and MIT are kept constant. In the proposed work, the optimum values of PIR and MIT, obtained from the abovementioned simulation work, have been utilized. The procedure of obtaining optimum target (Target-A) is already described in section 4.2.3.

4.3.3 Controlled switching device

The proposed methodology utilizes CSD to attain the optimum reclosing target. Mainly, a time delay has been added by CSD to convert random command into controlled command. This delay is derived from the analysis of data collected from different compensating sensors. Fig. 4.6 (a) shows the layout of CSD [74]. As shown in Fig. 4.6 (a), CSD collects voltages and current data from the real field using instruments transformers [55]. These data are stored in Data Storage and Evaluation Module (DSEM). The proposed algorithm has been processed in

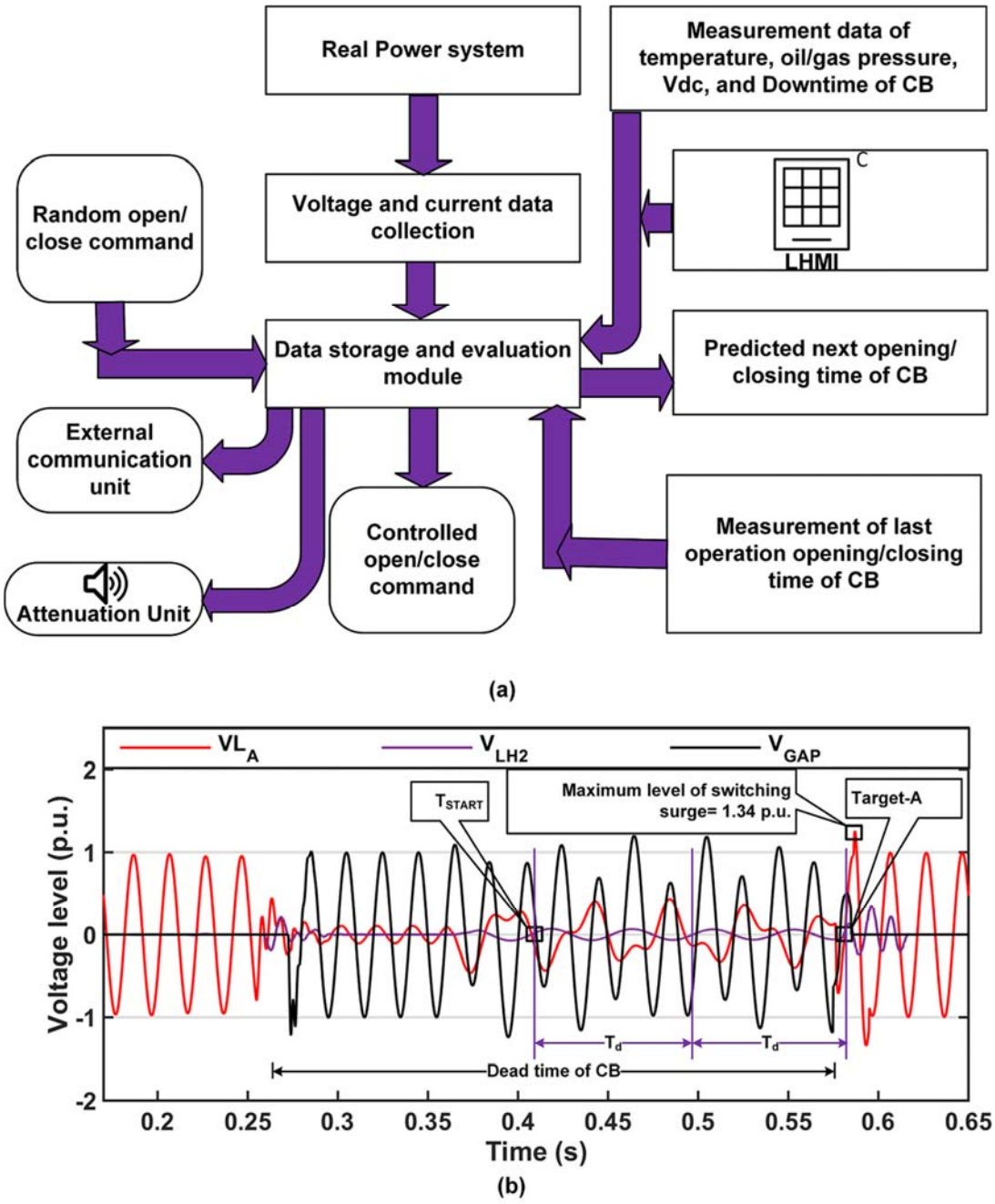

Fig. 4.6 (a) Layout of CSD, (b) assessment of the proposed methodology for 25% compensated SCTL during SLG fault.

this module. Further, in order to change energization/de-energization targets for different equipment to be switched, LHMI module is provided in CSD. The input command (opening/closing) is given to CSD using manual or SCADA mode. Once the random opening/closing command has been raised, the CSD converts it to controlled command by providing deliberate delay. This delay has been obtained based on evaluation of the real field voltages & currents data along with consideration of statistical and systematic variations of the CB. It is important to note that the MOT of CB changes due to statistical and systematic

variation. The CSD closely observes the systematic parameters such as temperature, oil/gas pressure, downtime, and control dc voltage of the CB using compensating sensors. Subsequently, the CSD counterbalances the effect of MOT scatter due to systematic variation using auto correction curves. However, it is difficult to compensate statistical deviations of the CB. Moreover, to predict the operating time for next operation of the CB, the MOT of the CB is also considered for the last operation.

The CSD also has different output ports such as external communication and alarm using which it can communicate with different IEDs located in S/S. In addition, the switching event has been captured by connecting DR with communication port. In case of abnormality, the annunciation port provides an alarm signal. The CSD also contains power supply unit that supplies different dc voltages to various modules.

4.3.4 Building of simulation cases

To assess performance of the proposed technique, large numbers of simulation cases have been generated by changing operational and systematic parameters. The summary of simulation cases generated are shown in Table 4.1

Table 4.1 Summary of simulation cases generated

Event	Parameter variation	Number of cases	Total cases generated
Fault condition	Line length (km): 290 and 450	(2)	2×2×3×3×2×3 ×3×3×3=5832
	Type of configuration: single ended and Double ended	(2)	
	Compensation levels : 25%, 50%, and 75%	(3)	
	Types of fault: A-G, B-G, C-G.	(3)	
	Resistance of fault (Ω): 0.01 and 100	(2)	
	Duration of fault (ms): 100, 150, and 220	(3)	
	Location of fault (% of line length): 0, 50, and 100	(3)	
	Load angle: 10^0 , 20^0, and 30^0	(3)	
	Inception angle of fault: 0^0, 90^0, and 135^0	(3)	
Number faulted cases generated			5832
No-fault condition	Line length (km): 290 and 450	(2)	2×2×3=12
	Type of configuration: single ended and Double ended	(2)	
	Compensation levels : 25%, 50%, and 75%	(3)	
Number of no-fault cases generated			12
Overall cases generated			5844

The parameters such as type of connection configurations of shunt reactor, line length, level of compensation, location of fault, fault duration, fault resistance, inception angle of fault,

types of fault, and load angle are varied. The total 5844 cases have been investigated in the presented work. Out of 5844 cases, 12 cases have been simulated for no-fault situation and 5832 cases have been generated for faulted situation. Here, in order to replicate the case of maloperation of the protection relay, no-fault condition has also been considered. Table 4.1 (b) shows results of one of the faulted cases during implementation of the proposed technique for a 400-km long SCTL with 25% compensation.

4.4 Performance evaluation of the proposed technique

Performance evaluation of the proposed methodology has been carried out considering varying compensation levels, impact of SA, and different values grid sources. Few of the results are discussed in the following sub-sections.

4.4.1 Effect of different compensation level

The performance of the proposed technique has been evaluated for two different compensation levels i.e. 25% and 75%. In this study, different SLG fault situations such as fault sustains for 100 ms, 150 ms, and 200 ms is represented as SLG1, SLG2, and SLG3, respectively. Further, no-fault condition is also considered. The simulation results obtained in terms of voltage profile over the entire length of the line for 25% and 75% compensation levels are shown in Fig. 4.7 (a) and (b), respectively. It is to be concluded from Fig. 4.7 (a) - (b) that the level of switching surge increases from sending-end (0% of line length) to receiving end (100% of line length). Further, at the mid-point of the transmission line, the switching surge attains a maximum value. Afterwards, it reduces gradually from the midpoint to the receiving end. It has been further noticed from Fig. 4.7 (a)-(b) that the highest switching surge (1.387 p.u.) is observed at the midpoint of the line during no-fault situation and with lowest compensation level (i.e. 25%). However, at remote end, its value is 1.35 p.u. Moreover, in case of no-fault situation, the switching surge attains higher value as compared to different SLG fault conditions. In addition, in case of faulted condition, the switching surge achieves the highest value during SLG fault with its presence for 100 ms compared to different SLG fault conditions. In addition, in case of faulted condition, the switching surge attains highest value during SLG fault with its existance up to 100 ms compared to other different type of faulted conditions.

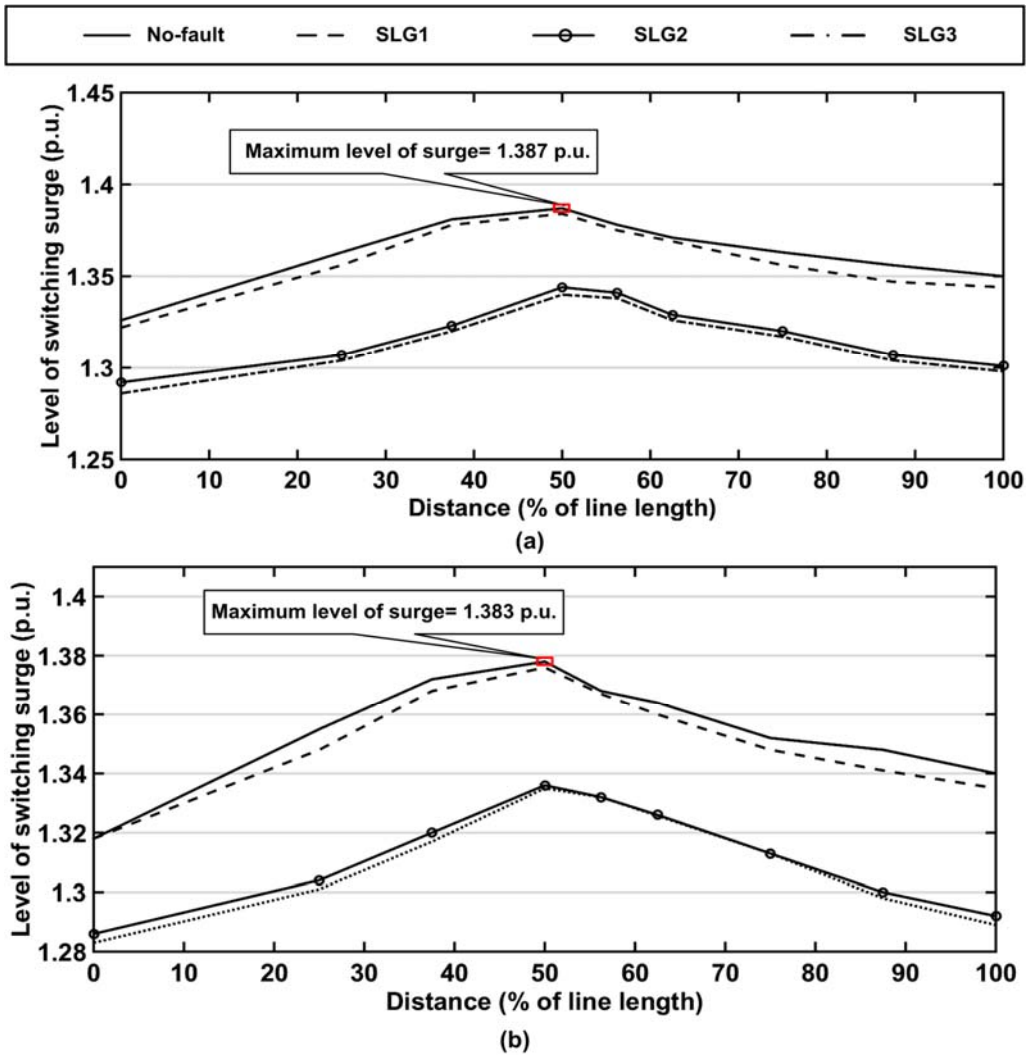

Fig. 4.7 Switching surge level during controlled SPAR of 400-km long SCTL with (a) 25%, (b) 75% compensation level.

4.4.2 Impact of SA

SA plays an important role in minimizing the level of switching surges. Hence, a simulation study has been performed considering absence/presence of SA during implementation of the proposed methodology. In this regard, the performance of the proposed scheme has been tested for all cases mentioned in Table 4.1. The results are shown in. It can be appreciated from Table 4.2 that the level of switching surge changes narrowly considering the effect of SA during re-energization of SCTL.

Table 4.2 Impact of SA

Different conditions	Level of compensations	Switching surge at the remote end of the line (p.u.)		
		With SA	Without-SA	Difference (p.u.)
No fault	25%	1.35	1.38	0.030
Faulted		1.344	1.375	0.031
No fault	50%	1.35	1.38	0.01
Faulted		1.342	1.36	0.018
No fault	75%	1.346	1.356	0.01
Faulted		1.34	1.345	0.005

4.4.3 Effect of different grid sources

In real field, grid contains various sources having different Short Circuit Current Levels (SCCLs). Therefore, in order to evaluate performance of the proposed technique, a simulation study has been performed considering three different sources (S1, S2 and S3). The parameters of these three sources along with outcome of the proposed technique in terms of level of switching surge are shown in Table 4.3. During this study, the same numbers of simulation cases, as mentioned in Table 4.1, have been analyzed. It can be concluded from Table 4.3 that the magnitude of switching surge alters narrowly due to the effect of different grid sources.

Table 4.3 Effect of different grid sources

Parameters		Line length (km)	Source (S1)	Source-1 (S2)	Source-2 (S3)
SCCL (A)		---	40×10^3	28×10^3	10×10^3
Sequence Impedance (Ω)	Positive	---	0.412+ j3.55	1.5 × S1	4.1 ×S1
	Zero	---	2.82 + j 10.1	1.5 × S1	4.1×S1
Level of switching surge (p.u.) during no-fault condition		400	1.35	1.34	1.34
Level of switching surge (p.u.) during faulted situation		400	1.34	1.337	1.336

4.4.4 Comparison of the proposed technique with reported controlled switching methodology

Nowadays, many manufacturers provide CBs that can achieve the closing target with a correctness of ±1ms. In this case, the mechanical and dielectric characteristics of the CB are designed with utmost care. The systematic and statistical deviations are mainly responsible for operating time variations in the CB. Different parameters such as change in the temperature, change in oil/gas pressure, change in battery voltage, and aging effect of the CB are liable for the systematic deviations of the CB. These deviations of the CB are counterbalanced by CSD using auto compensation curves. On contrary, it would not be possible to compensate change in MOT caused by statistical variation. Here, combined effect of MOT and decaying rate of

dielectric strength scatter of the order of 1 ms is considered. The combination of PIR-CB and CSD has been utilized by the proposed methodology whereas the PIR standalone methodology uses PIR only. A simulation study of controlled SPAR of 400-km long SCTL is performed using the proposed methodology and with PIR standalone methodology. For both techniques, different situations such as no-fault, various SLG faults (i.e. SLG fault with its presence up to 100 ms (SLG1), 150 ms (SLG2), and 200 ms (SLG3)) are analyzed. Here, two different compensation levels for SCTL (25% and 75%) have been considered. For all cases, the switching surge magnitude is measured at the remote end of the transmission line. Comparison between proposed technique and PIR standalone methodology in terms of level of switching surge for different fault conditions are shown in. Fig. 4.8

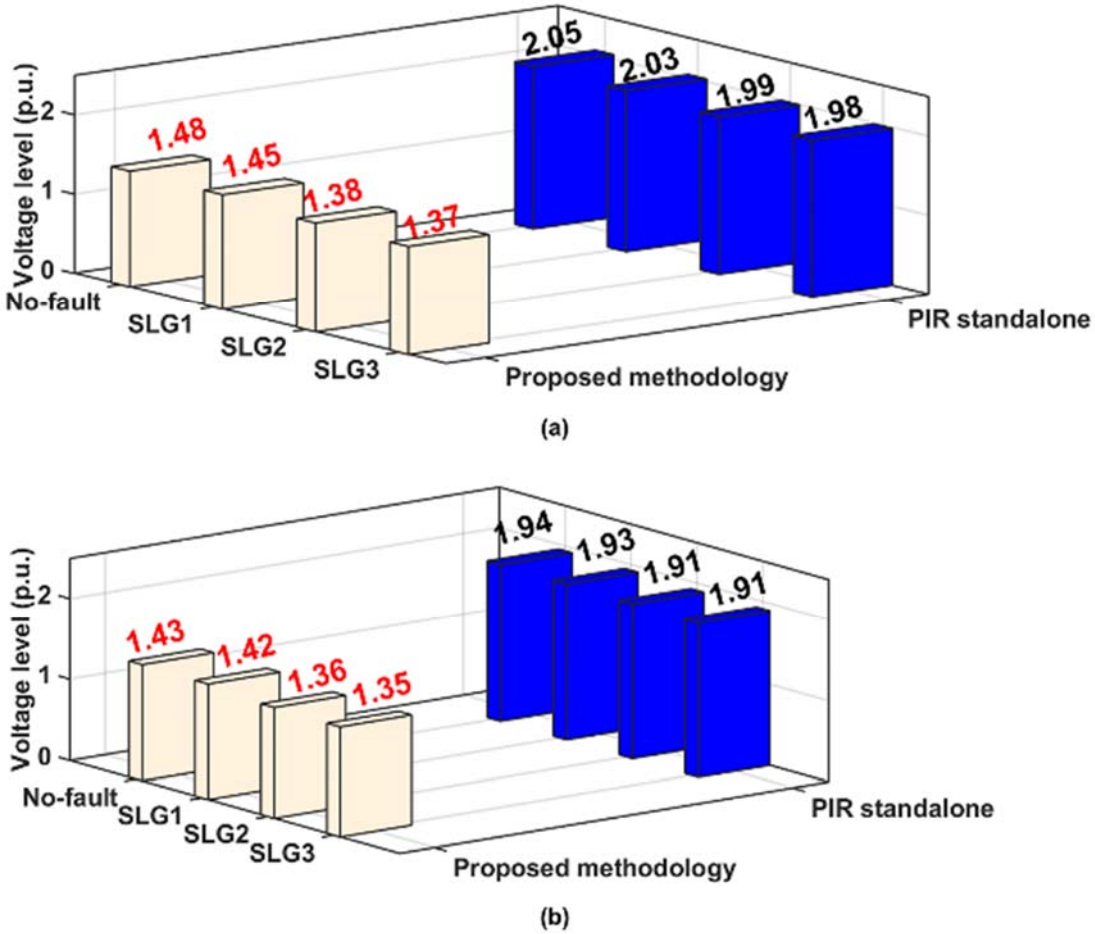

Fig. 4.8 Comparison between the proposed technique and PIR standalone methodology for (a) 25% and (b) 75% compensated SCTL.

It can be appreciated from Fig. 4.8 (a) that the highest magnitude of switching surge obtained using the PIR standalone methodology and the proposed technique is around 2.05 p.u. and 1.46 p.u., respectively, during no-fault condition. On the other hand, during faulted (SLG fault) situations, the maximum magnitude of switching surge obtained using PIR standalone methodology is almost 2.03 p.u. Conversely, for the same situation, the proposed technique generates a switching surge of 1.45 p.u only. Similarly, as observed from Fig. 4.8 (a) and (b), the highest magnitude of switching surge given by the PIR standalone methodology is always higher compared to the proposed technique for all situations. These results clearly indicate the effectiveness of the proposed scheme over the PIR standalone methodology.

4.4.5 Identification between temporary and permanent fault.

The proposed technique is also able to discriminate between permanent and temporary fault. In order to avoid closing of CB under faulted situation, it is required to identify whether the fault is temporary or permanent during dead time of the CB (i.e. 300 ms). For the ease of understanding, a simulation study has been carried out. In this study, following sequence has been followed.

(i) Occurrence of a SLG fault at 0.21 s.

(ii) Opening of remote end CB after duration of two cycle (i.e. at 0.25 s).

(iii) Opening of local end CB after one cycle of the opening of remote end CB (i.e. at 0.27 s).

(iv) Then the fault is cleared after 150 ms (i.e. at 0.36 s). At that instant, most of the trapped charge of the faulted phase has been drained to earth due to SLG fault whereas rest two phases are healthy.

From 0.36 s to 0.37 s, the trapped charge on faulted phase is increasing gradually due to the effect of mutual coupling with two other healthy phases. Around 0.37 s, the trapped charge of faulted phase attains almost magnitude of 0.5 p.u. compared to other two healthy phases. Subsequently, it will start oscillating with other two phases. In proposed algorithm, T_{START} is defined as an instant when zero crossing of V_{GAP} and V_{L2H} occurs simultaneously. The same has been observed from Fig. 4.9 (a). On contrary, during permanent fault, V_{L2H} attains almost zero value. In this case, it is not possible to identify T_{START}. This has been observed from Fig. 4.9 (b). Utilizing this fact, it is to be noted that the presented algorithm is capable to discriminate between temporary and permanent fault.

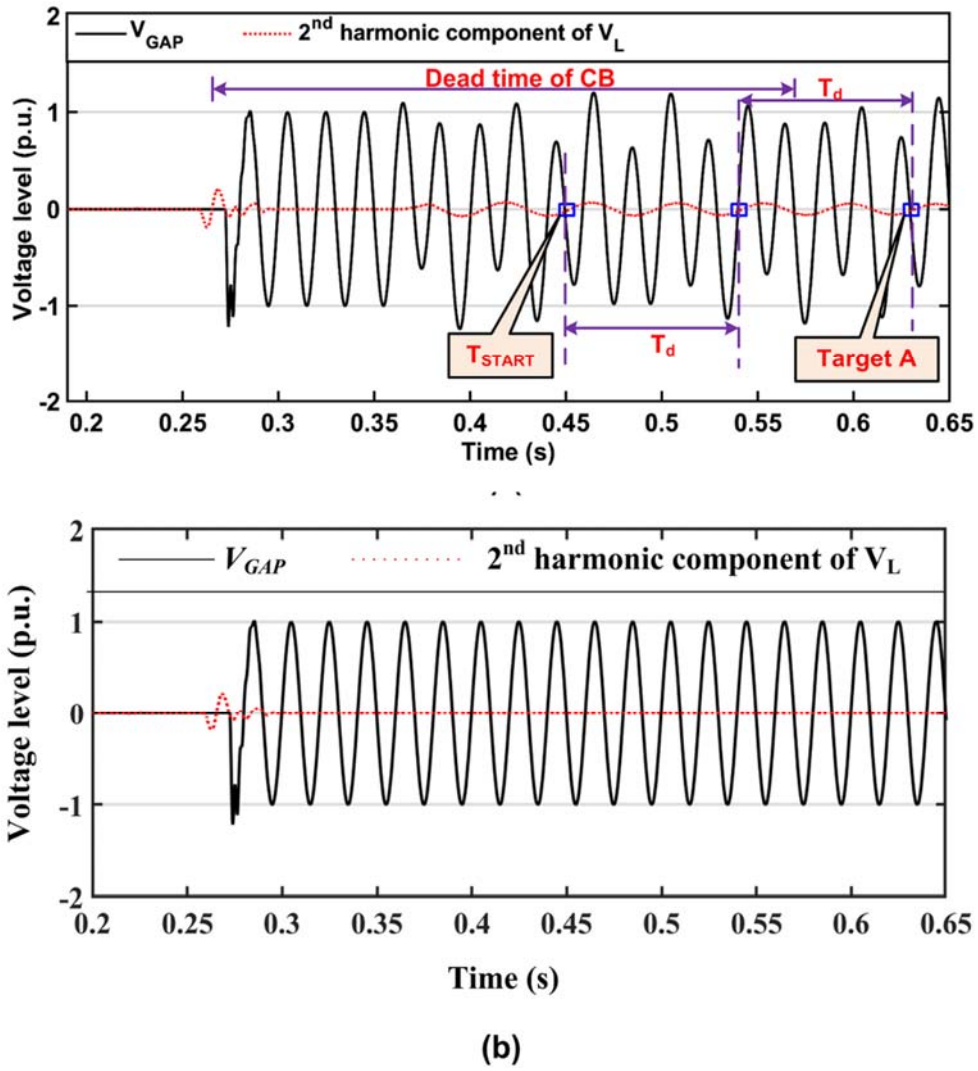

Fig. 4.9 Identification of (a) temporary and (b) permanent fault during SPAR of 25% compensated SCTL.

4.5 Summary

A new controlled SPAR methodology that effectively minimizes magnitude of the switching surge during re-closing of long SCTL using hybrid combination of CSD and PIR-CB is presented. The simulation model of 400 kV SCTL has been developed considering the existing power system network. Different cases are generated using PSCAD/EMTDC software package to assess performance of the proposed technique. The simulation cases are developed by changing systematic and operational parameters. Moreover, compared to the reported controlled switching methodology, the proposed technique can further minimize magnitude of the switching surge of the order of 40% for SCTL. The comparison between the proposed technique and PIR standalone methodology indicates effectiveness of the proposed scheme particularly when the effect of operating time scatter of the CB (of the order of ±1 ms) is taken into account.

At the same time, different parameters such as presence/absence of SA and source strength do not create any significant impact during implementation of the proposed technique. The presented work also discriminates between temporary and permanent fault.

Chapter 5

Controlled Energization of Shunt Reactor

5.1 Introduction

In this chapter, evaluation of controlled energization of shunt reactors for minimizing asymmetric dc component of charging current with circuit breaker having pre-insertion resistors is presented. Generally, CSD is used during de-energization as well as energization of shunt reactors. However, for substations configured with OHB or line connected to non-switchable reactor scheme, the PIR-CB can be utilized during switching of shunt reactor. This chapter presents an optimized controlled switching strategy, which minimizes the level of asymmetric dc component of charging current during energization of a shunt reactor using CSD with PIR-CB. This is achieved by optimizing the insertion instant, value and EIT of PIR. The validity of the proposed technique has been evaluated by generating a large number of simulation cases in PSCAD/EMTDC software package by changing rating & configuration of shunt reactor, EIT, insertion & removal instant and the value of PIR.

5.2 Uncontrolled energization of a shunt reactor

Uncontrolled energization of three-phase shunt reactor (either through simple CB or using PIR-CB) draws a high charging current due to the presence of an asymmetric dc offset component. Moreover, the PIR-CB will impose challenges to determine optimum making instant due to its resistance and EIT. Furthermore, dc offset component takes a long time to decay because of the large value of the time constant. This causes saturation of the core of the Current Transformer (CT), which in turn maloperates Restricted Earth Fault (REF) protection of the reactor. In fact, if the tripping happens during faulted condition than the chances of a generation of high frequency chopping overvoltages will be minimal due to large magnitude of fault current. Therefore, there will not be any probability of reignition in CB, which may result in severe damage to the inter-winding insulation of the shunt reactor. However, maloperation of REF relay leads to nuisance tripping of the reactor. In this condition, though the current to be interrupted by CB would not be as high as the fault current, the probability of reignition will be very high. In the worst case, it may damage the inter-winding insulation of the reactor. In such circumstances, mitigation of asymmetric dc component of charging current will reduce the possibility of malopearation of the protective device. In addition, this will also assist in increasing sensitivity of the protective device and hence, better performance will be obtained during high resistance earth faults [37].

Fig. 5.1 shows the simulation results during charging of an uncontrolled three-phase non-coupled 125 MVAr shunt reactor using simple CB and PIR-CB (400 Ω).

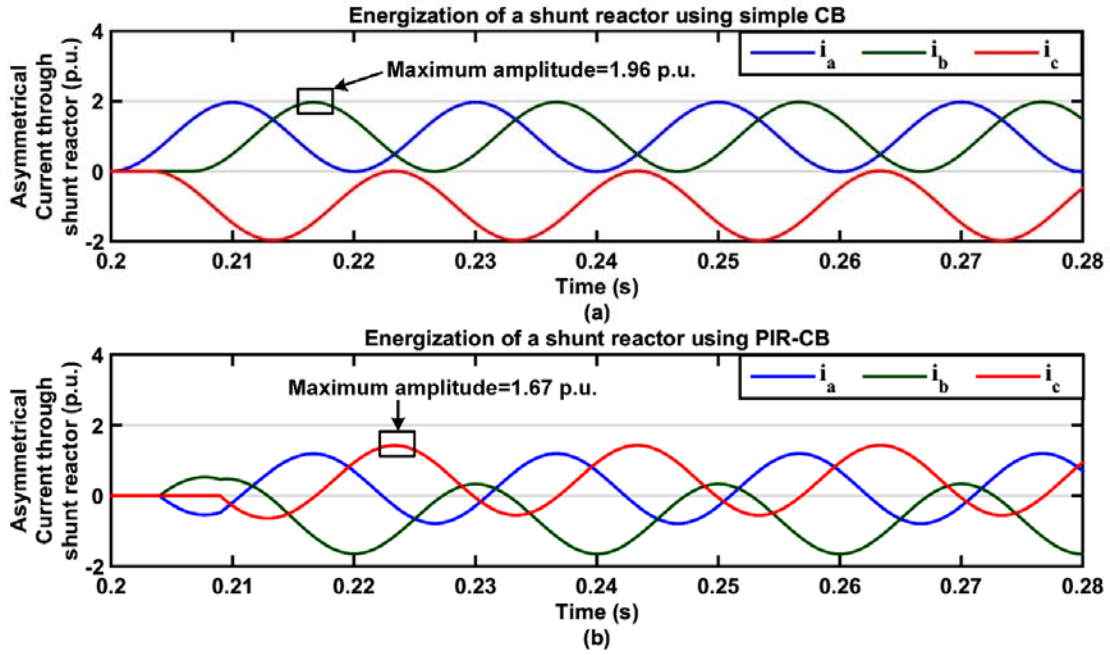

Fig. 5.1 Level of asymmetric current during uncontrolled energization of 125 MVAr shunt reactor using (a) simple CB and (b) PIR-CB.

In case of energization of a shunt reactor using simple CB, the circuit forms as the impedance of source appear to be in series with the impedance of a shunt reactor. Hence, the value of *X/R*= 62.879. Whereas in case of energization of 125 MVAr shunt reactor using PIR-CB, the additional resistance of PIR appears to be in series with the aforementioned combination (source impedance along with the impedance of a shunt reactor) for few milliseconds. Because of that, the value of *X/R* =3.0528. The closing of CB/PIR-CB has been carried out at gap voltage zero of each phase, which leads to maximum asymmetric decaying dc component in the charging current. Here, the short circuit current level of the source is taken as 38.20 kA. It has been observed from Fig. 5.1 that the maximum value of asymmetric charging current through the reactor is of the order of 1.96 p.u. and 1.67 p.u. for simple CB and PIR-CB, respectively. For non PIR-CBs, this asymmetry can be fully mitigated by energizing the reactor through an individual pole of CB at V_{GAP} peak. However, in case of PIR-CBs, further mitigation of asymmetric dc component of charging current demands careful evaluation of insertion instant, value, and EIT of PIR. The basic terminology related to PIR assembly is explained in the next sub-section.

5.3 Effect of PIR-CB during energization of a shunt reactor

5.3.1 Basic terminology of PIR

PIR is an assembly consisting of a resistor and two switches. The switch, which is used to insert PIR in series with the circuit, is known as interrupter whereas the switch that is utilized to bypass the PIR from the circuit is known as PIR switch [7]. There are mainly two types of PIR configurations used in practice (i) Series PIR and (ii) Parallel PIR. In case of series PIR, the interrupter is connected in series with PIR switch whereas for parallel PIR, it is connected in parallel with the PIR switch. Though electrical performance of both configurations offers coequal behaviour, in practice, series PIR is used due to its lower cost and lesser space requirement in comparison with the parallel PIR [7].

Fig. 5.2 shows single-line-diagram of a shunt reactor connected with the source using series PIR assembly. In Fig. 5.2, during energization of a reactor, electrical closing happens through the interrupter followed by PIR switch. The time laps between aforementioned two electrical making instants is known as EIT of PIR. On the other hand, the time gap between the mechanical closing of aforesaid switches is known as MIT [6], [7] .

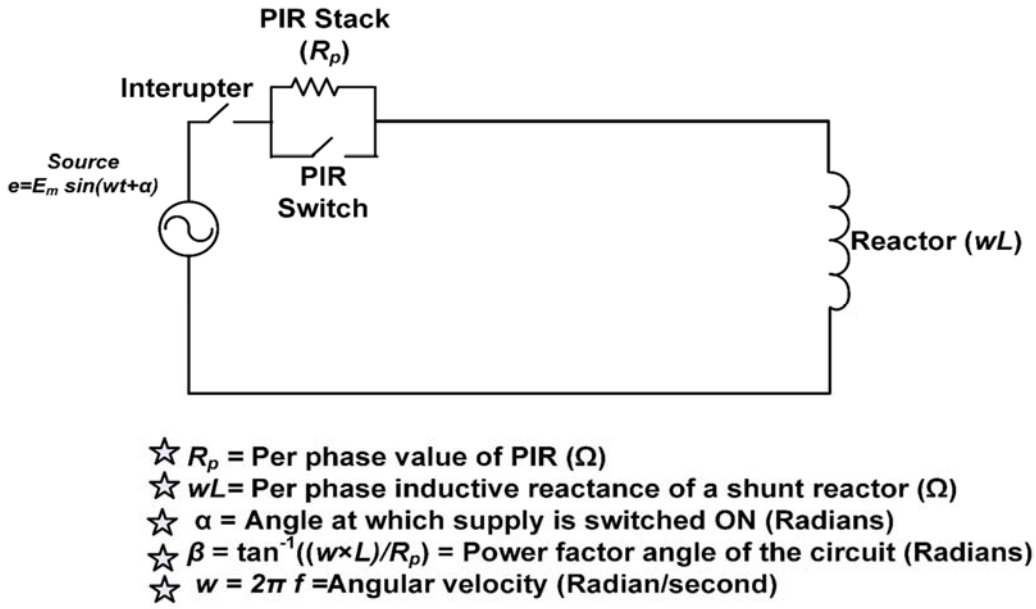

Fig. 5.2. Single-line-diagram to illustrate the behaviour of PIR.

5.3.2 Primary and secondary transient currents

With reference to Fig. 5.2, insertion and removal of PIR imposes primary and secondary transients across the contacts of CB as well as on the system. They are defined as under [1].

- Primary Current Transient (PCT): It is the maximum asymmetric charging current observed in the circuit for the time period up to which PIR is inserted in series with the reactor. It depends on the value of PIR and insertion angle of PIR (β).
- Secondary Current Transient (SCT): It is the sudden increase in the level of asymmetric charging current observed due to the sudden removal of PIR in series with the reactor. It depends on the value of PIR and EIT.

In order to discriminate between the above two transients, simulation of energization of 125 MVAr shunt reactor has been carried out using PSCAD/EMTDC software package with PIR-CB having EIT of 8 ms at an insertion angle (β). The simulation results are shown in Fig. 5.3. It has been observed from Fig. 5.3 that the value of PCT and SCT is of the order of 0.6 p.u. and 1.67 p.u., respectively. It is observed from Fig. 5.3 that the magnitude of SCT is always higher than the PCT. The objective of the proposed methodology is to minimize the level of SCT.

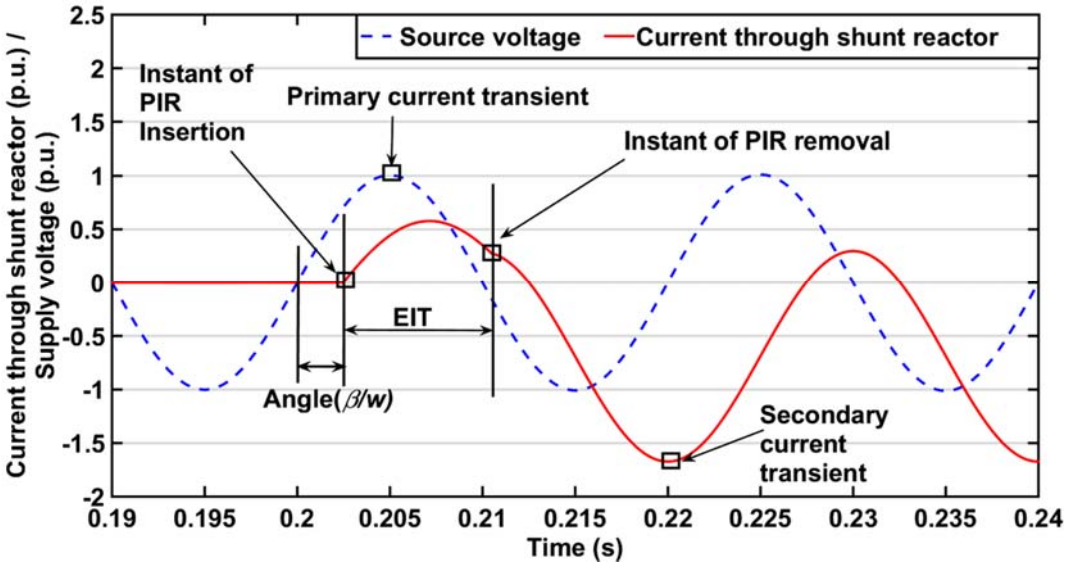

Fig. 5.3 Simulation results showing the level of primary and secondary current transients.

5.3.3 Application of PIR-CB with CSD

The single-line-diagram of OHB scheme having transmission line and a reactor connected through individual main CBs and shared by tie CB for back charging of both as an when needed (termed as "dia") is shown in Fig. 1.9 (a). In this case, CSD has been provided with PIR-CB on tie bay for controlled de-energization of the reactor to minimize the probability

of reignition [74]. Furthermore, in case of a line with non-switchable reactor bay, it is mentioned that minimum value of the secondary surge is obtained when the value of *R/Zc* = 1. It is to be noted from Fig. 1.9 (a) and (b) that the minimum value of secondary surge is lower in case when the closing target is half of the peak of the supply voltage compared to the closing target as the peak of the supply voltage.

With reference to Fig. 1.9 (b), the following bay operation topologies are considered.

(i) The transmission line can be used as uncompensated line by opening disconnector of the shunt reactor.

(ii) The transmission line can be used with compensation by connecting the shunt reactor.

(iii) The transmission line is disconnected by opening its disconnector and the line reactor is used as the bus reactor for reactive power compensation.

For condition (iii), in order to minimize the possibility of reignition with the PIR-CB of the line, the CSD has been provided for controlled de-energization of the reactor. Conversely, for conditions (i) & (ii), the CSD is usually bypassed. As discussed in the previous section, to mitigate SCT further, the controlled energization of the transmission line with PIR-CB can be performed with the same CSD. However, the settings of CSD for topology (iii) are entirely different than the ones used for bay operating topologies (i) and (ii) [73], [74].

5.4 Modelling of different apparatus used for simulation model

5.4.1 Modelling of PIR-CB

In order to improve the performance of controlled switching strategy, close coordination between the characteristic of CB and shunt reactor is necessary [62]. This is achieved by considering parameters of CB such as grading capacitor (C_G) and stray capacitance (C_S) at the time of modeling of CB. The parameters of PIR-CB are given in Appendix A3 and they are referred from [73]. For simplicity, single-phase representation, which is applicable to non-coupled reactors, is shown here. Later on, the same concept has been extended on three-phase shunt reactor having different configurations (Yg, Y, and Δ). This is elaborated in section 5.5.2.

5.4.2 Modelling of shunt reactor

The modelling of a 400 kV, 50 Hz shunt reactor is carried out using PSCAD/EMTDC software package [83]. A sampling frequency of 4 kHz has been used for a fundamental frequency (*f*) of 50 Hz. Fig. 5.4 shows single-line-diagram in which the shunt reactor (with three different configurations namely Y, Yg and Δ) is connected to the source through PIR-CB. Here,

two different ratings of shunt reactors (125 MVAr and 63 MVAr) are considered for simulation study.

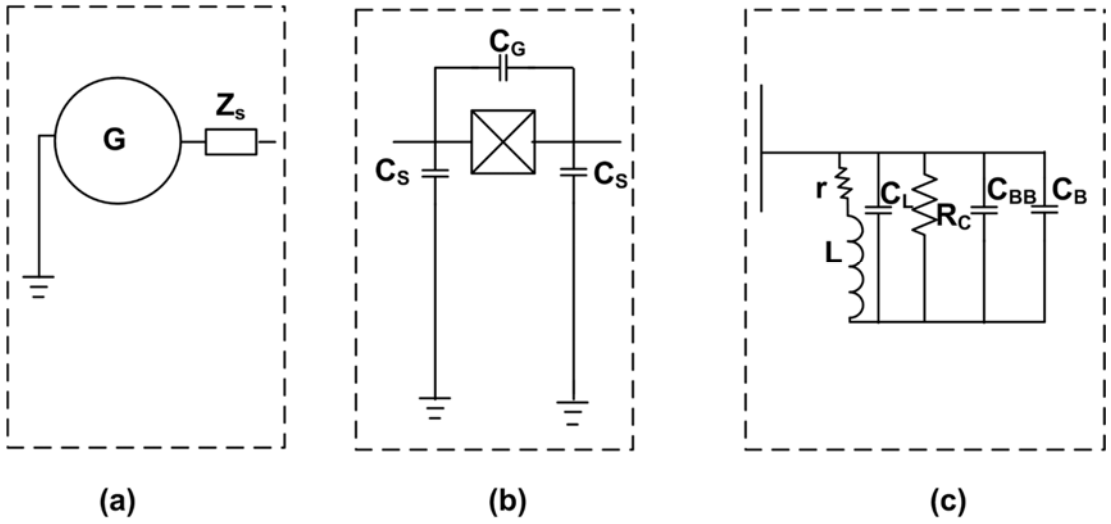

Fig. 5.4 Single-phase representation of simulation model of (a) source, (b) PIR-CB, and (c) shunt reactor having different connection configurations.

In order to observe the impact of Temporary Over Voltages (TOVs) along with the SCT, core loss component (R_C) of the reactor has also been considered in the simulation model. This includes various parameters such as the internal resistance of the reactor winding (r), the capacitance of reactor (C_L), a bus bar (C_{BB}) and bushings (C_B) along with the series inductance of the reactor (L). The details of these parameters are given in Appendix- A3 and they are referred from [5], [91], [105] . The presentation of different connection configurations of the shunt reactor have been given in section 5.5.2. As per IEC standard 60071-4, the effect of high frequency component (observed due to capacitance) is extremely important during de-energization of shunt reactor [106]. It is not necessary to consider the same during energization of the shunt reactor, as the energization is related to thermal (current) behaviour, which in this case is low frequency phenomenon. Moreover, to verify the effect of capacitance, a simulation study has been carried out. It has been observed from the results that the contribution of current due to the effect of capacitance (usually of the order of pF) is of the order of μA. This low amount of current does not have any significant effect on the proposed methodology where the magnitude of the asymmetric current is of the order of hundreds of ampere. Therefore, there is no need to consider the effect of capacitance in the modelling.

It is to be noted that gapped reactors mostly have an iron core with integrated airgaps resulting into high knee point voltage [4], [23]. At EHV & UHV levels, the knee point voltage

of transformer and shunt reactor is of the order of 1.1 p.u. and 1.25 - 1.5 p.u., respectively [107]. Furthermore, the voltage level reduces during energization of the shunt reactor as it absorbs reactive power from the system and there is the least probability of reaching the aforesaid high voltage level. Due to this fact, the core of shunt reactor never saturates.

5.4.3 Optimal insertion instant of PIR

In order to minimize the level of PCT, it is required to determine optimal insertion instant of PIR. This is achieved by performing mathematical analysis of energization of a shunt reactor using PIR-CB. In this presented work, the positive going zero-crossing of the supply voltage is taken as the reference for all the mathematical analysis. By applying Kirchhoff's Voltage Law (KVL) and Laplace transformation [1] in Fig. 5.2, the equation of instantaneous value of current is given by,

$$i = \frac{E_m}{\sqrt{R_p{}^2 + (w \times L)^2}} \left[\sin(wt + \alpha - \beta) - \sin(\alpha - \beta) e^{-\mu t} \right] \tag{5.1}$$

Where, μ represents the time constant of the circuit and β is the power factor angle. It is given by equation (5.2).

$$\beta = \tan^{-1}\left(\frac{w \times L}{R_p}\right) \text{ for single-phase circuit, } \beta = \tan^{-1}\left(\frac{w \times L_{eq}}{R_{eq}}\right) \text{ for three-phase circuit} \tag{5.2}$$

Where, L_{eq} and R_{eq} are the equivalent inductance and resistance of individual phase of the three-phase non-coupled shunt reactor, respectively. The details are given in section 3.4.2.

In equation (5.1), the first term indicates the steady state value of current whereas the second term represents the transient value of the current, which exponentially decays based on the time constant of the circuit (μ). It is to be noted from equation (5.1) that the optimal insertion angle is obtained when $\alpha = \beta$. Hence, power factor angle is the optimal insertion angle for PIR. In this situation, there would not be any transient component of current and only steady state component of current exists. Therefore, the optimal insertion instant ($T_{in\text{-}optimal}$) of PIR is given by,

$$T_{in\text{-}optimal} = \beta/(2 \times \pi \times f) \tag{5.3}$$

5.4.4 Optimal value of EIT

It is to be noted from Fig. 5.2 that the removal of PIR converts R-L circuit into an inductive circuit (neglecting the minor resistance offered by the shunt reactor). Therefore, based on KVL, the equation of supply voltage during removal of PIR is given by,

$$L \; {di}/{dt} = E_m \sin(wt + \alpha) \tag{5.4}$$

By integrating equation (5.4), the instantaneous value of current is given by,

$$i = -\left({E_m}/{(w \times L)} \right) \times \cos(wt + \alpha) + k \tag{5.5}$$

Where, k is the integration constant. By utilizing initial value theorem, it is given by,

$$k = \frac{E_m}{\sqrt{R_p{}^2 + (w \times L)^2}} \left(\sin(wt + \alpha - \beta) - \sin(\alpha - \beta) e^{-\mu t} \right) + \frac{E_m}{wL} \times \cos(wt + \alpha) \tag{5.6}$$

By substituting value of k & putting $\alpha = \beta$ in equation (5.5) and thereafter taking the first order differentiation, the time (t) at which the value of current through the shunt reactor is minimum is given by,

t = n ($\pi/(2 \times w)$) where, n = 1, 3, 5……N (an odd number) (5.7)

The time (t) is nothing but the time up to which the PIR has been inserted into the circuit and it is also known as EIT. Finally, the optimal removal instant ($T_{r\text{-optimal}}$) of PIR is given by,

$T_{r\text{-optimal}}$ = [{n×($\pi/(2 \times w)$} +(β/w)] (5.8)

It is observed from equation (5.8) that the optimum value of EIT is an odd multiple of $\pi/2$ radians at the time of energization of shunt reactor through PIR-CB. In this work, the optimal value of EIT for Yg shunt reactor is taken as $\pi/2$ radians whereas its value is 3 $\pi/2$ for Y/Δ configurations of shunt reactor. The selection criterion for the optimum value of EIT for each configuration of shunt reactor is explained in the section 5.6.1.

In order to determine the optimal value of PIR, by taking Fig. 5.2 as a reference, simulation of energization of two different ratings of three-phase shunt reactors, namely 125 MVAr and 63 MVAr, have been performed. The single-phase equivalent value of the said three-phase shunt reactor is 41.66 MVAr having $(w \times L)$ =1280 Ω/ph and 21 MVAr having $(w \times L)$=2540 Ω, respectively, with EIT = π/2 radians (5 ms). Moreover, the above simulations have been carried out by considering ±1 ms variation in insertion time (T_{in}) and removal time (T_r) of PIR. Furthermore, different values of PIR from 100 Ω to 1700 Ω have been considered and its effect on SCT is observed. Fig. 5.5 shows the variation in the level of SCT at different insertion and removal instant of PIR keeping the ratio of "$(w \times L)/R_p$" constant and vice-versa. It has been observed from Fig. 5.5 that the minimum level of SCT is achieved when the ratio of "$(w \times L)/R_p$" is 2.1 irrespective of the rating of the shunt reactor.

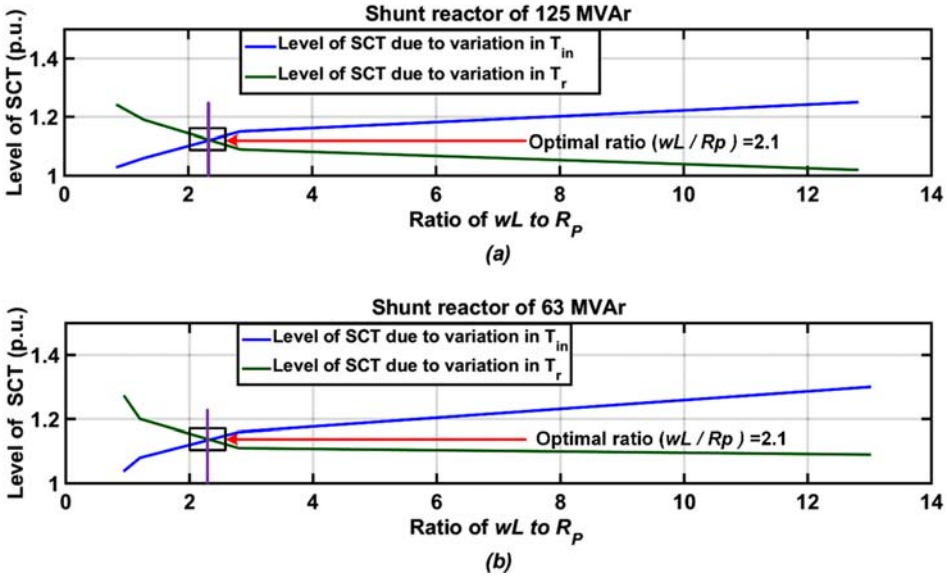

Fig. 5.5 Variation in the level of SCT against different ratio of $(w \times L)/Rp$ considering ±1 ms variation in T_{in} & T_r of PIR for (a) 125 MVAr and (b) 63 MVAr three-phase grounded shunt reactors.

5.5 Controlled energization of three-phase shunt reactors

5.5.1 Effect of mechanical scatter using non-PIR-CB

In practice, the energization of Yg three-phase shunt reactor has been carried out at gap voltage peak for the individual pole of the CB. On the other hand, in case of un-grounded shunt reactor, the optimal making instant is the peak of the supply side line-to-line voltage. In the later case, two phases are closed simultaneously whereas the remaining third phase will be closed after π/2 radians.

Based on controlled switching strategy, the summary of making targets for 3-phase Yg, Y, and Δ connected shunt reactor with non PIR-CB is shown in

. Using these making targets, the simulation study has been performed for energization of 125 MVAr shunt reactor considering ±1 ms mechanical scatter in closing time of the CB for all three connection configurations (Yg, Y, and Δ). Fig. 5.6 shows the simulation results in terms of charging current during energization of a Y connected shunt reactor.

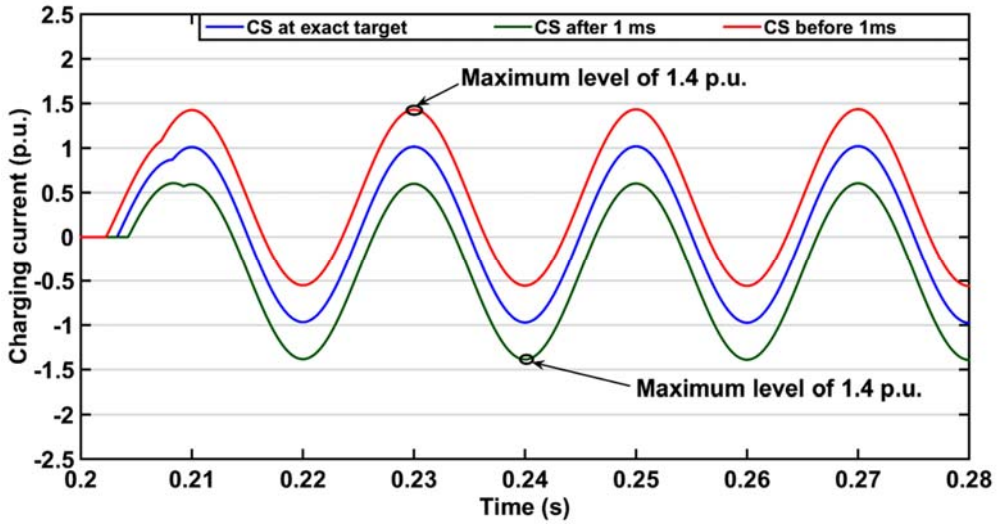

Fig. 5.6 Effect of mechanical scatter on the level of charging current during energization of a Y connected 125 MVAr shunt reactor.

It has been observed from Fig. 5.6 that the maximum deviation in the peak of asymmetric charging current is of the order of 1.4 p.u. considering mechanical scatter of ±1 ms of CB for Y connected shunt reactor.

Table 5.1 Summary of controlled closing targets for three-phase shunt reactor

Configuration of shunt reactor	A-Phase (Radians)	B-Phase (Radians)	C-Phase (Radians)
Yg	π/2	7π/6	5π/6
Y	π/3	π/3	5π/6
Δ	π/3	π/3	5π/6

5.5.2 Proposed methodology

By using the proposed methodology, the level of asymmetric dc component of charging current can be further reduced during energization of a shunt reactor with PIR-CB. In this regard, the same closing sequence (but different targets), as mentioned in section 1.2.2, have been used. The proposed methodology for each type of configuration of the shunt reactor is explained

below.

5.5.2.1 Yg connected shunt reactor

During energization of a three-phase non-coupled Yg shunt reactor, all the three-phases will behave as single-phase reactor as there would not be any inter-phase coupling. On the other end, for Y or Δ connected reactors, the current flows through the reactor only if two poles of CB are closed. In this regard, calculations of L_{eq} *and* R_{eq} are carried out for each configuration of shunt reactor separately.

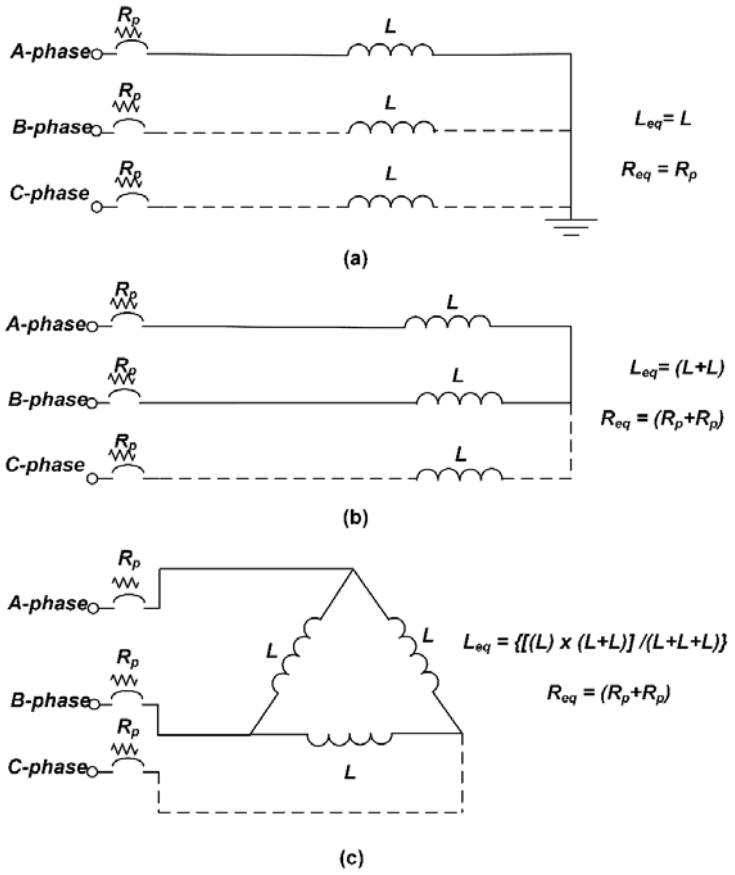

Fig. 5.7 Equivalent circuits for (a) Yg, (b) Y, and (c) Δ connected shunt reactor.

Fig. 5.7 shows an equivalent circuit of shunt reactor having three different configurations (Yg, Y, and Δ). It has been observed from Fig. 5.7 (a) that for Yg shunt reactor, L_{eq} is determined by considering per phase value of inductance *(L)*. Subsequently, by multiplying L_{eq} with w and then dividing the product ($w \times L_{eq}$) with the predetermined optimal ratio (2.1), R_{eq} is calculated. In this case, the optimal value of R_p is same as R_{eq}. Thereafter, β is calculated using equation (5.2).

5.5.2.2 Y connected shunt reactor

In case of energization of Y connected shunt reactor, two-phases are closed simultaneously followed by the closing of the remaining phase after π/2 radians. Hence, the optimal value of EIT will be 3π/2 radians instead of π/2 radians. As observed from Fig. 5.7 (b), due to the simultaneous closing of two phases, the value of *Leq* is determined by considering the series connection of two inductors by neglecting the remaining open circuited phase ($L_{eq} = L+L = 2L$). Subsequently, R_{eq} is determined using the predetermined optimal ratio. As two phases are closed simultaneously, the optimal value of R_p is determined by dividing R_{eq} by 2.1. Thereafter, β is determined using equation (5.2).

5.5.2.3 Δ connected shunt reactor

As observed from Fig. 5.7 (c), due to the simultaneous closing of two phases, the value of Leq is 2L/3 [Leq= (L+ L) || L]. Subsequently, the values of "w×Leq", Req, the optimal value of Rp and β will be calculated by following the same procedure as adopted in Y connected reactor. Table 5.2 shows the suggested insertion and removal targets for PIR during energization of shunt reactor having different connection configurations.

Table 5.2 Proposed insertion and removal targets for PIR during energization of shunt reactor.

Configuration of shunt reactor	Making target of Interrupter (PIR insertion target)			Making target of PIR switch (PIR removal target)		
	A-Phase (Radians)	B-Phase (Radians)	C-Phase (Radians)	A-Phase (Radians)	B-Phase (Radians)	C-Phase (Radians)
Yg	β	$\beta + 2\pi/3$	$\beta + \pi/3$	$\beta + \pi/2$	$[\beta + 2\pi/3] + (\pi/2)$	$[\beta + \pi/3] + \pi/2)$
Y	β	β	$\beta + \pi/2$	$\beta + 3\pi/2$	$\beta + 3\pi/2$	$[\beta + \pi/2] + 3\pi/2$
Δ	β	β	$\beta + \pi/2$	$\beta + 3\pi/2$	$\beta + 3\pi/2$	$[\beta + \pi/2] + 3\pi/2$

5.6 Performance of the presented technique

In order to evaluate the performance of the proposed methodology, a simulation study has been carried out for different values of PIR with the suggested optimal value of EIT. Three values of PIR have been used for evaluation purpose:

(i) Optimal value of PIR, as discussed in section 5.4.3, denoted by PIRoptimal

(determined from Req = (w×Leq)/2.1).

(ii) Value of PIR equal to per phase equivalent reactance of the reactor indicated by PIR1 (determined from Req = (w×Leq)).

(iii)Value of PIR equal to 2.1 times the value of per phase equivalent reactance of the reactor denoted with PIR2 (determined from Req = 2.1×(w×Leq)).

5.6.1 Validation of the proposed methodology for different values of PIR

Table 5.3 shows the maximum level of SCT during energization of three-phase shunt reactor having three different configurations (Yg, Y, and Δ) for optimal and two other values of PIR as discussed above.

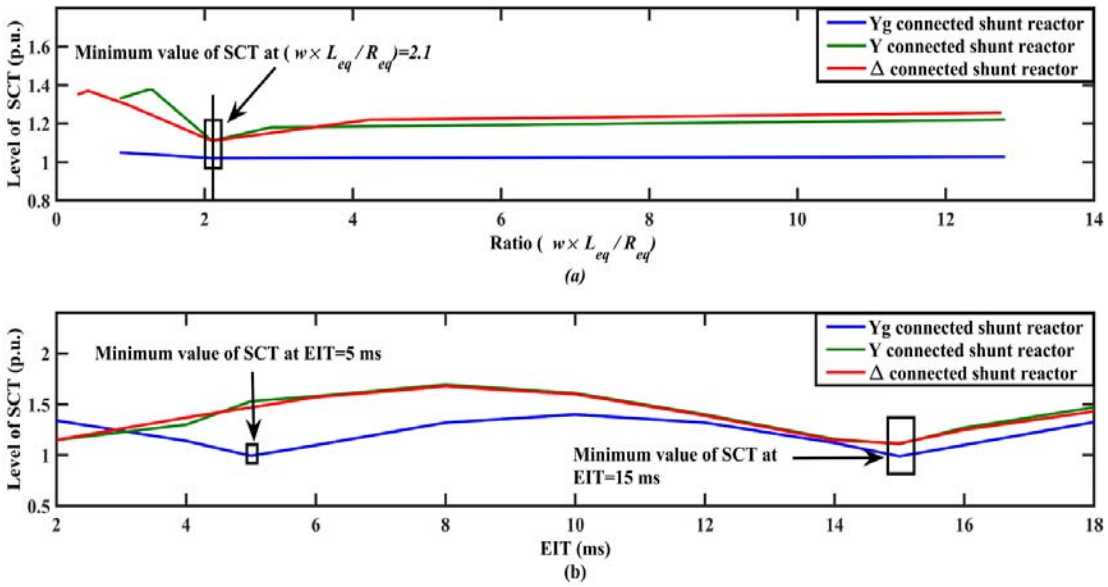

Fig. 5.8 Effect of (a) ($(w\times L_{eq})/R_{eq}$) ratio and (b) EIT on the level of SCT during energization of Yg, Y, and Δ connected 125 MVAr shunt reactor.

It is to be noted from Table 5.3that the level of SCT for optimal value of PIR is of the order of 1.02 p.u., 1.1 p.u., and 1.11 p.u. for Yg, Y, and Δ configuration of shunt reactor, respectively. Moreover, Fig. 5.8 (a) shows the simulation results of energization of 125 MVAr shunt reactor having different configurations (Yg, Y, and Δ) using various values of PIR and corresponding insertion angle β. It is to be noted from Fig. 5.8 (a) that the minimum value of SCT is obtained when $(w\times L_{eq})/R_{eq}$ =2.1.

Table 5.3 Comparison in terms of the level of SCT given by the proposed methodology for different values of PIR.

Value of PIR	Type of configuration	($PIR_{optimal}$)	PIR1	PIR2	EIT (Radians)
Maximum level of SCT (p.u.)	Yg	1.02	1.04	1.05	$\pi/2$
	Y	1.1	1.25	1.37	$3\pi/2$
	Δ	1.11	1.29	1.36	$3\pi/2$

5.6.2 Effect of EIT on the level of SCT

The performance of the proposed methodology has been evaluated during energization of 125 MVAr shunt reactor for three different configurations (Yg, Y, and Δ) with various values of EIT. Here, all the simulations are performed at optimal value of R_p and insertion angle of PIR = $\tan^{-1}((w \times L_{eq})/R_{eq})$. The simulation results in terms of the level of SCT are shown in Fig. 5.8 (b). It has been observed from Fig. 5.8 (b) that the maximum level of SCT is of the order of 1.47 p.u. (for EIT = 5 ms), 1.69 p.u. (for EIT = 8 ms), and 1.67 p.u. (for EIT = 8 ms) for Yg, Y, and Δ connected shunt reactor, respectively. It is clear from Fig. 5.8 (b) that the utilization of optimal value of EIT yields the minimum level of SCT. The similar kind of results are obtained for 63 MVAr shunt reactor. In addition, from Fig. 5.8 (a) and (b), it is to be noted that EIT has a larger influence on the level of SCT compared to the value of PIR [108].

5.6.3 Effect of mechanical scatter

The performance of the proposed methodology has been evaluated by considering effect of mechanical scatter of ±1 ms on PIR-CB during insertion (T_{in}) and removal instant (T_r) of PIR. For all simulation cases, when T_{in} is altered to create the mechanical scatter, T_r is considered to be unaltered and vice versa. Fig. 5.9 shows the simulation results in terms of the level of SCT given by the proposed strategy.

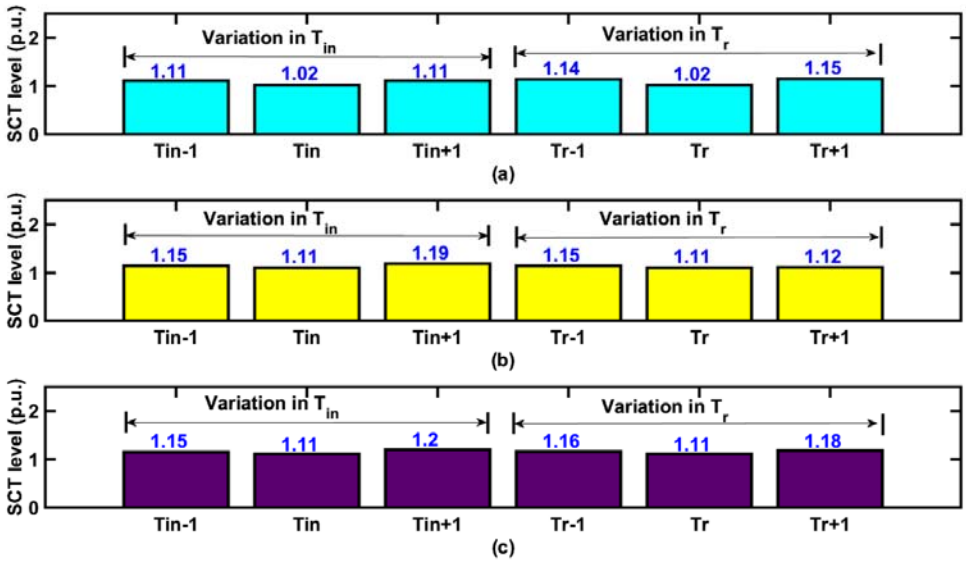

Fig. 5.9 The effect of ± 1 ms scatter of T_{in} and T_r of PIR on the level of SCT for (a) Yg, (b) Y, and (c) Δ connected 125 MVAr shunt reactor.

It is to be noted from Fig. 5.9 that the maximum level of SCT is of the order of 1.15 p.u., 1.19 p.u., and 1.2 p.u. for Yg, Y, and Δ connected shunt reactor, respectively. It is to be noted that, while the PIR is inserted in series with the reactor, the closing of an interrupter shall be done at power factor angle. On the other hand, the removal of PIR should happen at gap voltage peak due to inductive nature of the equivalent circuit.

5.7 Field results for switching of shunt reactor

At 400 kV and 765 kV voltage levels, PIR having a value of R_p = 400 Ω with EIT of 8 ms is used by the utilities in India for switching of transmission lines. The performance of the proposed methodology has been verified by taking actual values of PIR and EIT from an existing 765 kV Indian sub-station. For performance evaluation, PIR-CB, placed in tie bay for OHB scheme designed for line switching, has been used to back charge a non-coupled grounded reactor. During normal condition, the reactor is operated with non PIR-CB connected in main bay of the same "dia". Its rating is 240 MVAr at 765 kV system voltage.

Mostly, the shunt reactor is switched ON under light load condition when the voltage profile is higher than the rated value. In this case, the system voltage is found to be 810 kV on DR. It is to be noted that the achieved targets have been delayed in the range of 10^0 to 30^0. This is due to non-availability of an accurate value of RDDS for PIR-CB and also because of the scatter in interrupter as well as PIR contacts. It is observed that removal instant of PIR and gap voltage of PIR-CB also diverges. This leads to variation in MIT, which in turn changes EIT.

Three live energization operations for the aforesaid 765 kV, 240 MVAr non-coupled shunt reactor have been performed. The results in terms of waveform captured by DR for one of the sample cases is shown in Fig. 5.10.

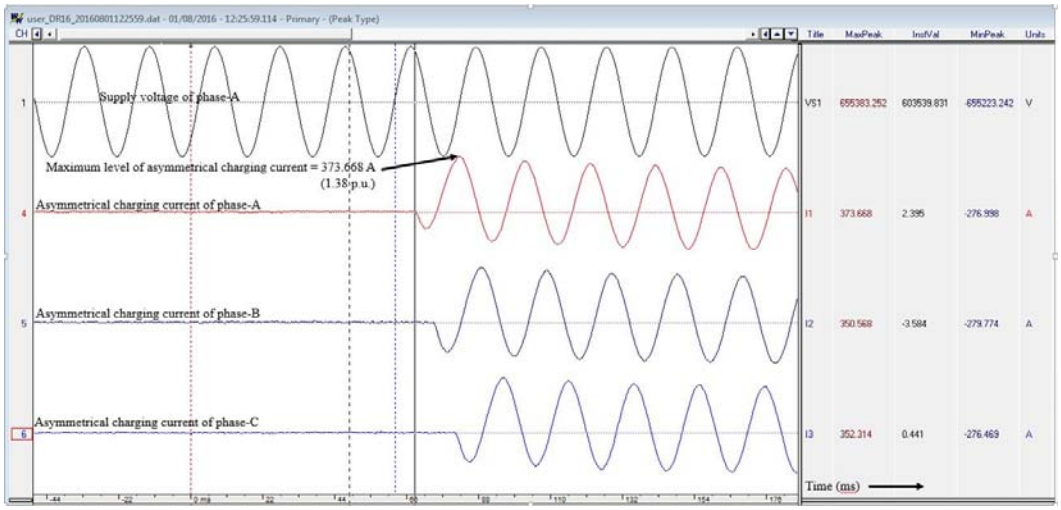

Fig. 5.10 Field results of energization of Yg 240 MVAr shunt reactor.

In order to validate the proposed methodology, a simulation study has also been carried out by taking the parameters of PIR-CB (Value = 400 Ω and MIT = 8 m) same as actual field. Hence, the system voltage is taken as 810 kV. Moreover, energization of individual phase is carried out at same instance as that observed during the live switching operations. The simulation results are summarized in Table 5.4

Table 5.4 Comparison between field and simulation results.

Sr No.	DR No		Optimal Target (Degree)	Insertion angle of PIR (Degree)			Maximum level of asymmetric charging current for individual phase (p.u.)					
							Observed during field switching			Obtained from simulations		
				A	B	C	A	B	C	A	B	C
For 240 MVAr shunt reactor												
1	Field	1	β=80.73 & EIT = 8 ms	99	114	102	1.36	1.33	1.32	1.32	1.48	1.41
2		2		112.5	96	88.5	1.38	1.296	1.303	1.388	1.219	1.13
3		3		117	91.5	97.5	1.35	1.28	1.28	1.43	1.17	1.24
4	Simulation		β=80.73 & EIT = 8 ms	β	β	β	-	-	-	1.16	1.13	1.1
5			β=80.73 & EIT=5 ms	β	β	β				1.02	1.013	1.011
For 180 MVAr shunt reactor												
6	Field		β=83.028 & EIT = 8 ms	85.5	82.5	84	1.041	1.063	1.1	1.06	1.071	1.1

During POW switching, the accuracy of closing/opening of CB contacts depends on the characteristics of CB [23]. Recently, the new generation of high voltage Sulpher hexaflouride (SF6) CBs offers the making target accuracy up to 0.5 ms [23]. By utilizing aforementioned high-speed CB, the optimal making target has been achieved with an accuracy of 0.5 ms, which limits the asymmetric charging current up to 1.1 p.u. In this regard, energization of a Yg connected 180 MVAr shunt reactor has been performed on an existing 765 kV Indian substation using latest PIR-CB (PIR = 400 Ω & EIT= 8 ms). In this case, the PIR has been inserted at an optimal angle β for each phase. The results in terms of waveform captured by DR of energization of Yg connected 180 MVAr shunt reactor is shown in Fig. 5.11. It has been observed from Fig. 5.11 that these results are almost mapped with simulation results of

(case no. 6). It is to be noted that the insertion angle of PIR is with reference to positive going zero-crossing of the voltage of individual phase. It can be observed from Table 5.4 that the asymmetric dc component achieved from the simulations and that obtained from live switching closely matches with a maximum error of just 9%.

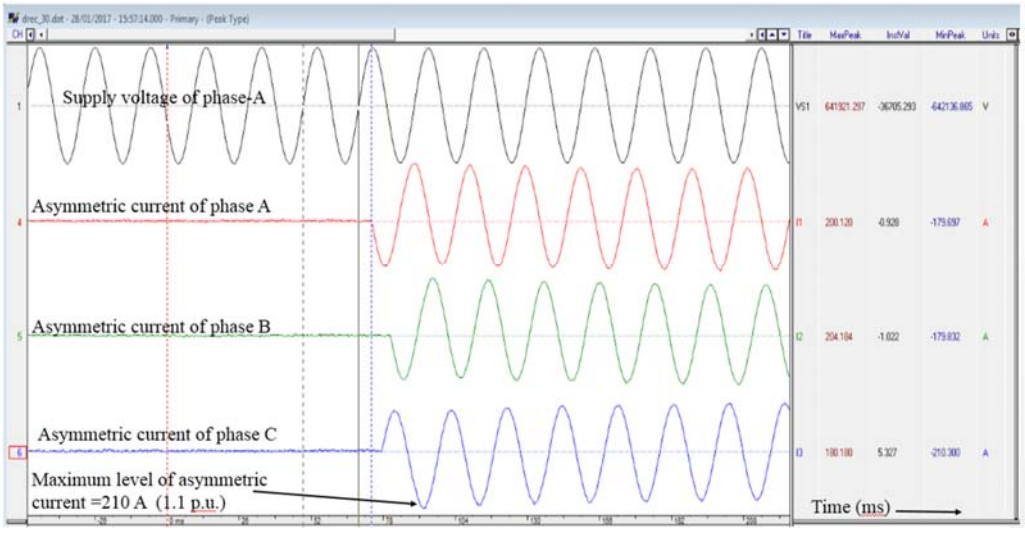

Fig. 5.11 Field results of energization of Yg 180 MVAr shunt reactor.

This validates the applicability of the suggested methodology in the real field. Finally, the summary of the comparative evaluation of field results with the proposed methodology is shown in Table 5.5.

.

Table 5.5 Summary of comparative evaluation of field results with the proposed methodology for non-coupled Yg shunt reactor with PIR of 400 Ω.

Closing angle (Radians)	Mechanical Scatter (ms)	Maximum level of asymmetric charging current (p.u.)	EIT (ms)
$\pi/2$	None	1.36	8
β	±1	1.29	
	None	1.16	
		1	5
β	± 0.5	1.1	8

It can be well appreciated that the level of the asymmetric dc component of charging current is limited up to 1.16 p.u. using the proposed methodology. It utilizes PIR-CB, which is actually designed for transmission line application (PIR = 400 Ω and EIT = 8 ms) having a making target accuracy of ±1 ms and ± 0.5 ms.

5.8 Summary

A new methodology is presented, which effectively minimizes the asymmetric dc component of charging current during energization of a shunt reactor by utilizing CSD along with PIR-CB. The presented technique depends on optimization of insertion instant, EIT and the value of PIR. The performance of the proposed methodology has been evaluated by modeling an existing 400 kV, shunt reactor employed in OHB and line connected to non-switchable reactor scheme using PSCAD/EMTDC software package. A large numbers of data set have been generated by varying rating & configuration of shunt reactor, EIT, insertion & removal instant and the value of PIR. The results indicate that the presented technique limits the magnitude of asymmetric dc component present in charging current between 1.02-1.11 p.u. for various configurations of shunt reactor. Considering ± 0.5 ms and ± 1 ms scatter in closing time of interrupter and PIR bypass switch, the proposed methodology reduces the level of charging current of the order of 4%, 26%, and 37% for Yg, Y, and Δ configuration of shunt reactor. Moreover, the mitigation achieved upon applying the suggested targets during three live energization operations for a non-coupled 240 MVAr shunt reactor with PIR-CB designed for line switching application at 765 kV level is also presented. By comparing actual field results with simulations, the maximum error of 9% has been observed, which validates the applicability of the proposed method in the real field.

Chapter 6

Controlled Energization of an unloaded Power Transformer

6.1 Introduction

This chapter presents application of the controlled switching device for reducing the level of inrush current and TVD during energization of an unloaded power transformer using circuit breaker having PIR. As mentioned in section 1.4.3, controlled energization of an unloaded power transformer has been carried out at peak of V_{GAP}. However, in real field, due to the effect of MOT scatter of the CB, the level of inrush current attains high value during energization of an unloaded power transformer. In order to understand effect of MOT scatter, detail study of operating mechanism of the CB has been required. This includes in depth knowledge of auxiliary contact used as a feedback for CSD, tolerance of CB contacts closing, and effect of aging of CB in tolerance. Further, the level of inrush current during controlled energization also depends on the type of power transformer such as electrically coupled and magnetically coupled. The modelling of a complete system consisting of a power source, PIR-CB, and two types of power transformers (electrically and magnetically coupled) has been carried out using PSCAD/EMTDC software package. The results obtained from the simulations are compared with the results acquired during energization of similar transformers in real field.

6.2 Controlled energization of an unloaded power transformer

6.2.1 Recent practices used in the field

In practice, three kinds of switching strategies are used for mitigation of inrush current during controlled energization of an unloaded power transformer.

(i) In the first method, energization of an unloaded power transformer is done at gap voltage peak without considering the level of residual flux. However, this is compromised solution.

(ii) The second strategy is to energize the transformer when the magnitude of the residual flux is same as the prospective flux. Here, the level of residual flux is estimated by integrating the load side voltage.

(iii) The recent practice in Asia region is to perform controlled de-energization before the controlled energization of a transformer. This controlled de-energization brings the lowest possible value of the residual flux.

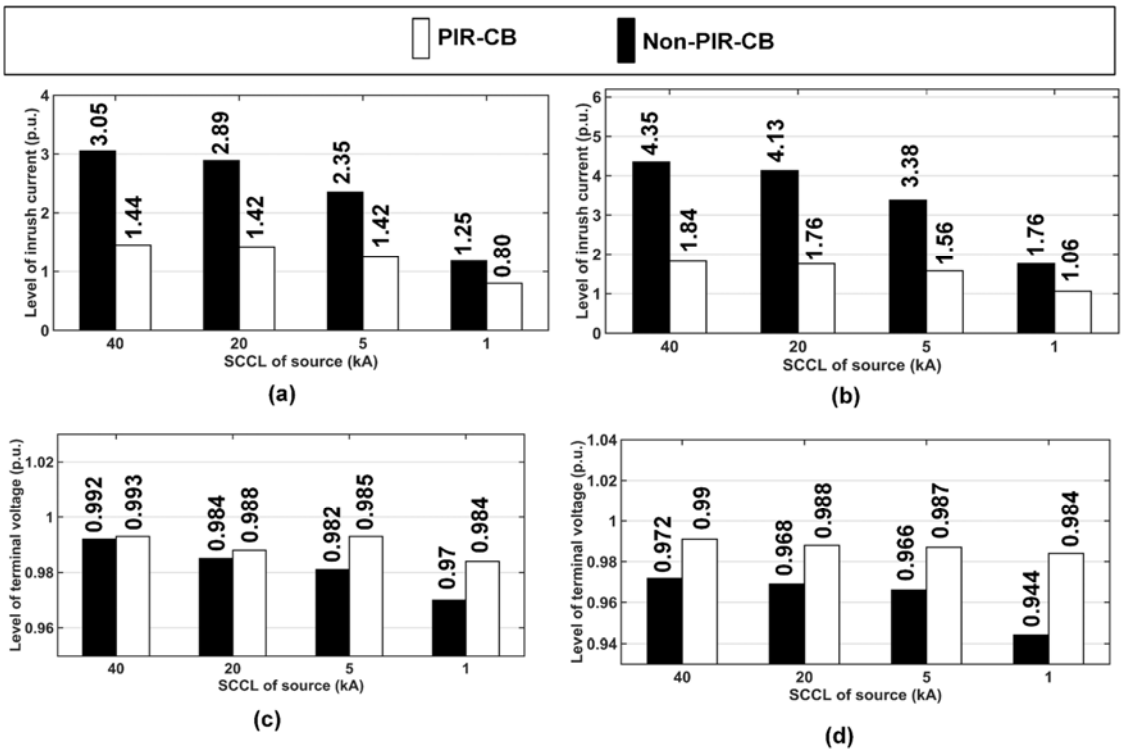

Fig. 6.1 Simulation results during controlled energization of a power transformer (a), (c): Level of inrush current and terminal voltage without scatter (b), (d): Level of inrush current and terminal with scatter.

While energizing an unloaded power transformer using aforementioned strategies, the main difficulty is the achievement of the optimal making target due to MOT scatter of the CB. Moreover, in order to accomplish the optimal making target, all controlled switching strategies (including the recent one) have utilized non-PIR-CB.

In order to evaluate the performance of PIR-CB against non-PIR-CB using strategy (i), a simulation study has been carried out. Here, controlled energization of a 500 MVA, Yg/Y/ Δ connected magnetically coupled unloaded power transformer has been performed using different SCCL of the source (40 kA, 20 kA, 5 kA, and 1 kA). Moreover, this simulation study has been done considering the highest level of remanence. In the above study, the value of PIR and MIT of PIR-CB is taken as 400 Ω and 10 ms, respectively [7]. The level of remanence in phase-A, B, and C is considered as '0.9' p.u., '-0.45' p.u, and '-0.45' p.u., respectively. The phase-A is closed at peak of the gap voltage whereas, other remaining phases are closed at 5ms after closing of phase-A. The simulation results without considering the effect of MOT scatter are shown in Fig. 6.1 (a) and (b). Conversely, the simulation results considering the effect of MOT scatter of the order of ±1 ms are shown in Fig. 6.1 (c) and (d). It has been observed from Fig. 6.1 that after considering the effect of MOT scatter, the maximum level of inrush current using non-PIR-CB

and PIR-CB is of the order of 4.35 p.u. and 1.84 p.u., respectively. On the other hand, the minimum level of terminal voltage using non-PIR-CB and PIR-CB is of the order of 0.944 p.u. and 0.984 p.u., respectively. The voltage may go further down in case of weak grid systems, which further leads to higher impact on other plants connected with the same network.

The controlled switching strategy (ii) may not be utilized in cases where load side voltage measurement is not available. In fact, the load side voltage measurement in the transformer is not required for protection purpose except in power plant. Conversely, for the controlled switching strategy (iii), energization of an unloaded transformer is initially performed at the peak of gap voltage by neglecting the level of residual flux after controlled de-energization. During this energization, the pattern of inrush current has been captured through DR. Thereafter, the simulation study has been done using the same system parameters and the similar pattern of inrush current is obtained. Based on the simulation results, the MOT scatter of CB, optimal closing targets, and the level of remanence have been evaluated.

6.2.2 Effect of PIR-CB during energization of an unloaded power transformer

It has been observed from Fig. 6.1 that there is an improvement in the maximum level of inrush current and the transient voltage profile during energization of an unloaded power transformer using PIR-CB compare to non-PIR-CB (conventional methodology). Utilizing this fact, this chapter explores energization of an unloaded power transformer using PIR-CB.

The PIR-CB contains two switches (namely interrupter and PIR switch) with PIR per phase. The details of various configurations of PIR, their behaviours, and the advantages of different configurations are reported in the literature [6], [103]. In practice, the hybrid combination of PIR-CB with controlled switching device can be implemented without any additional efforts. One of the examples of this combination is the utilization of one-and-half breaker scheme. The single-line-diagram of one-and-half breaker scheme is shown in Fig. 6.2 (a). As shown in Fig. 6.2 (a), controlled switching device is provided on the tie bay to improve the level of inrush current and transient voltage performance during controlled energization of a power transformer whereas PIR-CB has been used for energization of an uncompensated transmission line [74]. During energization of an unloaded transformer, the PIR has been inserted by closing an interrupter first and it is bypassed by closing the PIR switch after completion of MIT. As the electrical and mechanical closing instants of interrupter are dissimilar, the EIT and MIT of PIR-CB are also different from each other. It is to be noted that the time lapse between the electrical closing of interrupter and PIR switch is known as EIT whereas the time lapse between the mechanical closing of an interrupter and PIR switch is defined as MIT [6], [7], [103].

It can be well appreciated that any CB with PIR can be designed based on the MIT, which is a fix value. Conversely, the EIT will depend on shape & magnitude of gap voltage and values of RDDS of an interrupter & a PIR switch. The above fact can be visualized from Fig. 6.2 (b), which shows the simulation results during energization of 500 MVA unloaded (Yg/Y/Δ connected) transformer using PIR-CB. Here, the value of PIR and MIT of PIR-CB is taken as 400 Ω and 10 ms, respectively. It has been observed from Fig. 6.2 (b) that the electrical and the mechanical closing instants of an interrupter are dissimilar due to high gap voltage. Conversely, these closing instants for PIR switch are overlapped with each other due to high value of RDDS and low value of the gap voltage.

6.3 Network modelling

6.3.1 Modelling of a power transformer

As mentioned in section 1, modelling of two types of power transformers are carried out for their controlled energization using PIR-CB.

(i) (Yg, Y, Δ: 765, 400, 33), 1500 MVA, a bank of three 1-Φ (electrically coupled) transformer.

(ii) (Yg, Yg, Δ: 400, 220, 11), 500 MVA, 3-limb (magnetically coupled) transformer.

The modelling of both aforementioned power transformers is carried out using PSCAD/EMTDC software package [83], [109]. A sampling frequency of 1 kHz has been used for a fundamental frequency of 50 Hz. Fig. 6.2 (c) shows a single-line-diagram, which represents modelling of power transformers, PIR-CB, and source. The parameters of power transformer are given in Appendix A4. Generally, in order to optimize the design and also to limit the no-load losses in the range of 0.5% to 1% of its nominal MVA rating, the EHV and UHV power transformers (400 kV and above) are designed for the knee point voltage of 1.1 p.u. On the other hand, shunt reactors are designed for the knee point voltage as high as 1.25-1.3 p.u. due to their comparatively lower MVA rating [110]. Furthermore, in order to maintain the system stability at EHV and UHV level, the system voltage never exceeds 1.1 p.u. during healthy condition [47], [110]. Hence, during energization, shunt reactor rarely saturates whereas the probability of saturation of the core in EHV and UHV transformer is fairly high. Moreover, the level of saturation (remanence flux) during energization of a power transformer depends on operating flux density and its B-H characteristic. The saturation characteristic is modelled in PSCAD considering material of the core, characteristic of B-H curve, and no-load losses of the model used in the power transformer. Moreover, the required level of remanence flux for individual phases of the power transformer is achieved by connecting dc current source of appropriate

magnitude just prior to its energization [56]. While modelling the transformer, it is to be noted that the algebraic sum of the residual flux of all three windings remains zero for magnetically coupled transformer as it is made up of three limb assembly. This concept is also applicable to electrically coupled transformer as one of its winding is connected in Δ.

6.3.2 Modelling of PIR-CB

In order to mitigate the switching transients, close coordination between CB and load side apparatus is highly desirable [62]. Therefore, the modelling of PIR-CB replicating actual operating condition is extremely important. To achieve this, the resistance, mechanical & electrical insertion and removal instants and hence, MIT shall be chosen with utmost care. If power transformer saturates during no-load energization, it offers very low inductance, which results into the very high level of inrush current. However, insertion of an additional resistor (using PIR-CB) during energization of transformer would improve the inrush current and transient performance of the connected network [111]. The parameters of PIR–CB are mentioned in Appendix-A4. These parameters are calculated using reference [7]. In the proposed work, series PIR configuration has been used throughout the simulation study [112].

6.3.3 Modelling of different grid sources

The modelling of source with different SCCL has been carried out using PSCAD/EMTDC software. The parameters of source are given in Appendix-A4.

6.4 Energization of a power transformer using PIR-CB

In this section, performance evaluation of the proposed methodology, during energization of an unloaded power transformers (one is electrically and the other is magnetically coupled) with PIR-CB, is presented. As the proposed methodology is based on controlled strategy (iii) controlled de-energization is performed prior to controlled energization of the transformer. Here, the same PIR, which is mainly designed for the transmission line energization, is used during energization of the power transformer. The value of MIT and PIR is considered as 10 ms and 400 Ω, respectively. The minimization in the level of inrush current along with reduction in TVD, which is one of the important power quality issues are the main objectives of the proposed methodology. In order to achieve the above objectives, the step-by-step procedure followed for the evaluation purpose is shown in Fig. 6.3.

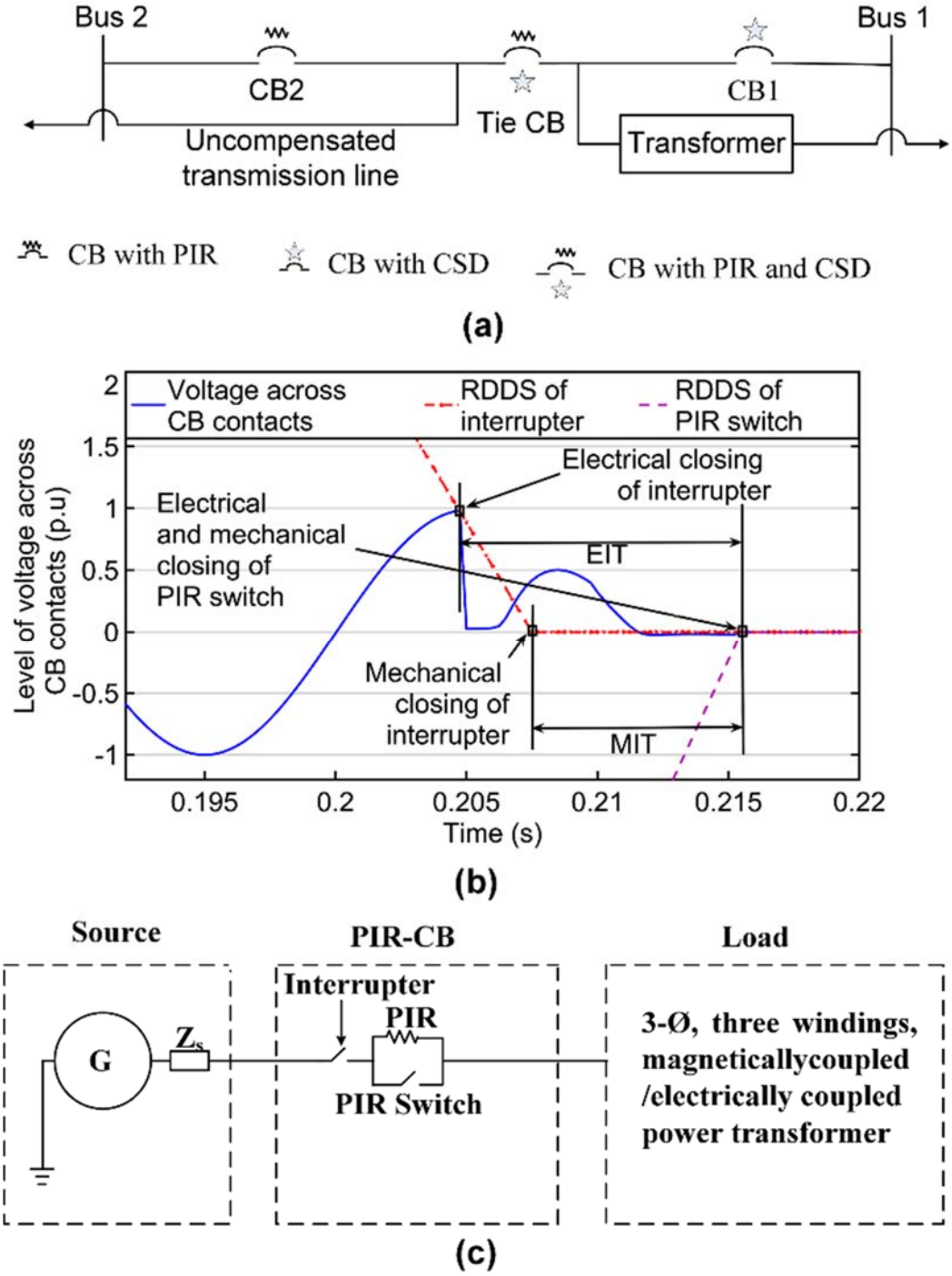

Fig. 6.2 (a) Single line diagram of one-and-half breaker scheme, (b) simulation results showing a conceptual view of EIT and MIT of PIR-CB, and (c) modelling of source, PIR-CB, &power transformer.

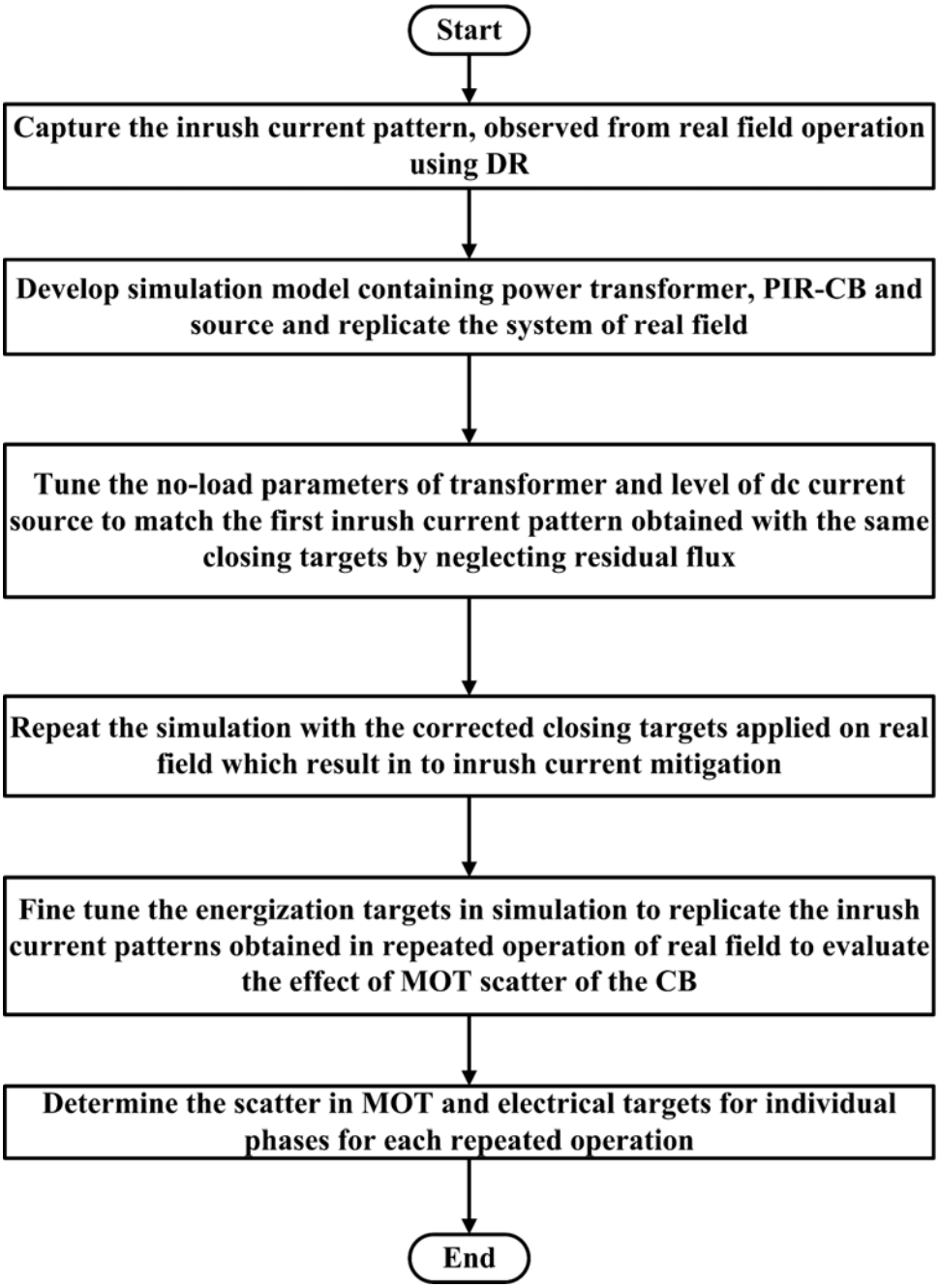

Fig. 6.3 Step by step procedure for evaluation study.

In the first step, controlled de-energization is performed to lock the level of residual fluxes linking with the individual phase. In the next step, controlled energization is performed with the suggested targets, as mentioned in [58], for coupled power transformers by neglecting residual fluxes. The pattern of inrush current of individual phase, during this energization, is captured using DR. This pattern is used to evaluate the level of remanence flux for individual phase using PSCAD simulations. Consequently, corrections required in controlled energization

targets are evaluated to minimize inrush currents for all three-phases. In the next step, another real switching operation is performed with corrected targets and the inrush current for individual phase is recorded. This process of controlled de-energization and energization of the transformer is repeated 2-3 times to ensure the repeatability of inrush current mitigation. However, due to statistical scatter in MOT of an interrupter and PIR switch of the PIR-CB, slight variation in the mitigation effect is observed in subsequent operations. Consequently, the scatter in MOT and electrical targets for individual phase are evaluated for each repeated operation.

6.5 Field results and discussion

6.5.1 Parameters responsible for MOT scatter of the CB

The MOT of CB changes due to statistical and systematic variations [103]. The systematic variation in MOT is due to external parameters such as variation in the ambient temperature, dc battery supply voltage and aging effect (time after installation). On the other hand, statistical parameters cannot be controlled. The latest generation of controlled switching relay has facility to compensate MOT variation using appropriate correction curves. Hence, the minor deviation in mitigation, which is observed during the successive operation will be mainly due to statistical variation. The importance of variation in MOT of the CB with respect to controlled switching application is explored in IEC 62271-302 standard. The main objective of this standard is to explain various ways to examine the suitability of the CB to meet the requirements of controlled switching. It is to be noted that the targets reported in the literature of application of controlled switching are electrical closing targets. During controlled energization of the power transformer, these targets are attained through the mechanical closing targets of the CB. However, in practice, the actual mechanical closing time ('T_{mech}') of the CB has been determined by collecting the feedback from the closure of the auxiliary contact ('52-A', normally open), which is located on main shaft of the CB. This auxiliary contact will attain the same kind of displacement that is attained by the main contact of the CB. The mechanism is set in such a way that the auxiliary contact is closed after the main contact of the CB. Moreover, it can be appreciated that the auxiliary contact has inherent variation (tolerance). This tolerance shall be maintained in the range of ± 0. 5 ms to replicate statistical variation of main contact timing with a good amount of accuracy. This is required to ensure repeatability of mitigation effect of inrush current on successive operations. These aforementioned variations are well understood from Fig. 6.4 (a) - (c). It has been observed from Fig. 6.4 (a) that the optimal closing target of the main contact of CB is 'k1'. However, due to the effect of the statistical variation, the actual mechanical closing of the main contact of CB either advances ('ko') or delays ('k2') by 0.5 ms. Similarly, 52-A contact also introduces an inherent tolerance of the order of ±0.5 ms

(as shown in Fig. 6.4 (b)). As explained earlier, the closing of the main contact of CB is determined based on the feedback received from the auxiliary contact. Utilizing this fact and considering the combined effect of statistical variation in main contact timing of CB and tolerance of the auxiliary contact, in extreme condition, the correction in MOT for the next operation of the CB may advance ('Δx') or delay ('Δy') by ±1 ms (as shown in Fig. 6.4 (c)). It is to be noted that the actual operating time of the main contact may advance by 0.5 ms and correction may delay by 0.5 ms resulting into closing time correction in next operation by 1 ms in an incorrect way. Moreover, the controlled switching system with auxiliary contact feedback must be tuned for repetitive inrush current mitigation. Consequently, the observed inrush current variation in successive operations shall be acceptable. In real field, it is observed that aforementioned effect results in to inrush current variation in the range of 0.25 p.u in successive operations. Moreover, the aforementioned range may vary depending on characteristic of apparatus such as CB, power transformer and grid source. Furthermore, MOT of the CB, over a period of time, varies from 0.1 ms to 1.2 ms due to aging effect in a systematic manner. Considering 50 ms as the ideal MOT of CB, Fig. 6.4 (d) shows the variation in the MOT of the CB due to aging effect. It is to be noted that the above values are only for explanation purpose and does not replicate any CB characteristics and also differ from breaker to breaker. Furthermore, the major disturbance such as heavy short circuit will result into the rapid aging of the CB [103]. Moreover, the variation in MOT of the CB contact is tracked using auxiliary contact, which again changes either by Δx or Δy duration. Hence, it is very difficult to predict the actual MOT variation of the CB for any operation.

In order to observe variation in electrical closing target due to the MOT scatter (of the order of ±1 ms), a simulation study has been carried out. In this study, controlled energization of a 500 MVA magnetically coupled power transformer has been performed considering the high level of remanence (0.9 p.u. in phase A and -0.45 p.u in both B and C phases) using PIR-CB (400 Ω, MIT=10 ms). The simulation results are shown in Fig. 6.5. It has been observed from Fig. 6.5 that the electrical closing target shifts from point 'a' to point 'b' due to the effect of MOT scatter of the CB (due to shifting of mechanical closing target from 'c' to 'd'). It is to be noted that the value of RDDS of the CB also has inherent statistical scatter in the range of 10 % to 20% with respect to the time after installation of the CB. However, in order to avoid complexity, this effect has been ignored. It is to be further noted from Fig. 6.5 that for chosen value of MIT, the mechanical insertion & removal instant of PIR changes due to statistical variation in the main contact and the PIR switch contact. When this is projected on gap voltage,

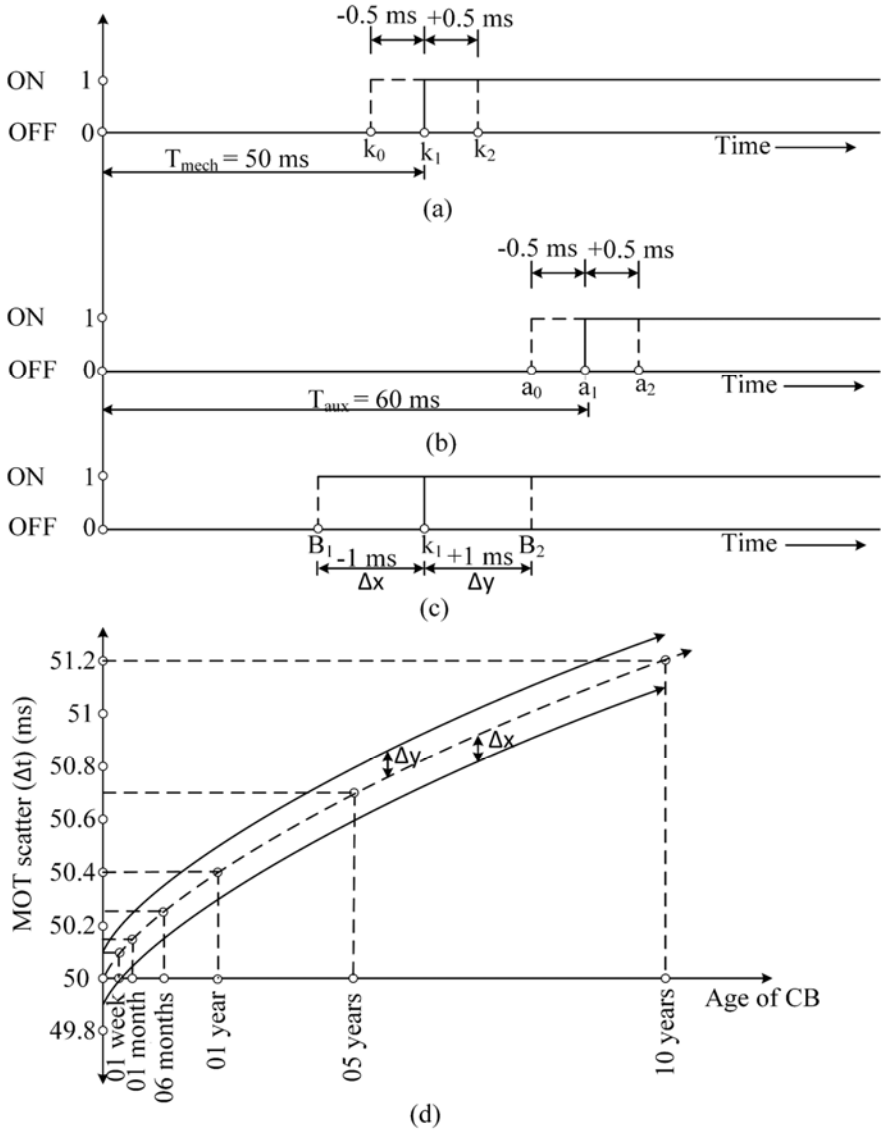

Fig. 6.4 Effect on MOT of CB due to (a) statistical scatter of main contact,(b) tolerance of auxiliary contact, (c) considering both (a) & (b), and (d) aging effect.

it results into change in electrical insertion & removal instant of PIR. This may further magnify the variation in EIT depending upon the nature of gap voltage and statistical scatter of an interrupter and PIR switch. Further, it can be observed that the electrical and mechanical removal of PIR switch is almost same (as shown by zoom portion 'p' in Fig. 6.5) due to rapid decay in the level of gap voltage (from 'S1' to 'S2') after insertion of the PIR. The value of EIT changes (EIT1 to EIT2) widely in comparison to fixed value of MIT

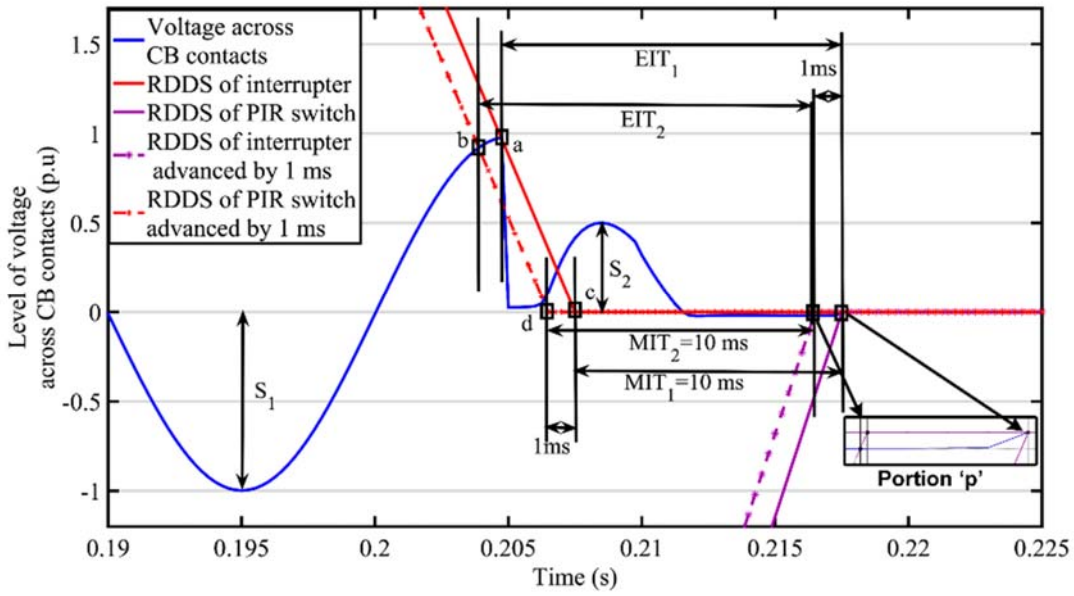

Fig. 6.5 Effect of mechanical scatter on electrical closing target and EIT of PIR-CB

6.5.2 Experimental field set-up

The details of power system network, from which the field results are obtained, is shown in Fig. 6.6. The single-line-diagram of one-and-half breaker scheme is shown in Fig. 6.6 (a). The connection of various inputs to controlled switching device from the transformer bay equipment such as command circuit, busbar side CCVT, auxiliary contacts of CB, substation SCADA, etc. are shown in Fig. 6.6 (b). The details of the layout are explained as under.

In an Asia Pacific region, most of the substations at EHV and UHV level are equipped with one-and-half-breaker scheme. In order to minimize the level of switching transients, this scheme has PIR-CB connected at one-end (bay) for the switching of the transmission line and controlled switching device on other-end (bay) for the application of controlled switching of the power transformer.

It is important to note that the 'tie-bay CB' of the one-and-half-breaker scheme contains both PIR-CB and controlled switching device to perform the switching of the transmission line and power transformer, respectively. In the proposed methodology, this tie-bay CB has been used to perform controlled energization of an unloaded power transformer using PIR-CB. The details of this PIR-CB with controlled switching device are shown in Fig. 6.6 (b).

(i) Input data module: The controlled switching device acquires real-time data of busbar side voltage and transformer side current signals through instrument

transformers of the transformer bay. The current signal is converted into voltage signal using I-V converter. Thereafter, it is fed to data evaluation module of controlled switching device through Analog to Digital Converter (ADC). On the other hand, the voltage signal is fed directly to the data evaluation module of controlled switching device using ADC. The close/open commands from SCADA/manual switch are connected to controlled switching device and the output commands to trip coil and closing coil of CB are wired from respective output terminals of controlled switching device. Furthermore, in case of problem with operation of controlled switching device, there is an additional provision for manual mode operation of the CB, which bypasses or blocks operation of CB through the controlled switching device.

(ii) Controlled Switching Device: Once the random opening or closing command has been initiated, the prime function of the controlled switching device is to convert this random opening/closing command into controlled opening/closing command by introducing an intentional time delay in the CB operation. This intentional time delay has been calculated based on voltage and current data acquired from the actual field. Moreover, based on the type of load to be switched such as transmission line, transformer, shunt-reactor, and shunt capacitor, evaluation of the optimum switching targets will be carried out by the controlled switching device. For this purpose, different settings are provided in controlled switching device. Various modules of controlled switching device with their respective tasks have been listed below.

(iii) Data storage module: The function of this module is to store the data acquired by the ADC.

(iv) Data evaluation module: This module performs following tasks.

- It analyses the voltage and current signals acquired from the real field.
- It evaluates the MOT for last operation of the CB by collecting the feedback from an auxiliary contact.
- It detects zero crossing of busbar side voltages for individual phases. This will be used for evaluating optimum output command for individual poles of CB after considering their operating times of the CB. This is known as adaptive operating time functionality and it is based on the auto-compensating curve fitting technique.

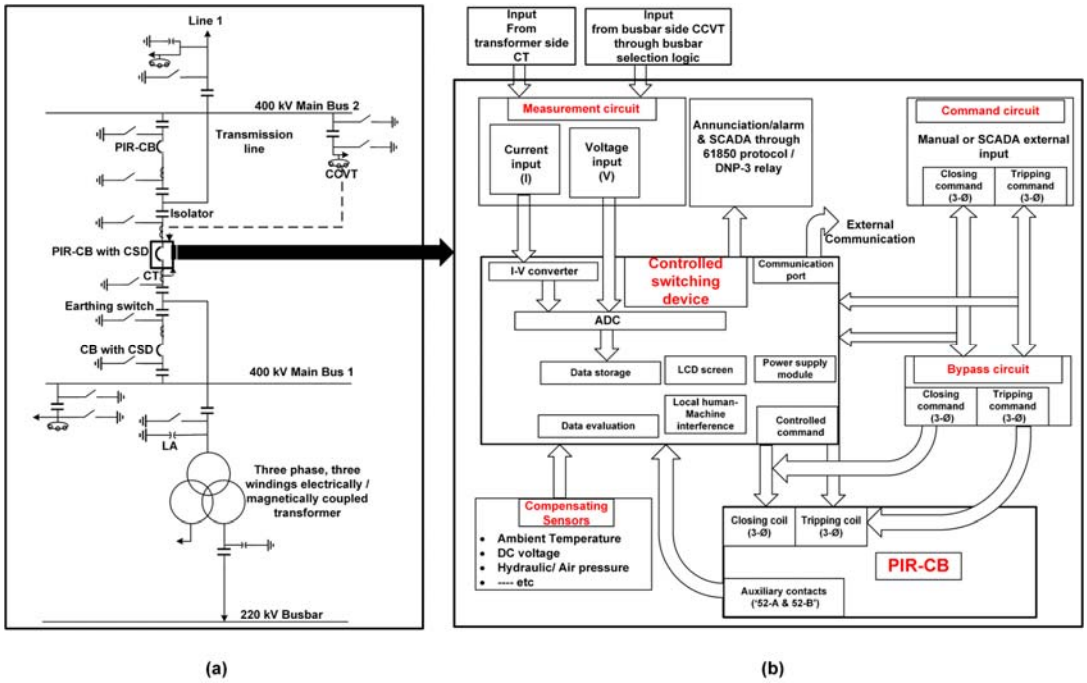

Fig. 6.6 Details of field set-up (a) single-line-diagram of one-and-half breaker scheme and (b) connection between different ports, controlled switching device, and CB

- Variation in different parameters such as ambient temperature, dc supply voltage, and hydraulic/air pressure of the CB are responsible for change in the MOT of the CB. This else otherwise, would result into incorrect determination of the actual switching targets. Required compensation factor in operating time of individual poles of CB (both close and open) has been evaluated based on data collected from compensating sensors. Hence, this module calculates an intentional time delay after the initiation of input close or open command considering all the above-mentioned parameters, which are required to be considered as they are responsible for change in the MOT of the CB.

(v) Power supply module: The function of this module is to supply various levels of dc voltages to different modules of the controlled switching device.

(vi) Communication module: Various IEDs have been installed at the controlled room of the substation. They support different communication protocols such as IEC 61850-8-1, IEC 61850-9-2LE, and Hyper Text Transfer Protocol (HTTP) over Ethernet. They are connected to Ethernet-based communication systems via the

RJ-45 connector or fiber-optic multimode LC connector. All the information and controls are regulated through different communication protocols. However, the horizontal communication (Generic object oriented substation events (GOOSE)) between the IEDs is enabled through IEC 61850-8-1 communication protocol. The connection of disturbance recorder or the files of captured waveforms have been accessed using IEC 61850.

(vi) Human interference and LCD screen: Separate port for human interference is placed with monitoring screen. This port is mainly used to employ particular setting out of different available settings for the switching of various power apparatus in controlled switching device.

(vii) Circuit Breaker: MOT of the CB varies due to systematic and statistical variations. Various compensation sensors are used to achieve required correction in operating time of CB due to change in external parameters such as ambient temperature, dc supply voltage, and hydraulic/air pressure of the CB. It also contains assembly of pre-insertion resistor.

6.6 Field results during energization of a power transformer using PIR-CB

In one-and-half breaker scheme, it is usual practice to use PIR of the order of 400 Ω for the energization of transmission line. The same value has been utilized by the proposed scheme during energization of transformers. Moreover, the literature reported in the field of controlled switching applications depicts that strategies used during energization of an unloaded power transformer depend on connection configuration of the winding [58]. When energization is performed on Yg connected winding side of the transformer with electrical and/or magnetic coupling, the resultant fluxes for remaining two phases change dynamically after energization of first phase. The nature of these dynamic fluxes, in case of the magnetically coupled transformer, may exhibit completely different behaviour compared to an electrically coupled transformer. Consequently, the performance is evaluated for both types of transformer, which is part of an existing Indian power system network. These transformers are:

(i) Bank of three 1-Φ transformers with delta connected tertiary (electrically coupled, 1500 MVA)

(ii) Three-limb transformer (magnetically coupled, 500 MVA).

In case of a bank of three 1-Φ transformers with delta connected tertiary winding, all three transformers are electrically coupled but magnetically de-coupled. Hence, the level of

dynamic fluxes does not change widely. Whereas in case of three limb transformer, all the three windings are magnetically coupled, which results into very strong coupling between three-phases. Because of that, the level of dynamic flux changes widely due to the higher sensitivity of the magnetic circuit. Considering PIR of 400 Ω and MIT of 10 ms for both the transformers, various field cases generated during controlled energization of an unloaded transformer are depicted in Table 6.1.

Table 6.1 Summary of field cases generated

Sr. No	Type of transformer	Number of operation to judge the level of remanence and optimal closing targets	Number of operations to minimize the effect of MOT scatter of CB	Total
1	Electrically coupled	01	03	04
2	Magnetically coupled	01	02	03

6.6.1 Controlled energization of an electrically coupled transformer

The rating of an electrically coupled transformer is 1500 MVA and its configuration is Yg/Y/Δ: (765 kV)/(400 kV)/(33 kV). The energization has been carried out at 765 kV, Yg winding side. It is to be noted that the achieved mechanical targets have been deviated in the range of 100 to 200 because of non-availability of statistical MOT scatter of an interrupter & a PIR switch, tolerance of auxiliary contact, and accurate value of RDDS. The total four energization operations have been performed on this transformer. The actual field results, in terms of recorded waveform captured by DR for one of the cases out of four cases, are shown in Fig. 6.7 (a). At the same time, the simulation results given by the suggested methodology are also shown in Fig. 6.7 (b) and (c). It can be observed that the field results closely match with the simulation results.

The simulation results showing comparison between the proposed methodology (PIR-CB) and conventional methodology (non-PIR-CB) during controlled energization of this transformer is shown in. It has been observed from that the remanence level of individual phase is maintained very low using controlled de-energization of the transformer. Afterwards, based on the estimated level of remanence flux on individual phase, the energization targets for the next energization are optimized. The controlled energization of the transformer is repeated after performing controlled de-energization. There is a necessity to check the repeatability of the inrush mitigation and the variation in the mitigation effect due to statistical scatter of the main contact and tolerance of the auxiliary contact of the CB.

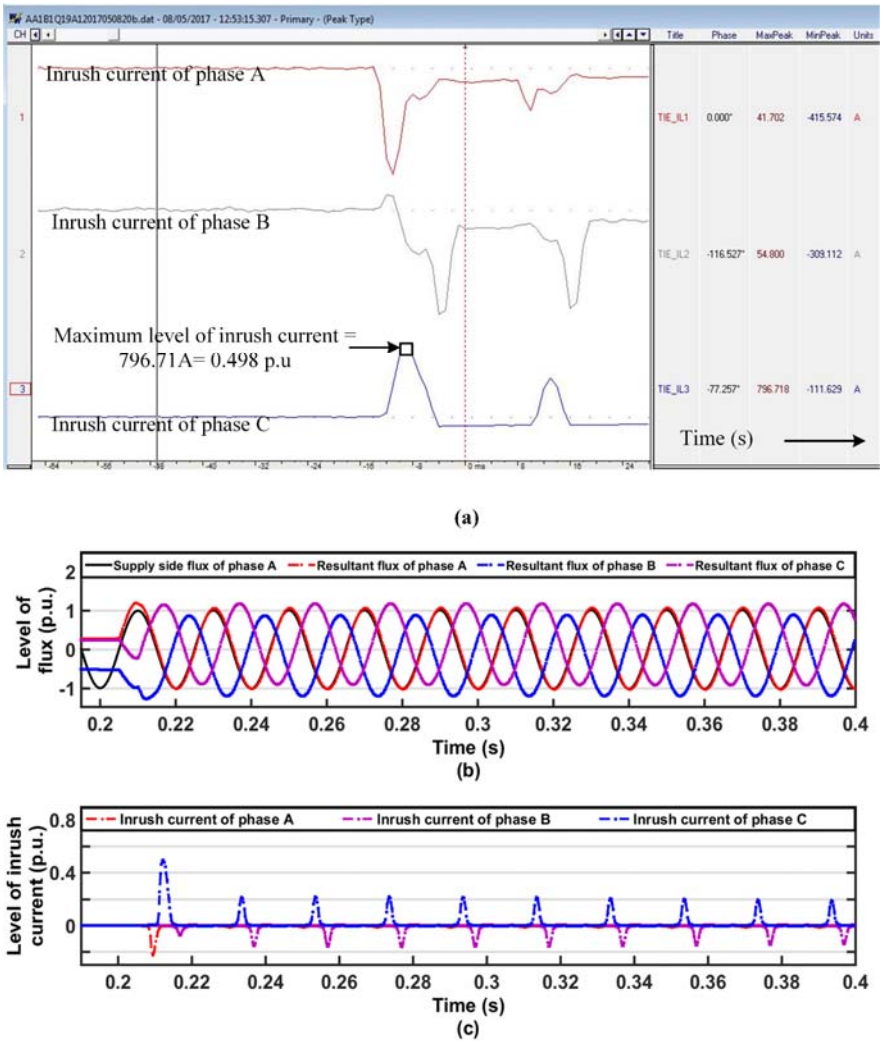

Fig. 6.7 Controlled energization of 765 kV, 1500 MVA electrically coupled transformer (a) field results, (b) simulation results in terms of level of fluxes, and (c) simulation results in terms of level of inrush currents., 1500 MVA electrically coupled transformer (a) field results, (b) simulation results in terms of level of fluxes, and (c) simulation results in terms of level

Subsequently, the level of inrush current gradually reduces after every repetitive energization of an unloaded transformer. The same has been observed from Table 6.2 as the level of inrush current reduces from 0.53 p.u. to 0.26 p.u. It is to be noted from Table 6.2 that the level of inrush current during controlled energization of power transformer using conventional methodology (non-PIR-CB) reduces from 1.98 p.u. to 0.54 p.u. during subsequent operations. The reduction in the level of inrush current is very high compared to the proposed methodology based on PIR-CB. Moreover, Table 6.3 shows comparison between simulation results and field results in terms of level of inrush current. In addition, comparative evaluation in terms of TVD between the proposed methodology (PIR-CB) and conventional methodology (non-PIR-CB) is also shown in Table 6.3 .

Table 6.2 Simulation results showing comparison between proposed methodology (PIR-CB) and conventional methodology (non-PIR-CB) during controlled energization of electrically coupled transformer.

Sr. No.	Operating mechanical time scatter from optimal making target (Degree)			Level of remanence estimated from case (1) (p.u.)			Maximum level of inrush current for individual phase (p.u.)					
							Proposed methodology (PIR-CB)			Conventional methodology (non-PIR-CB)		
	A	B	C	A	B	C	A	B	C	A	B	C
1	0	0	0	-	-	-	-0.25	-0.18	0.53	-0.61	-0.6	1.98
2	-14.5	0.18	-0.18	0.235	0.265	-0.5	0.03	-0.33	0.023	-1.45	0.11	1.14
3	9.9	-13.32	-18.9				-0.34	0.06	0.30	-0.02	0.79	-0.55
4	9.9	-12.68	-12				0.02	-0.26	0.15	0.02	-0.54	0.27

Table 6.3 Comparison between simulation and field results given by proposed methodology and conventional methodology (non-PIR-CB) in terms of inrush current and TVD for electrically coupled transformer.

Sr. No.	Maximum level of inrush current for individual phase (p.u.)						Minimum level of subsequent transient voltage dip (p.u.)	
	Simulation results			Field results			Proposed methodology (PIR-CB)	Conventional methodology (non-PIR-CB)
	A	B	C	A	B	C		
1	-0.25	-0.18	0.53	-0.26	-0.19	0.5	0.989	0.983
2	0.03	-0.33	0.023	0.024	-0.32	0.02	0.991	0.986
3	-0.34	0.06	0.30	-0.34	0.06	0.29	0.995	0.987
4	0.02	-0.26	0.15	0.02	-0.25	0.15	0.996	0.987

It has been observed from Table 6.3 that the field results are almost in close conformity with the simulation results. Furthermore, the minimum level of TVD using PIR-CB and non-PIR-CB is of the order of 0.989 p.u. and 0.983 p.u., respectively. The variation in TVD is minimal when the performance of non-PIR and PIR-CB is compared due to the fact that SCCL of the grid source is quite high (of the order of 40 kA).

6.6.2 Controlled energization of a magnetically coupled transformer

In case of magnetically coupled transformer, the 11 kV tertiary winding is not connected in delta. However, the three-phases are magnetically coupled because of three limb construction. The rating of this transformer is 500 MVA and its configuration is Yg/Yg/Δ: (400 kV)/(220 kV)/(11 kV). The total three energization operations have been performed. The field results, in terms of recorded waveform captured by DR for one of the sample case, are shown in Fig. 6.8 (a). The simulation results using the suggested methodology are also shown in Fig. 6.8 (b) and (c).

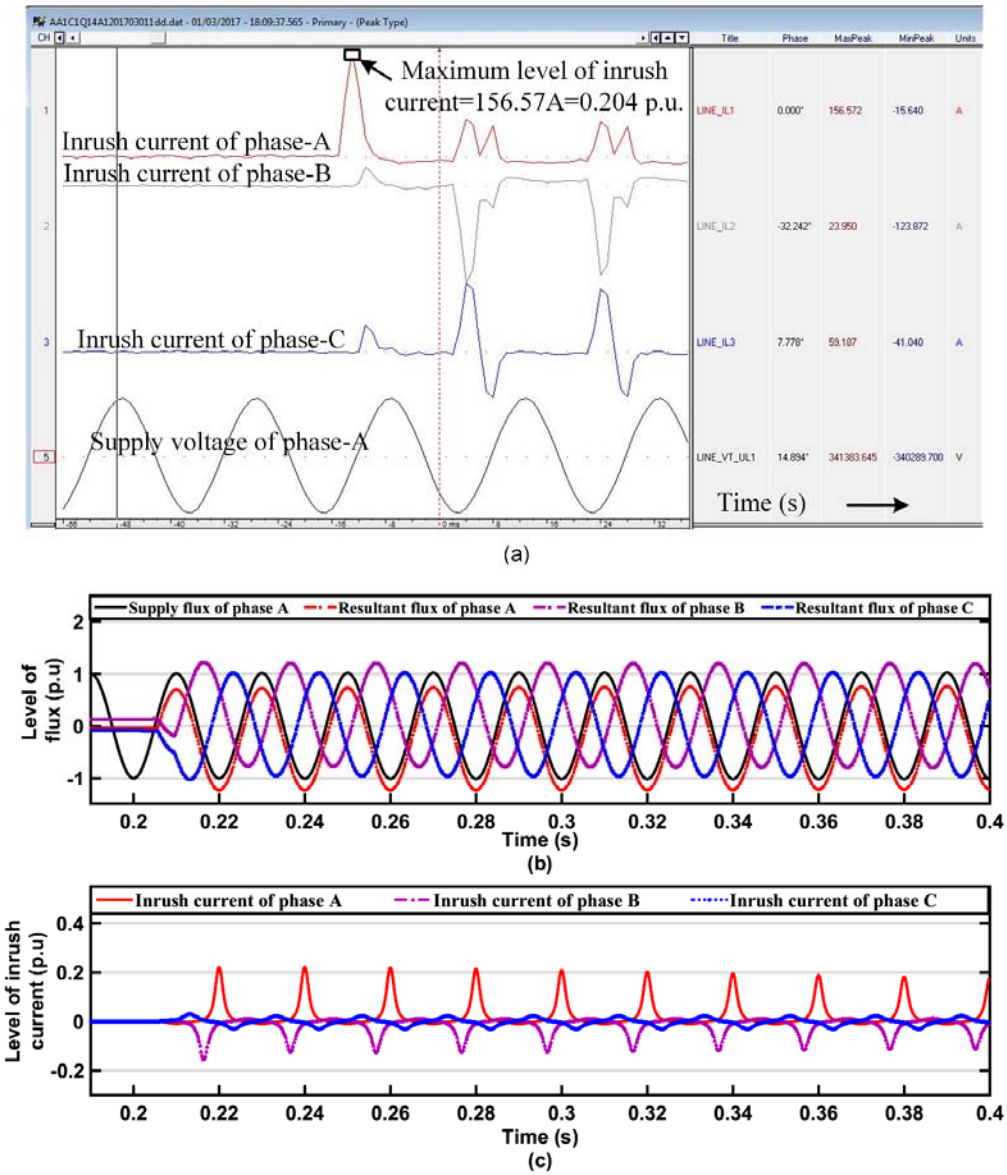

Fig. 6.8 Controlled energization of 400 kV, 500 MVA magnetically coupled transformer (a) field results, (b) simulation results in terms of level of fluxes, and (c) simulation results in terms of level of inrush currents.

It is to be noted from Fig. 6.8 that due to the effect of MOT scatter of CB and low level of remanence, the maximum level of inrush current obtained from field and simulation study is of the order of 0.204 p.u. and 0.22 p.u, respectively.

The simulation results showing comparison between the proposed methodology (PIR-CB) and conventional methodology (non-PIR-CB) during controlled energization of magnetically coupled transformer is shown Table 6.4. It has been observed from Table 6.4that the level of inrush current using the proposed methodology reduces from 0.22 p.u. to 0.11 p.u. during subsequent energization of power transformer whereas in case of conventional methodology the same has been reduced from 0.89 p.u. to 0.52 p.u. This clearly indicates

superiority of PIR-CB based proposed methodology over non-PIR-CB based conventional methodology in terms of inrush current mitigation.

Table 6.4 Simulation results showing comparison between proposed methodology (PIR-CB) and conventional methodology (non-PIR-CB) during controlled energization of magnetically coupled transformer.

Sr. No.	Operating mechanical time scatter from optimal making target (Degree)			Level of remanence estimated from case (1) (p.u.)			Level of inrush current for individual phase (p.u.)					
							Proposed methodology (PIR-CB)			Conventional methodology (non-PIR-CB)		
	A	B	C	A	B	C	A	B	C	A	B	C
1	0	0	0	-	-	-	0.22	-0.15	-0.03	-0.05	-0.262	0.86
2	12.6	09	01	-0.04	0.14	-0.1	-0.11	0.04	0.04	-0.105	0.07	0.71
3	5.4	11.7	5.4				-0.05	-0.08	0.11	0.08	-0.58	0.08

Table 6.5 Comparison between simulation results and field results given by proposed methodology (PIR-CB) and conventional methodology (non-PIR-CB) in terms of inrush current and TVD for magnetically coupled transformer.

Sr. No.	Maximum level of inrush current for individual phase (p.u.)						Minimum level of subsequent transient voltage dip (p.u.)	
	Simulation results			Field results			Proposed methodology (PIR-CB)	Conventional methodology (non-PIR-CB)
	A	B	C	A	B	C		
1	0.22	-0.15	-0.031	0.20	-0.16	-0.05	0.997	0.992
2	-0.11	0.04	0.04	-0.11	0.04	0.04	0.998	0.994
3	-0.05	-0.08	0.11	-0.04	-0.08	0.093	0.999	0.999

Table 6.5 shows comparison between simulation results and field results in terms of level of inrush current during energization of magnetically coupled power transformer. In addition, comparative evaluation in terms of TVD between the proposed methodology (PIR-CB) and conventional methodology (non-PIR-CB) is also shown in Table 6.5. It has been observed from Table 6.5 that the field results are almost equal to the simulation results. Moreover, the minimum level of TVD using PIR-CB and non-PIR-CB is of the order of 0.9972 p.u. and 0.9923 p.u., respectively. The variation in TVD is minimal when the performance of non-PIR and PIR-CB is compared due to the fact that SCCL of the grid source is quite high (of the order of 40 kA)

6.7 Summary

This chapter presents an application of controlled switching device for the minimization of the level of inrush current and TVD during energization of an unloaded power transformer using PIR-CB. This evaluation is done during energization of an existing Indian EHV power transformer for electrically and magnetically coupled design configurations. Accurate simulation model, which consists of the equivalent power source, PIR-CB, and coupled

transformer has been developed to compare the simulation results with that of real field results. The effect of statistical scatter, systematic scatter of interrupter & PIR switch and tolerance of auxiliary contact (used as a feedback element by controlled switching device) is well elaborated along with the aging effect of PIR-CB. Moreover, the impact of change in EIT and MIT due to aforementioned variations on consistency of mitigation results of inrush and TVD has been analyzed. The field results for energization of both electrically and magnetically coupled transformers are compared with that obtained from simulation performed in PSCAD by accurate modelling of the representative system. The close match between field results and that obtained with simulation for both electrically and magnetically coupled transformer validate the suggested methodology. Moreover, MOT scatter due to statistical and systematic variations in CB is inevitable. The effect of MOT scatter due to systematic variation can be compensated by controlled switching device whereas the scatter due to statistical variation is unavoidable. Because of statistical variation of CB, the actual closing instant differs from the optimal closing instant. The effect of statistical scatter on the level of inrush current can be minimized using the PIR-CB based proposed methodology.

Chapter 7 Conclusions and Future Scope

7.1 Conclusions

In order to improve efficiency, reliability and performance of the power system network, researchers are finding the ways to minimize the numbers of abnormal conditions generated during different events. The switching is one of such event. Sometimes, switching of transmission lines and power apparatus cause severe switching transients. These switching transients create loss of life for different power apparatus, deterioration of quality of power, malopeartion of protective relay, and disturbance in communication circuit of the power system network. Moreover, in order to promote generation of green energy, the penetration of renewable sources in the power system has been also increased. However, due to limited hours availability of these renewable resources, the number of switching events in the power system network has been increased. This may create problems for the power system network due to which the economical aspect of the system has been compromised.

In past, PIR-CB has been used to minimize the level of switching transients. However, PIR-CB cannot mitigate the level of switching transients completely. Mainly, there are two types of switching, namely (i) uncontrolled switching and (ii) controlled switching. In case of uncontrolled switching of transmission line, it may develop switching surge of the order of 3 p.u. This may damage the insulation of the power component connected with the same line. Moreover, this may create flash over at the load side. Sometimes, switching transients may cause malopeartion of the protection relay.

In case of uncontrolled switching of shunt reactor, it draws high amount of inrush current from the supply. As the inrush current contains asymmetric dc component, the core of the instrument transformers may saturate due to which protective relay may maloperate. Hence, the reliability, power quality, and efficiency of the power system can be deteriorated. Further, in case of uncontrolled energization of the power transformer, it draws very high level of inrush current from the supply, which contains different harmonics components and dc offset. Subsequently, it deteriorates quality of power supply and may develop TVD for the power apparatus connected with the same line. Consequently, the performance of the power apparatus is degraded.

In order to rectify the above problems, an attempt has been made in this thesis. Following are major conclusions of the research work carried out in this thesis.

1. Initially, controlled energization targets for fully and partially discharged UCTL and

SCTL has been determined using supply side voltage as a reference. In this presented work, frequency domain model of PSCAD/EMTDC software package has been used for modelling of the transmission line, which is commonly used for transient study. The sampling frequency of the order of 1 kHz has been selected for the fundamental frequency of 50 Hz. A large numbers of simulation cases have been generated by varying the system parameters such as type of fault, fault duration, compensation level, fault distance, load angel, and instant of fault inception. Here, supply voltage signal is considered as the reference signal. In case of energization of fully discharged UCTL/SCTL and partially discharged SCTL, zero crossing instant of the supply voltage is considered as an optimal target. Whereas in case of a partially discharged UCTL, the optimal closing target is half of the peak voltage magnitude having polarity same as trapped charge considered for an optimal closing target. In order to evaluate performance of the proposed technique, a simulation study has been carried out. In this study, performance of the proposed methodology has been evaluated considering effect of MOT scatter, impact of SA, and different SCCL of the grid sources. It has been observed that the proposed technique limits the level of the switching surge up to 1.9 p.u. during energization of fully/partially discharged UCTL/SCTL. This shows wide range of applicability of the proposed technique.

2. In the second approach, line side voltages have been analyzed to obtain the optimal controlled switching target during energization of a partially discharged SCTL. In the presented work, modelling of SCTL has been carried out in PSCAD/EMTDC environment considering one of the existing 400 kV Indian power transmission system network. Large numbers of simulation cases have been generated by varying system parameters such as compensation level, type of fault, fault distance, length of line, duration of fault, instant of fault inception, and load angel. In order to determine the optimal controlled switching target, DFT analysis of line side voltages has been performed. The assessment of the proposed technique has been carried out considering effect of MOT scatter of the CB, impact of SA, and different SCCL of the sources. It has been noticed that the proposed technique controls the level of switching surge up to 1.5 p.u. Moreover, comparison of the proposed scheme with the existing scheme proves the superiority of the proposed technique.

3. In third approach, controlled switching targets for SPAR of SCTL has been determined using line side voltages. The simulation model has been developed in PSCAD/EMTDC environment considering an existing 400 kV Indian transmission network. In order to assess the performance of the proposed technique, a simulation study has been carried

out. Large numbers of simulation cases have been generated by varying power system parameters such as fault duration, load angel, instant of fault inception, fault distance, and compensation level. Further, the proposed technique has been tested considering effect of MOT scatter of the CB and different SCCL of the grid sources. It has been observed that the proposed technique is able to limit the level of switching surge up to 1.6 p.u. Lastly, it has been observed from comparative evaluation of the proposed scheme with the existing scheme that the proposed scheme outperforms in terms of the level of switching surge generated.

4. Shunt reactors are widely used in power system network at 400 kV and above level for reactive power management. As they switched ON and OFF multiple times in a day, their uncontrolled energization draws high charging current from the supply. This creates high thermal stress in the winding of the shunt reactor. Further, this charging current contains asymmetric dc component, which takes very long time to decay. Moreover, as the asymmetric dc component saturates the instrument transformers, it may cause malopeartion of the protective relay. Mathematical analysis has been carried out and optimal controlled switching targets for energization of the shunt reactor has been determined. The simulation model has been developed in PSCAD/EMTDC software package. The proposed technique has been tested considering different connection configurations of the shunt reactor. Moreover, the effect of MOT scatter of the CB is also analyzed. Field results obtained by implementing the proposed technique are also discussed. It has been observed that the proposed technique is capable to restrict the level of charging current up to 1.1 p.u., which validates wide range of applicability of the proposed technique.

5. Power transformer is a very important and expensive equipment of the power system network. Though, it is switched ON and OFF occasionally, its switching becomes more frequent due to deregulation of power system network along with incorporation of private power producers especially renewable energy sources. Uncontrolled energization of power transformer draws very high level of inrush current from the source. This inrush contains asymmetric dc component and different harmonics component, which degrades power quality, and may develop severe thermal stresses in the winding of the transformer. The high magnitude of inrush current also creates TVD for the equipment connected with the same line. The level of inrush current depends on winding resistance, residual magnetic field, and point on wave switching instant. In order to limit the level of inrush current during controlled energization of a power transformer, it is essential to minimize the effect of MOT scatter of the CB. In this work, detailed study of the

parameters, which are responsible for the MOT scatter of the CB, has been carried out. Further, the behaviour of dynamic fluxes are different for electrically and magnetically coupled power transformers. The simulation model of both types of transformers has been developed in PSCAD/EMTDC environment. In order to evaluate the wide range of applicability of the proposed technique, it is tested for both electrically and magnetically coupled power transformers. Field results for implementation of the proposed technique for electrically (1500 MVA, 765 kV) and magnetically (500 MVA, 400 kV) coupled power transformers have been discussed. It has been observed that the proposed technique effectively limits the level of inrush current within 1.0 p.u. At the end, comparative evaluation of the proposed technique with the existing technique proves the supremacy of the proposed scheme.

7.2 Future scope

As none of the research work is complete, there is always a scope of further improvement. Hence, it is almost impossible to determine controlled targets for the transmission line having different connection configurations. The suggested area, which can be explored in the field of application of the controlled switching, are mentioned below.

1. Nowadays, shunt and series compensated transmission lines are used to transfer bulk amount of power in real field. Consequently, there is a need to develop new controlled switching technique that limits the level of switching surge during closing/reclosing of hybrid combination of series and shunt compensated transmission lines.

2. In order to improve reliability, performance, and efficiency of the power system, it is required to develop a new controlled SPAR scheme for transmission line having series and shunt compensation.

3. The application of controlled switching of transformer with complex connection configuration and design such as zigzag connection and phase shifting transformer can be explored.

4. In real field, effect of mechanical operating time scatter of the CB is one of the barrier for successful implementation of controlled switching technology. Development of high speed CB would be one of the area to be examined for further research.

Research Publications

1. Published/Accepted in International Jounals

[1]. K. A. Bhatt, B. R. Bhalja, and U. Parikh, "Evaluation of controlled energization of shunt reactors for minimizing asymmetric dc component of charging current with circuit breaker having pre-insertion resistors," *Int. J. Electr. Power Energy Syst.*, vol. 93, pp. 340–351, Dec. 2017.

[2]. K. A. Bhatt, B. R. Bhalja, and U. B. Parikh, "Evaluation of controlled energization of an unloaded power transformer for minimizing the level of inrush current and transient voltage distortion using PIR-CBs," *IET Gener. Transm. Distrib.*, vol. 12, no. 11, pp. 2788–2798, Jun. 2018.

[3]. K. A. Bhatt, B. R. Bhalja, and U. Parikh, "Controlled switching technique for minimization of switching surge during energization of uncompensated and shunt compensated transmission lines for circuit breakers having pre-insertion resistors," *Int. J. Electr. Power Energy Syst.*, vol. 103, pp. 347–359, Dec. 2018.

2. Communicated in International Jounals

[1]. K. A. Bhatt and B. R. Bhalja, "An approach for controlled energization/re-energization of shunt compensated transmission lines," in *IET Gener. Transm. Distrib*, April. 2018. Major revision has been submitted on March 15, 2019

[2]. K. A. Bhatt and B. R. Bhalja, "An approach for controlled single phase auto reclosing technique for shunt compensated transmission lines," in *Int. J. Electr. Power Energy Syst,* 2018. Major revision submitted on April 7, 2019.

Appendix-A

A1. System Parameters for simulation model of transmission lines

Base source data	
Positive sequence impedance (Ω)	0.4115 + j 3.546
Zero sequence impedance (Ω)	2.822 + j 10.08
Transmission line parameter	
Rated voltage (kV)	400
Rated frequency (Hz)	50
Positive sequence impedance	0.017272 + j 0.3135 Ω/km
Zero sequence impedance	0.277 + j 1.04 Ω/km
Positive sequence capacitance	14.88 nF/km
Zero sequence capacitance	9.8 nF/km
Ground Clearance	9.39 meters
Spacing between two phase conductors	7.74 meters
Positive sequence impedance	0.017272 + j 0.3135 Ω/km
Zero sequence impedance	0.277 + j 1.04 Ω/km
Positive sequence capacitance	14.88 nF/km

A2. System Parameters for simulation model

Source parameters (both ends)	
Positive sequence impedance (Ω)	0.4115 + j 3.546
Zero sequence impedance (Ω)	2.822 + j 10.08
Transmission line parameters	
Positive sequence impedance (Ω/km)	0.0173 + j 0.314
Zero sequence impedance (Ω/km)	0.277 + j 1.04
Positive sequence capacitance (nF/km)	14.87
Zero sequence capacitance (nF/km)	10.82
Ground clearance (meters)	9.39
Spacing between two phase conductors (metres)	7.74
Length of UCTL (km)	200
Length of SCTL (km)	315 and 400
Parameters of Neutral Grounding Reactor	
Rated voltage	5.5 kV
Rated current	10 A
Reactance	932.9 Ω
Frequency	50 Hz

A3. System Parameters for simulation model of shunt reactor

Base source data	
Positive sequence impedance (Ω)	0.4115 + j 3.546
Zero sequence impedance (Ω)	2.822 + j 10.08
PIR-CB data	
Rated voltage (kV)	400
Rated frequency (Hz)	50
Stray capacitance (C_S) of PIR-CB (pF)	20
Configuration of PIR	Series
Grading capacitance (C_G) of PIR-CB (pF)	1500
Shunt reactor data	
Inductance (Ls) of reactor of 125 MVAr/ 63 MVAr (H)	4.074/8.084
Rated frequency (Hz)	50
Capacitance (C_{BB}) of bus-bar (pF)	17
Resistance of reactor I for 125 MVAr/63MVAr (Ω)	20/12
Capacitance (C_L) of reactor (pF)	28
Capacitance (C_B) of bushing (pF)	23
Resistance I to represent core loss (MΩ)	320

A4.System Parameters

Base source data

Parameter		Short Circuit Current Level (SCCL) of source (kA)			
		40	20	05	01
Positive sequence impedance (Ω)	765 kV	0.64+j5.53	1.28+j11.07	5.12+j44.3	25.69+j 221.31
	400kV	0.199+j1.71	0.398+j3.43	1.59+j13.7	7.95+j68.48
Zero sequence impedance (Ω)	765 kV	5.25+j18.75	10.5+j37.50	42.47+j52.13	2.9.93+j750.11
	400kV	1.55+j5.56	3.11+j11.11	12.45+j44.48	62.26+j222.39

PIR-CB data

Rated voltage (kV)		765 400
Rated frequency (Hz)		50
Configuration of PIR		Series
RDDS of interrupter (kV/ms)	765 kV	218
	400 kV	109
RDDS OF PIR switch (kV/ms)	765 kV	283.4
	400 kV	142

Power transformer data

Rated frequency (Hz)	50
Magnetizing current	1.0% of rated full load current
Knee point voltage	1.1 p.u.

References

[1] A. Greenwood, *"Electrical Transients in Power Systems,"* 2 nd ed. New York, USA: John Wiley & Sons.INC., 1991.

[2] Rakosh Das Begamudre, *Extra high voltage AC transmission Engineering*, 4th ed. New age international, 2011.

[3] B. R. Bhalja, R. P. Maheshwari, and N. Chothani, *Protection And Switchgear*, 2ND ed. New delhi: Oxford University press, 2017.

[4] D. Goldsworthy, T. Roseburg, D. Tziouvaras, and J. Pope, "Controlled Switching of HVAC Circuit Breakers: Application Examples and Benefits," in *61st Annual Conference for Protective Relay Engineers*, 2008, no. April, pp. 520–535.

[5] IEEE Standard C37.015-2009, "IEEE Draft Guide for the Application of Shunt Reactor Switching," New York, 2017.

[6] C. Wagner and J. Bankoske, "Evaluation of Surge Suppression Resistors in High-Voltage Circuit Breakers," *IEEE Trans. Power Appar. Syst.*, vol. PAS-86, no. 6, pp. 698–707, Jun. 1967.

[7] H. Heiermeier and R. B. Raysaha, "Power Testing of Preinsertion Resistors: Limitations and Solution," *IEEE Trans. Power Deliv.*, vol. 32, no. 4, pp. 1688–1695, Aug. 2017.

[8] A. C. Legate, J. H. Brunke, J. J. Ray, and E. J. Yasuda, "Elimination of closing resistors on EHV circuit breakers," *IEEE Trans. Power Deliv.*, vol. 3, no. 1, pp. 223–231, Jan. 1988.

[9] IEEE Power & Energy Society, "IEEE Guide for Automatic Reclosing of Circuit Breakers for AC Distribution and Transmission Lines," New York, 2012.

[10] D. E. Hedman, I. B. Johnson, C. H. Titus, and D. D. Wilson, "Switching of Extra-High-Voltage Circuits II-Surge Reduction with Circuit-Breaker Resistors," *IEEE Trans. Power Appar. Syst.*, vol. 83, no. 12, pp. 1196–1205, Dec. 1964.

[11] H. B. Thoren, "Reduction of Switching Overvoltages in EHV and UHV Systems," *IEEE Trans. Power Appar. Syst.*, vol. PAS-90, no. 3, pp. 1321–1326, May 1971.

[12] F. Faria Da Silva, C. L. Bak, U. S. Gudmundsdóttir, W. Wiechowski, and M. R. Knardrupgård, "Use of a pre-insertion resistor to minimize zero-missing phenomenon and

switching overvoltages," in *2009 IEEE Power and Energy Society General Meeting, PES '09*, 2009.

[13] R. Gerald Colclaser, C. L. Wagner, and E. . Donohue, "Multistep Resistor Control of Switching Surges," *IEEE Trans. Power Appar. Syst.*, vol. PAS-88, no. 7, July, pp. 1022–28, 1969.

[14] H. Soloot, A. Gholami, E. Agheb, A. Ghorbandaeipour, and P. Mokhtar, "Investigation-of-Transmission-Line-Overvoltages-and-their-Deduction-Approach," *Int. J. Electr. Electron. Eng.*, vol. 3, no. 5, pp. 1070–1078, 2009.

[15] CIGRE Task Force 13.00.1, "Controlled switching: A state of the art survey- part I," *ELECTRA*, vol. 162, pp. 65–96, Oct. 1995.

[16] CIGRE Task Force 13.00.1, "Controlled switching A state of the art survey- part II,, ELECTRA, 1996.," in *ELECTRA*, 1996, pp. 1–26.

[17] CIGRE WG A3.35, "Present and Future of Controlled Switching," in *CIGRE -IEC colloquium*, 2016, pp. 1–11.

[18] S. Brahma *et al.*, "Guest Editorial Power System Protection," *IEEE Trans. Power Deliv.*, vol. 31, no. 4, pp. 1785–1786, 2016.

[19] I. Kamwa, A. K. Pradhan, and G. Joos, "Robust Detection and Analysis of Power System Oscillations Using the Teager-Kaiser Energy Operator," *IEEE Trans. Power Syst.*, vol. 26, no. 1, pp. 323–333, Feb. 2011.

[20] S. Das and T. Sidhu, "Detecting synchrophasors computed over fault/switching transients," *IET Gener. Transm. Distrib.*, vol. 8, no. 9, pp. 1616–1625, 2014.

[21] K. A. Bhatt, B. R. Bhalja, and U. Parikh, "Controlled switching technique for minimization of switching surge during energization of uncompensated and shunt compensated transmission lines for circuit breakers having pre-insertion resistors," *Int. J. Electr. Power Energy Syst.*, vol. 103, pp. 347–359, Dec. 2018.

[22] IEEE Working Group on switching surges of the transmission and distribution comittee, "Switching Surges, Part III: Field and Analyzer Results for Transmission Lines Past, Present, and Future Trends," *IEEE Trans. Power Appar. Syst.*, vol. PAS-89, no. 2, pp. 173–189, 1970.

[23] ABB High Voltage Products, "Controlled Switching Buyer's and Application Guide,"

Ludvika, Sweden, 2013.

[24] H. Seyedi and S. Tanhaeidilmaghani, “New controlled switching approach for limitation of transmission line switching overvoltages,” *IET Gener. Transm. Distrib.*, vol. 7, no. 3, pp. 218–225, Mar. 2013.

[25] International Electrotechnical Commission, “IEC-TR-62271-302, ‘Hogh-voltage switchgear and control gear,’” 2010.

[26] B. K. Panigrahi, S. R. Samantaray, and R. Dubey, “Adaptive distance protection scheme for shunt-FACTS compensated line connecting wind farm,” *IET Gener. Transm. Distrib.*, vol. 10, no. 1, pp. 247–256, 2016.

[27] S. Gajare and A. K. Pradhan, “Synchrophasor-Based Intelligent Autoreclosing Scheme for Series Compensated Transmission Lines,” *IEEE Trans. Power Deliv.*, vol. 32, no. 5, pp. 2255–2262, 2017.

[28] M. K. Jena, B. K. Panigrahi, and S. R. Samantaray, “Online detection of tripped transmission line to improve wide-area SA in power transmission system,” *IET Gener. Transm. Distrib.*, vol. 12, no. 2, pp. 288–294, 2018.

[29] P. K. Dash, A. K. Pradhan, G. Panda, and A. C. Liew, “Adaptive relay setting for flexible AC transmission systems (FACTS),” *IEEE Trans. Power Deliv.*, vol. 15, no. 1, pp. 38–43, 2000.

[30] M. Pazoki, Z. Moravej, M. Khederzadeh, and N.-K. C. Nair, “Effect of UPFC on protection of transmission lines with infeed current,” *Int. Trans. Electr. Energy Syst.*, vol. 26, no. 11, pp. 2385–2401, Nov. 2016.

[31] A. R. Abhyankar, S. A. Soman, and S. A. Khaparde, “Optimization approach to real power tracing: An application to transmission fixed cost allocation,” *IEEE Trans. Power Syst.*, vol. 21, no. 3, pp. 1350–1361, 2006.

[32] V. C. Nikolaidis, N. Savvopoulos, A. S. Safigianni, and C. D. Vournas, “Adjusting third zone distance protection to avoid voltage collapse,” *Proc. - 2014 Power Syst. Comput. Conf. PSCC 2014*, 2014.

[33] V. C. Nikolaidis, “Combining Tranmission Line Protection with Voltage Stability Monitoring,” *2018 Power Syst. Comput. Conf.*, pp. 1–7.

[34] C. M. Smith and N. C. Nair, “Development of a new open test platform for protective

relay," in *TENCON 2010 - 2010 IEEE Region 10 Conference*, 2010, pp. 586–591.

[35] W. Carpenter, *IEEE Guide for Protective Relay Applications to Transmission Lines*, vol. 1999. New York, USA: IEEE SA Standards Board.

[36] S. Das, T. S. Sidhu, M. R. D. Zadeh, and Z. Zhang, "A Novel Hybrid Differential Algorithm for Turn to Turn Fault Detection in Shunt Reactors," *IEEE Trans. Power Deliv.*, vol. 32, no. 6, pp. 2537–2545, 2017.

[37] Z. Gajic, H. Birger, and M. Fahrudin, ""HV Shunt Reactor Secrets for Protection Engineer "," in *30st Western Protective Relaying Conference*, 2003, pp. 1–29.

[38] A. Župan, B. Filipović-Grčić, and D. Filipović-Grčić, "Transients caused by switching of 420 kV three-phase variable shunt reactor," *Electr. Power Syst. Res.*, 2016.

[39] C. D. Tsirekis and N. D. Hatziargyriou, "Control of Shunt Capacitors and Shunt Reactors Energization Transients," *System*, 2003.

[40] ABB High Voltage Products, "Instrument Transformers Application Guide Installations with ABB Outdoor Instrument Transformers," Ludvika, Sweden, 2015.

[41] K. Venkatesh and K. S. Swarup, "Estimation and elimination of DC component in digital relaying," *2012 Int. Conf. Power, Signals, Control. Comput. EPSCICON 2012*, 2012.

[42] K. A. Bhatt, B. R. Bhalja, and U. Parikh, "Controlled switching technique for minimization of switching surge during energization of uncompensated and shunt compensated transmission lines using circuit breaker having pre-insertion resistors," *Int. J. Electr. Power Energy Syst.*, vol. 93, pp. 340–351, 2017.

[43] T. Kobayashi *et al.*, "Application of controlled switching to 500-kV shunt reactor current interruption," *IEEE Trans. Power Deliv.*, vol. 18, no. 2, pp. 480–486, Apr. 2003.

[44] I. Ugleši and B. Filipovi, "Transients Caused by Uncontrolled and Controlled Switching of Circuit Breakers," in *The international Symposim on High-Voltage Technique*, 2013, no. November, pp. 1–8.

[45] S. Sharma and A. R. Abhyankar, "Loss Allocation for Weakly Meshed Distribution System Using Analytical Formulation of Shapley Value," *IEEE Trans. Power Syst.*, vol. 32, no. 2, pp. 1369–1377, 2017.

[46] S. F. Abdelsamad, W. G. Morsi, and T. S. Sidhu, "Probabilistic Impact of Transportation Electrification on the Loss-of-Life of Distribution Transformers in the Presence of

Rooftop Solar Photovoltaic," *IEEE Trans. Sustain. Energy*, vol. 6, no. 4, pp. 1565–1573, 2015.

[47] CIGRE Working group C4.307, "Transformer energization in Power Systems : A Study Guide," 2014.

[48] J. M. Solanki, S. Khushalani, and N. N. Schulz, "A multi-agent solution to distribution systems restoration," *IEEE Trans. Power Syst.*, vol. 22, no. 3, pp. 1026–1034, 2007.

[49] M. R. Khalghani, S. Khushalani-Solanki, J. Solanki, and A. Sargolzaei, "Cyber disruption detection in linear power systems," *2017 North Am. Power Symp. NAPS 2017*, pp. 2–7, 2017.

[50] J. H. Brunke and K. J. Frohlich, "Elimination of Transformer Inrush Currents by Controlled Switching — Part I : Application and Performance Considerations," *IEEE Trans. Power Deliv.*, vol. 16, no. 2, pp. 281–285, Apr. 2001.

[51] J. H. Brunke and K. J. Frohlich, "Elimination of Transformer Inrush Currents by Controlled Switching — Part II : Application and Performance Considerations," *IEEE Trans. Power Deliv.*, vol. 16, no. 2, pp. 281–285, Apr. 2001.

[52] Z. Moravej, D. N. Vishwakarma, and S. P. Singh, "Application of radial basis function neural network for differential relaying of a power transformer," *Comput. Electr. Eng.*, vol. 29, no. 3, pp. 421–434, May 2003.

[53] T. S. Sidhu and M. S. Sachdev, "Online identification of magnetizing inrush and internal faults in three-phase transformers," *IEEE Trans. Power Deliv.*, vol. 7, no. 4, pp. 1885–1891, 1992.

[54] B. Kovan, F. De Leon, D. Czarkowski, Z. Zabar, and L. Birenbaum, "Mitigation of inrush currents in network transformers by reducing the residual flux with an ultra-low-frequency power source," *IEEE Trans. Power Deliv.*, vol. 26, no. 3, pp. 1563–1570, 2011.

[55] K. A. Bhatt, B. R. Bhalja, and U. B. Parikh, "Evaluation of controlled energisation of an unloaded power transformer for minimising the level of inrush current and transient voltage distortion using PIR-CBs," *IET Gener. Transm. Distrib.*, vol. 12, no. 11, pp. 2788–2798, Jun. 2018.

[56] M. Tripathy, R. P. Maheshwari, and H. K. Verma, "Power Transformer Differential Protection Based On Optimal Probabilistic Neural Network," *IEEE Trans. Power Deliv.*, vol. 25, no. 1, pp. 102–112, Jan. 2010.

[57] IEEE Std. 1159, “IEEE Recommended Practice for Monitoring Electric Power Quality.,” New York, 2009.

[58] U. Parikh and B. R. Bhalja, “Mitigation of magnetic inrush current during controlled energization of coupled un-loaded power transformers in presence of residual flux without load side voltage measurements,” *Int. J. Electr. Power Energy Syst.*, vol. 76, pp. 156–164, Mar. 2016.

[59] M. Nagpal, T. G. Martinich, A. Moshref, K. Morison, and P. Kundur, “Assessing and limiting impact of transformer inrush current on power quality,” *IEEE Trans. Power Deliv.*, vol. 21, no. 2, pp. 890–896, 2006.

[60] K. S. Swarup and S. P. Valsan, “Protective relaying for power transformers using field programmable gate array,” *IET Electr. Power Appl.*, vol. 2, no. 2, pp. 135–143, Mar. 2008.

[61] F. de Leon, A. Farazmand, S. Jazebi, D. Deswal, and R. Levi, “Elimination of Residual Flux in Transformers by the Application of an Alternating Polarity DC Voltage Source,” *IEEE Trans. Power Deliv.*, vol. 30, no. 4, pp. 1727–1734, Aug. 2015.

[62] U. Parikh and B. R. Bhalja, “Challenges in field implementation of controlled energization for various equipment loads with circuit breakers considering diversified dielectric and mechanical characteristics,” *Int. J. Electr. Power Energy Syst.*, vol. 87, pp. 99–108, May 2017.

[63] M. Hb De Grijp and R. A. Hopkins, “Controlled switching of shunt capacitors,” in *AFRICON, 1996., IEEE AFRICON 4th, Stellenbosch, 24-27 September*, 1996, pp. 874–879.

[64] T. Chang and W. Chen, “Pre-insertion Resistor of Switching Shunt Capacitor Banks.”

[65] CIGRE Working group 13.07, “‘Controlled switching of HVAC circuit breakers, guide for application lines, reactors, capacitors, transformers—Part 2,’” *Electra*, pp. 43–73, Aug-1999.

[66] H. A. Darwish, A.-M. Taalab, E. S. Ahmed, and O. P. Malik, “Experimental evaluation of power differential relay for transmission line protection,” in *2009 IEEE/PES Power Systems Conference and Exposition*, 2009, pp. 1–7.

[67] K. Seethalekshmi, S. N. Singh, and S. C. Srivastava, “A classification approach using support vector machines to prevent distance relay maloperation under power swing and

voltage instability," *IEEE Trans. Power Deliv.*, vol. 27, no. 3, pp. 1124–1133, 2012.

[68] D. Kang and R. Gokaraju, "A New Method for Blocking Third-Zone Distance Relays during Stable Power Swings," *IEEE Trans. Power Deliv.*, vol. 31, no. 4, pp. 1836–1843, 2016.

[69] K. Froehlich *et al.*, "Controlled closing on shunt reactor compensated transmission lines. I. Closing control device development," *IEEE Trans. Power Deliv.*, vol. 12, no. 2, pp. 734–740, Apr. 1997.

[70] K. N. Srivastava and S. C. Srivastava, "Chaos in Power Systems Using Facts Devices," *IEEE Trans. Circuits Syst. -I*, vol. 45, no. 1, pp. 72–78, 1998.

[71] S. C. Srivastava, S. Chakrabarti, and A. Sharma, "Multi-agent-based dynamic state estimator for multi-area power system," *IET Gener. Transm. Distrib.*, vol. 10, no. 1, pp. 131–141, 2016.

[72] N. Kumar, H. Gupta, and S. P. Singh, "Prototype scheme for differential protection of power transformer using ANN," *2008 40th North Am. Power Symp.*, 2008.

[73] ABB, "Live Tank Circuit Breakers Application Guide," Ludvika, Sweden, 2013.

[74] ABB substation automation products, "Switchsync ™ PWC600 Product Guide," Vesteras, Sweden, 2013.

[75] H. Ito, "Controlled switching technologies, state-of-the-art," in *IEEE/PES Transmission and Distribution Conference and Exhibition*, 2002, vol. 2, pp. 1455–1460.

[76] C. Thomas and R. Hedin, "Switching Surges on Transmission Lines Studied by Differential Analyzer Simulation," *IEEE Trans. Power Appar. Syst.*, vol. PAS-88, no. 5, pp. 636–645, May 1969.

[77] P. C. V. Esmeraldo, J. Amon F, F. M. S. Carvalho, A. C. C. Carvalho, and S. A. Morais, "Circuit-breaker requirements for alternative configurations of a 500 kV transmission system," *IEEE Trans. Power Deliv.*, vol. 14, no. 1, pp. 169–175, 1999.

[78] K. Froehlich *et al.*, "Controlled Closing on Shunt Reactor Compensated Transmission Lines Part 2: Application of Closing Control Device for High-speed Autoreclosing on BC Hydro 500 kV Transmission Line K.," *IEEE Trans. Power Deliv.*, vol. 12, no. 2, pp. 734–740, 1997.

[79] K. M. C. Dantas, W. L. A. Neves, and D. Fernandes, "An Approach for Controlled

Reclosing of Shunt-Compensated Transmission Lines," *IEEE Trans. Power Deliv.*, vol. 29, no. 3, pp. 1203–1211, Jun. 2014.

[80] P. Mestas, M. C. Tavares, and A. M. Gole, "Implementation and Performance Evaluation of a Reclosing Method for Shunt Reactor-Compensated Transmission Lines," *IEEE Trans. Power Deliv.*, vol. 26, no. 2, pp. 954–962, Apr. 2011.

[81] X. Luo, C. Huang, and Y. Jiang, "Improved digital algorithm for adaptive reclosing for transmission lines with shunt reactors," *IET Gener. Transm. Distrib.*, vol. 10, no. 9, pp. 2066–2070, Jun. 2016.

[82] O. Dias and M. C. Tavares, "Comparison between traditional single-phase auto reclosing and adaptive technique based on harmonic content measurement," *IET Gener. Transm. Distrib.*, vol. 11, no. 4, pp. 905–914, 2017.

[83] Manitoba-HVDC Research Center, "PSCAD/EMTDC User's Manual Version 4.2." Winnipeg, Canada, pp. 1–492, 2005.

[84] R. J. Rajotte, C. Charpentier, S. Breault, H. H. Le, H. Huynh, and J. Desmarais, "Field tests of a circuit breaker synchronous control," *IEEE Trans. Power Deliv.*, vol. 10, no. 3, pp. 1301–1309, 1995.

[85] W. Y. Lee, K. Y. Park, J. K. Chong, B. Y. Lee, and H. J. Kim, "A Method to Decide the Switching Instants of Controlled Switching Circuit Breaker for Shunt Reactors," in *IEEE/PES Transmission and Distribution Conference and Exhibition*, 2002, vol. 3, October, pp. 1760–65.

[86] S. Paudyal, G. Ramakrishna, and M. S. Sachdev, "Application of equal area criterion conditions in the time domain for out-of-step protection," *IEEE Trans. Power Deliv.*, vol. 25, no. 2, pp. 600–609, 2010.

[87] S. R. Samantaray and P. K. Dash, "Decision Tree based discrimination between inrush currents and internal faults in power transformer," *Int. J. Electr. Power Energy Syst.*, vol. 33, no. 4, pp. 1043–1048, May 2011.

[88] B. Bhargava, A. H. Khan, A. F. Imece, and J. DiPietro, "Effectiveness of pre-insertion inductors for mitigating remote overvoltages due to shunt capacitor energization," *IEEE Trans. Power Deliv.*, vol. 8, no. 3, pp. 1226–1238, Jul. 1993.

[89] M. A. Atefi and M. Sanaye-Pasand, "Improving controlled closing to reduce transients in HV transmission lines and circuit breakers," *IEEE Trans. Power Deliv.*, vol. 28, no. 2,

pp. 733–741, 2013.

[90] Section-37, “the Indian Electricity Rules , 1956.” pp. 45–48, 2000.

[91] L. Prikler, G. Bdn, and G. B~nfai, “EMTP models for simulation of shunt reactor switching transients,” *Electr. Power Energy Syst.*, vol. 19, no. 4, pp. 235–240, 1997.

[92] International Electrotechnical Commission, “IEC 61869-3, "Instrument transformers-part 3,” Geneva, Switzerland, 2011.

[93] K. M. C. Dantas, W. L. A. Neves, G. A. Cardoso, and L. C. Fonseca, “Real Time Implementation of Transmission Line Controlled Switching,” in *International Conference on Power Systems Transients (IPST2011) June 14-17*, 2011, pp. 1–6.

[94] M. Kezunovic, L. Kojovic, V. Skendzic, C. W. Fromen, D. R. Sevcik, and S. L. Nilsson, “Digital models of coupling capacitor voltage transformers for protective relay transient studies,” *IEEE Trans. Power Deliv.*, vol. 7, no. 4, pp. 1927–1935, 1992.

[95] P. Bornard, J. Tesseron, J. Bastide, and M. Nourris, “Field Experience of Digital Fault Recorders and Distance Relay in EHV Substations,” *IEEE Trans. Power Appar. Syst.*, vol. PAS-103, no. 1, pp. 133–139, Jan. 1984.

[96] O. A. S. Youssef, “Combined fuzzy-logic wavelet-based fault classification technique for power system relaying,” *IEEE Trans. Power Deliv.*, vol. 19, no. 2, pp. 582–589, 2004.

[97] A. V. De Carvalho, A. R. F. Freire, and H. M. De Oliveira, “Transient interaction between coupling capacitors voltage transformers and transmission lines,” in *IEEE Power and Energy Society General Meeting, PES ’09*, 2009, pp. 1–8.

[98] E. Nashawati, O. E. Delivery, N. Fischer, B. Le, D. Taylor, and S. E. Laboratories, “Impacts of Shunt Reactors on Transmission Line Protection,” in *38th Annual Western protective relay conference, Washington, USA,18-22 October*, 2011, no. 2, pp. 1–16.

[99] A. Ukil and R. Ivanovi, “Application of Abrupt Change Detection in Power Systems Disturbance Analysis and Relay Performance Monitoring,” *IEEE Trans. Power Deliv.*, vol. 22, no. 1, pp. 59–66, Jan. 2007.

[100] M. Stanek, “Analysis of circuit breaker controlled switching operations - From manual to automatic,” in *Proceedings of the Universities Power Engineering Conference*, 2015, vol. 2015-Novem.

[101] B. R. Bhalja, R. P. Maheshwari, and N. Chothani, *Protection and Switch gear*, 2 nd. New

delhi, India: Oxford University press, 2011.

[102] P. Sorrells and A. Benitez, "Power transformer neutral grounding reactor application and distribution feeder protection issues at CenterPoint Energy," in *58th Annual Conference for Protective Relay Engineers, 2005.*, 2005, vol. 2005, pp. 27–39.

[103] K. A. Bhatt, B. R. Bhalja, and U. Parikh, "Evaluation of controlled energization of shunt reactors for minimizing asymmetric DC component of charging current with circuit breaker having pre-insertion resistors," *Int. J. Electr. Power Energy Syst.*, vol. 93, pp. 340–351, Dec. 2017.

[104] CIGRE Task Force 13.00.1, "Controlled switching A state of the art survey- part I.," in *ELECTRA*, 1995, pp. 1–34.

[105] F. K. Basha and M. Thompson, "Practical EHV reactor protection," in *2013 66th Annual Conference for Protective Relay Engineers, CPRE 2013*, 2013.

[106] R. Atte, R. Atte, R. Atee, and O. No, "IEC TR 60071-4 'Insulation co-ordination –Part-4,'" Geneva, Switzerland.

[107] T. Committee, I. Power, and E. Society, *IEEE Std C57.21™-2008 (Revision of IEEE Std C57.21-1990), IEEE Standard Requirements, Terminology, and Test Code for Shunt Reactors Rated Over 500 kVA*, vol. 2008, no. August. 2008.

[108] J. Hu, B. Bisewski, R. Sherry, M. Dalzell, M. Zavahir, and C. Bartzsch, "Converter Transformer Inrush Control Using Hybrid Pre-insertion Resistors and Point-on-Wave Switching in the New Zealand HVDC System," in *CIGRE sessions*, 2016, pp. 1–8.

[109] *' User's Guide on PSCAD/EMTDC Power System Simulation Manual'*, 4th ed. Manitoba, Canada, 2005.

[110] T. Committee, I. Power, and E. Society, *IEEE Std C57.21™-2008 (Revision of IEEE Std C57.21-1990), IEEE Standard Requirements, Terminology, and Test Code for Shunt Reactors Rated Over 500 kVA*, vol. 2008, no. August. 2008.

[111] CIGRE Working group C4.307, "T 'Transformer Energization in Power System: A Study Guide' , Working Group C4.307, February 2014.," *E-CIGRE*, vol. 1, no. February, p. 11, 2014.

[112] V. Switchgear, *IS/IEC 62271-203: 2003, " High Voltage Switchgear and Controlgear."* New delhi: Bureau of Indian Standard, 2008.